# INVESTIGATION ON FRICTION STIR WELDING OF DISSIMILAR ALUMINIUM ALLOYS AA 7075 AND AA 1200 BUTT JOINTS

**BY**

**ATTAH, Ileh Benjamin**
**PhD/SEET/2016/910**

**THESIS SUBMITTED TO THE POSTGRADUATE SCHOOL, FEDERAL UNIVERSITY OF TECHNOLOGY, MINNA, NIGERIA IN PARTIAL FULFILMENT OF THE REQUIREMENT FOR THE AWARD OF THE DEGREE OF DOCTOR OF PHYLOSOPHY (PhD) IN MECHANICAL ENGINNERING (INDUSTRIAL& PRODUCTION)**

**OCTOBER, 2021**

# ABSTRACT

Dissimilar aluminium alloys of AA1200 and AA7075 have significant applications in automobile sector, aerospace, defence and shipping industries. These alloys faces problems like hydrogen solubility, formation of aluminium oxides, solidification shrinkage etc when welded with fusion welding process. Friction stir welding is the process which is able to successfully weld these dissimilar alloys of aluminium. Process parameters like rotational speed, welding speed, tool design, vertical force plays important role in determining the joint properties. Rotational speed and welding speed has its major role in producing the necessary frictional heat to plasticise the material which on solidification produces the weld joint. After developing workable process parameters (process window) from preliminary welds, the welds are taken on rotational speed of 900 rpm to 2100 rpm and welding speed for 30 mm/min to 90 mm/min using the response surface methodology approach. The tool geometries were varied as tapered tool (TT) and tapered threaded tools (TTT). The tensile test performed shows that the ultimate tensile strength for the TT ranges from 118-152.48 MPa translating to a joint efficiency range of 65.78-84.71%, microhardness ranges from 77-99.72 HV, while for TTT the ultimate tensile strength ranges from 130.52-161.84% translating to a joint efficiency of 72.52-90.32 %, microhardness ranges from 77.8-105.75 HV . Rotational speed of 1500 rpm, Traverse speed of 60 mm/min and Tilt Angle of 2º were obtained as optimal welding parameters for the tapered (TT) and tapered threaded tools (TTT) and Tapered threaded tool weldment gave better mechanical properties. The result of the corrosion test performed revealed that TTT weldment performed better at optimal level in terms of corrosion resistance with a corrosion rate of 0.497 mm/year as against 0.698 mm/year obtained using the tapered tool (TT). The microstructures obtained using both tool geometries revealed presence of onion ring formation which is an indication of mixing or material coalescence at the optimal level of parameters. It was recommended that compressive and bending strengths of the weldment of the two dissimilar aluminium alloys should be evaluated, friction stir welding in lap configuration arrangement should be conducted on the two dissimilar alloys for other application purposes, further research should be performed on the effect of residual stress on the weldment and that the effect of the axial load on the mechanical properties of the weldments be investigated.

# TABLE OF CONTENTS

**Contents**                                                                 **Page**

# LIST OF TABLES

## LIST OF FIGURES

# LIST OF PLATES

# ABBREVIATIONS

| | |
|---|---|
| AA | Aluminium Alloy |
| FSW | Friction Stir Welding |
| AS | Advancing Side |
| RS | Retreating Sides |
| TRS | Tool Rotational Speed |
| TTT | Tapered Threaded Tool |
| TT | Tapered Tool |
| FSWELD | Friction Stir weld |
| HAZ | Heat Affected Zone |
| TMAZ | Thermo-mechanically Affected Zone |
| mm/min | Millimetre per minute |
| rpm | Revolutions Per minute |
| TWI | The Weld Institute |
| UTS | Ultimate Tensile Strength |
| IIT KGP | Indian Institute of Technology Kharagpur |
| GRG | Grey Relational Generating |
| GRC | Grey Relational Coefficient |
| Grade | Grey Relational Grade |

# CHAPTER ONE

## 1.0                          INTRODUCTION

### 1.1     Background to the Study

Friction Stir Welding (FSW) is a solid state welding process invented and patented by The Welding Institute (TWI) in the United Kingdom in 1991 for butt and lap welding of metals and plastics. It is a joining technique that employs plastic deformation to create solid state joints between wider ranges of materials which are used in the manufacturing industries and can be used for materials that are difficult to weld using fusion welding (Thomas *et al.,* 1991). They have been used in production of vehicles bonnets, wheel rims (Smith *et al.,* 2012) and vessels bulkheads and decks (Gesto *et al*., 2008) and freezing plants (Midling *et al.,* 1999). The mechanical properties of the friction stir welded materials are higher than the conventional welding joints. Friction stir welding process has been used to successfully weld both similar and dissimilar alloys. The friction stir welding technology is considered to be the most significant metal joining process due to its environmental friendliness, energy efficiency and its broadness and the process is currently used for many applications and employed in many industries such as aerospace, marine, railway and electrical. The benefits of friction stir welding being that it generates no harmful fumes, no solidification cracking, results in reduced distortion and improved weld quality for the proper parameters, adaptable to all positions and are a relatively quiet process (Hussain & Quardri, 2010).

The joining of two dissimilar materials such as aluminium (Al) and copper (Cu) is of great demand for industrial applications. The need to join these materials is due to the thermal and mechanical properties they possess, such as a high corrosion resistance and a high electric conductivity. However, aluminium and copper are difficult to weld using the conventional welding processes due to the thermal properties of both materials. The

current conventional welding methods result in the formation of hard and brittle intermetallic phases at the interface of the joint (Akinlabi, 2012). These phases will eventually result in cracks.

The use of friction stir welding to join these two materials result in improved contact surface, improved current flow and less resistance. Friction Stir Welding consumes little energy and no gas or flux is used, therefore making the process environmentally friendly. The improvements lead to energy savings; this will lead to a global energy consumption decrease if the method is implemented on a global scale (Akinlabi, 2012).

The friction stir welding technology produces high quality welds but to achieve all these, there are several parameters that need to be addressed during the welding process of materials. The welding process parameters, tool geometry, joint design and heat generation exert a significant effect on the material flow pattern and temperature distribution thus influencing the microstructural evolution and the properties of the materials being welded (Leal *et al.*, 2010). Several researchers have successfully joined aluminium to copper using the friction stir welding process (Akinlabi *et al.,* 2011; Esmaeili *et al.,* 2011; Akinlabi *et al.,* 2012). Tool shoulders are designed in a way such that frictional heat is generated on the surface and subsurface of the specimens being welded. The shoulder and pin combination work hand in hand. In situations where thin sheets are to be welded, the shoulder produces the most deformational and frictional heat. During the welding of thick specimens, the main heating is produced by the pin. The most important parameter of the shoulder is the diameter because it has significant effect on the amount of frictional heat generated (Byung-Wook *et al.,* 2010). The larger the shoulder diameter, the larger the pressure force which causes changes in the weld shape. The response surface methodology is a collection of mathematical and statistical techniques for experimental model building. By careful design of experiments, the

objective is to optimise a response (output variables) which is influenced by several independent variables (input variables).

Response surface methodology is a collection of mathematical technique useful for developing and optimizing processes (Myers & Montgomery, 2002). It is extensively applicable in situations where several input variables potentially influence some performance measures or quality characteristics of the process. It implies that performance measure or quality characteristics are called responses while input variables are sometimes called independent variables and are subject to the control of the Scientist or Engineer.

Response surface methodology consists of experimental strategy for exploring the space of the process or independent variables, empirical statistical modeling to develop an appropriate approximating relationship between the yield and the process variables, and optimization methods for finding the values of the process variables that produce desirable values of the response. (Myers & Montgomery, 2002).

## 1.2    Statement of the Research Problem

The difficulties faced in welding aluminium and other non-ferrous metals are more severe in fusion (conventional welding process) resulting in defects such as cracks and porosity as well as emission of toxic fumes and smokes than in the solid state welding. The friction stir welding process is more suitable for welding aluminium alloys especially in aerospace vehicles.  It has been established that a great number of fasteners and rivets are used in aerospace vehicles, apart from the weight which these fasteners and rivets (1000, 000 rivets on each wing of the aircraft) adds to the aircraft they are equally susceptible to crevice corrosion (Caio-Palumbo *et al.*, 2017). The application of friction stir welding eliminates this additional weight imposed on the aircraft. Also, toxic fumes

and smoke is generated with conventional welding techniques but friction stir welding is a green and environmental friendly technology. Lastly, the mechanical properties of the weldment are dependent upon the process parameters and if not properly selected can lead to production of defective weldment. The optimisation of these parameters becomes imperative in order to produce defect- free weldment.

## 1.3    Aim and Objectives of the Study

The aim of this work is to investigate friction stir welding of dissimilar aluminium alloy butt joints and determine the effect of the welding parameters on the mechanical properties of the weldment, establish a suitable joining parameters for producing defect-free weldment. The objectives are to: -

   i.    determine the effect of friction stir welding parameters (rotational speed, welding speed and tool tilt angle) on the mechanical properties of weldment of two dissimilar aluminium alloys.

  ii.    determine single response optimal welding parameters and percentage contributions to mechanical properties of the weldment using (S/N) signal to noise ratio and analysis of variance (ANOVA), respectively

 iii.    develop empirical models for the mechanical properties of the weldment based on experimental results.

  iv.    determine multi- response optimal welding parameters using grey relational analysis (GRA).

   v.    evaluate the corrosion behaviour of the optimised weldment using potentiodynamic polarisation (PDP).

  vi.    examine microstructure of the optimised weldment using scanning electron microscopy and optical microscopy.

## 1.4    Justification of the Study

Light weight and good surface finish are desirable qualities in welding for specific applications especially in aerospace vehicles (João-pedro, 2014). Riveting and conventional (fusion) welding technique applied in aerospace joints are associated with heavy weight and crevice corrosion therefore, resulting in poor joint strength and eventually damage under service condition over time. Also, aluminium alloys are difficult to weld conventionally due to high reflectivity and thermal conductivity, the inter-metallic phase in the conventional (fusion) welding lowers the toughness of the weldment and causes cracks during and after the welding. With friction stir welding, all these defects are reduced in the weldment.

**CHAPTER TWO**

**2.0**             **LITERATURE REVIEW**

**2.1**     **Welding and Its Classification**

Welding is a fabrication process whereby two or more parts are fused together by means of heat, pressure or both forming a joint as the parts cool. Welding is usually used in metals and thermoplastics. The completed welded joint is referred to as weldment. Some materials are considered unweldable which is a term used in Engineering to describe two parts which cannot be joined together by welding techniques. The parts that are joined are known as parent materials while the materials added in order to form the joints are called filler metals or consumables (TWI, 2015).

A weld is made when separate pieces of material to be joined together combine to form one piece when heated to a temperature high enough to cause softening or melting. Filler material is typically added to strengthen the joint. Welding is a dependable, efficient and economic method for permanently joining similar metals. In other words, you can weld steel to steel or aluminum to aluminum, but you cannot weld steel to aluminum using traditional welding processes. Welding is used extensively in all sectors of manufacturing, from earth moving equipment to the aerospace vehicles.

The number of different welding processes has grown in recent years. These processes differ greatly in the manner in which heat and pressure (when used) are applied, and in the type of equipment used. There are currently over 50 different types of welding processes; the electric arc welding is the most common form. The most popular processes are shielded metal arc welding, gas metal arc welding and gas tungsten arc welding (TWI, 2015).

Welding can be classified into two general categories namely: Fusion welding and solid state welding process. They can be further broken down into various processes as indicated in Figure 2.1 (Tri-state Fabricators, 2010).
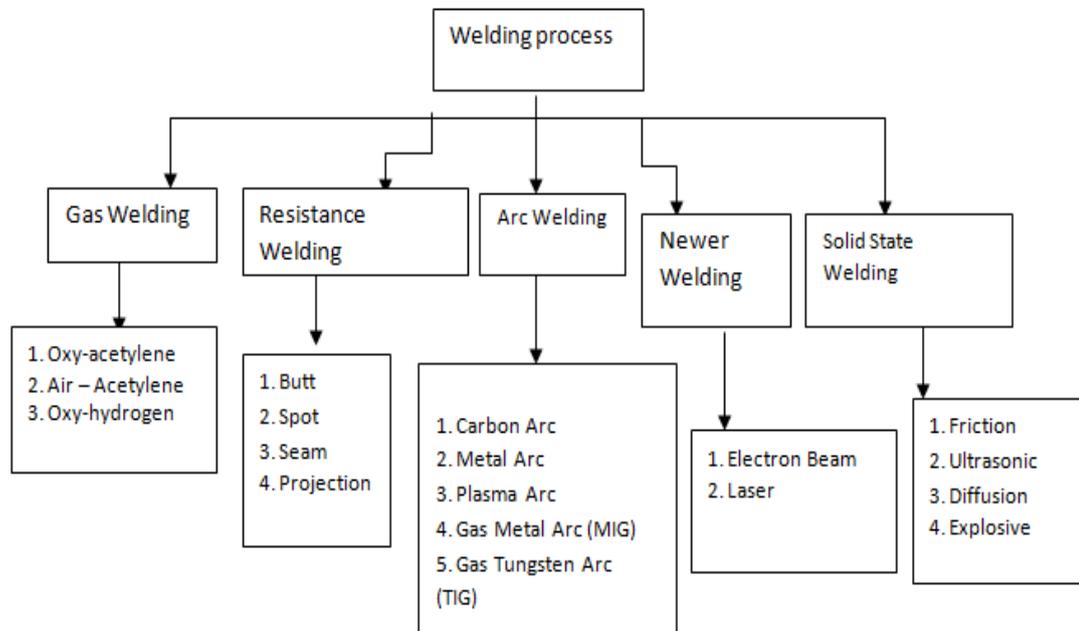


**Figure 2.1: Classification of Welding processes (Tri-state fabricators, 2010)**

### 2.1.2    Solid state welding

Solid state welding refers to joining processes in which coalescence results from the application of pressure or a combination of heat and pressure. If heat is applied, the temperature in the process is below the melting temperature of the metal being welded. It is a welding process that requires no filler metal and in which metallurgical bonding is achieved with little or no melting of base metal. Some examples include friction welding, ultrasonic and diffusion welding (Vural, 2014).

### 2.2    Friction Welding Processes

Friction welding process is a solid state welding process in which coalescence of material is achieved by the frictional heat between two surfaces in contact. In friction welding, no

external heat source is required as the heat is generated within the system (Vural, 2014)**.** There are various friction welding processes such as:

**(i)    Direct Drive Friction Welding Process**

In direct drive friction welding process, the workpieces to be welded are clamped rigidly in a fixed unit and a rotating chuck assembly and the rotating part is accelerated to a predetermined rotational speed. During the rotation the fixed workpiece is pushed against the rotating part and the rotation and the axial force continue for a predetermined duration (until the production of the appropriate heat input). Then, the rotation stops quickly and at "zero speed" the axial force increases until the end of the process (Pantelis, 2014).

**(ii)    Inertia Friction Welding Process**

The workpieces to be welded are clamped rigidly in a fixed unit and a rotating chuck assembly. The rotating spindle (including the one part and any required flywheels) is accelerated to a predetermined rotational speed, storing the energy required for welding, the spindle is then disconnected from the drive source and the flywheel begins to rotate. Simultaneously, the ram assembly moves the non rotating part axially to force both workpieces together at a predetermined calculated thrust load. While the parts are thrust together, the produced friction converts kinetic energy stored in the rotating spindle and flywheel assemblies into heat at the interface of the parts, and finally into mechanical work of the plasticized metals (Pantelis, 2014).

**(iii)    Linear Vibration Welding Process**

This is a welding process in which the workpieces move against each other in a linear direction. The frictional force between the two parts generates heat which plasticizes their interface; static load acting on the moving part promotes flow of the plasticized material hence generating the weld. This method can be applied on pieces with uniform surface and sufficient width (Pierce Industries, 2018).

**(iv)     Orbital Friction Welding Process**

This is a process whereby the center of one component moves relative to the other component around a two dimensional curve to provide the rubbing action. The two workpieces are rotated around their longitudinal axes in the same direction with the same angular speed. The two longitudinal axes are parallel with a small distance offset. When the motion of the components has stopped and, before the application of friction pressure, the parts are correctly aligned to form a weld (Maalekian *et al.*, 2008).

**(v)     Radial Friction Welding Process**

Residual friction welding process involves rotation and radial compression of a solid beveled ring into a V-preparation provided by the pipe ends, a mandrel is located in the bore, at the weld location, to prevent collapse of the pipe ends and penetration of upset metal formed during the weld sequence. The ring, made from a compatible material, is more sharply beveled than the pipes to promote metal flow from the base of the weld reparation (Pierce Industries, 2018).

## 2.3     Friction Stir Welding

Friction stir welding is a solid state joining technique in which a cylindrical tool is rotated and traversed along the proposed joint edges and the frictional heat generated by the tool causes plastic deformation of the materials and forms a weld (Thomas *et al,* 1991)

### 2.3.1   Material flow

The material flow during friction stir welding is separated in two kinds of flow:

   a.   Material flow due to pin: layer by layer

   b.   Material flow due to shoulder: material from retreating side (RS) is transferred through the shoulder surface at the top of the advancing side (AS) (Kumar *et al*., 2008).

**2.3.1.1 Welding forces**

During welding a number of forces acts on the friction stir welding tool:

a. A downwards force necessary to maintain the position of the tool at or below the material surface. Some friction-stir welding machines operate under load control but in many cases the vertical position of the tool is preset and so the load will vary during welding.

b. The traverse force acts parallel to the tool motion and is positive in the traverse direction. Since this force arises as a result of the resistance of the material to the motion of the tool it might be expected that this force will decrease as the temperature of the material around the tool is increased.

c. The lateral force may act perpendicular to the tool traverse direction and is defined here as positive towards the advancing side of the weld.

d. Torque is required to rotate the tool, the amount of which will depend on the down force and friction coefficient (sliding friction) and/or the flow strength of the material in the surrounding region (Buchibadu *et al*., 2017).

**2.3.1.2 Generation and flow of heat**

For any welding process it is, in general, desirable to increase the travel speed and minimize the heat input as this will increase productivity and possibly reduce the impact of welding on the mechanical properties of the weld. At the same time it is necessary to ensure that the temperature around the tool is sufficiently high to permit adequate material flow and prevent flaws or tool damage. When the traverse speed is increased, for a given heat input, there is less time for heat to conduct ahead of the tool and the thermal gradients are larger. At some point the speed will be so high that the material ahead of the tool will be too cold and the flow stress too high, to permit adequate material movement, resulting

in flaws or tool fracture. If the "hot zone" is too large then there is scope to increase the traverse speed and hence productivity (Frigaard *et al*, 2001).

The welding cycle can be split into several stages during which the heat flow and thermal profile will be different as follows:

a. Dwell. The material is preheated by a stationary, rotating tool to achieve a sufficient temperature ahead of the tool to allow the traverse. This period may also include the plunge of the tool into the workpiece.

b. Transient heating. When the tool begins to move there will be a transient period where the heat production and temperature around the tool will alter in a complex manner until an essentially steady-state is reached.

c. Pseudo steady-state. Although fluctuations in heat generation will occur the thermal field around the tool remains effectively constant, at least on the macroscopic scale.

d. Post steady-state. Near the end of the weld heat may "reflect" from the end of the plate leading to additional heating around the tool (Frigaard *et al.*, 2001)

Heat generation during friction-stir welding arises from two main sources: friction at the surface of the tool and the deformation of the material around the tool (Qi & Chao, 1999). The heat generation is often assumed to occur predominantly under the shoulder, due to its greater surface area, and to be equal to the power required to overcome the contact forces between the tool and the workpiece.

## 2.3.2 Welding tool

The welding tool of friction stir welding plays a prominent role in the welding process which has an impact on the mechanical properties and quality of microstructure of the

material. Therefore, the tool is designed carefully and it should have ideally higher mechanical properties than weld materials. The difficulty in tool design is in finding proper tool material;

The materials that can withstand the high temperatures that are experienced during friction stir welding are the high-temperature tool materials and they are thus suitable for the process. Materials that are hard enough to withstand wear during welding is also very important and should be considered during selection of tool material..

Rai *et al.* (2011) reviewed and examined several important aspects of friction stir welding tools such as tool material selection, geometry and load bearing ability, mechanisms of tool degradation and process economics. The geometrical parameter of friction stir welding is tool designed with D/d ratio (shoulder/pin ratio). The shoulder diameter (D) is decided with pin diameter (d), so that the ratio of D/d should be 3. The tool shoulder applies a pressure to the material to constrain the plasticized material around the pin and generates heat through friction and plastic deformation in a relatively thin layer under the shoulder surfaces. Elangovan *et al*. (2009) studied the influence of five different tool pin profiles on the formation of friction stir processing zone. The five-tool pin profiles, i.e., straight cylindrical, tapered cylindrical, threaded cylindrical, triangular and square pins to fabricate the joints are shown in Figure 2.2



(a) Straight cylindrical   (b) Threaded cylindrical   (c) Tapered cylindrical   (d) Square   (e) Triangle
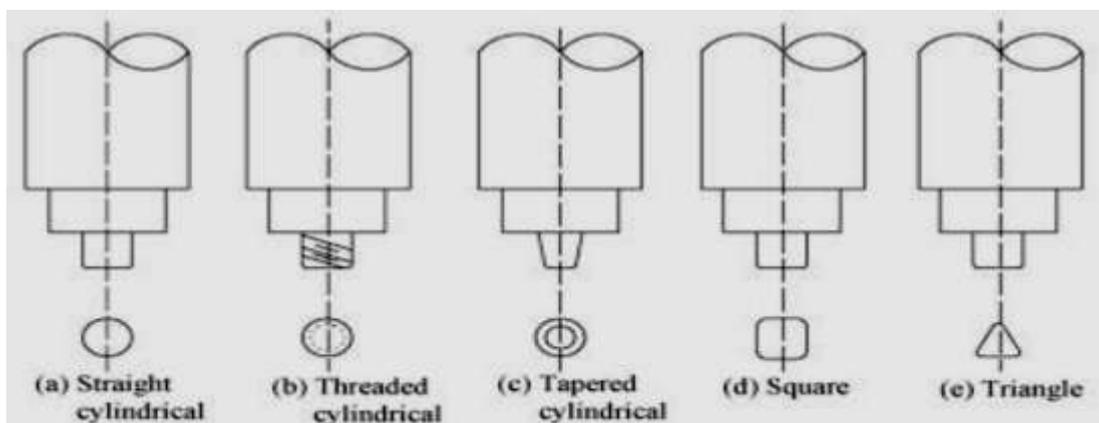
Figure 2.2**:** Schematic diagram of different types of FSW pin profile (a) Straight cylindrical, (b) threaded cylindrical, (c) Tapered cylindrical, (d) Square and (e) Triangle (Elangovan *et al.*, 2009)

There are three types of friction stir welding or processing tools based on the number of pieces making the tools. They are fixed, adjustable and self-retracting. The fixed friction stir welding tool corresponds to a single piece of the device comprising of shoulder and probe (Tozaki *et al.,* 2010; Bakavos & Pragnell, 2009; Bakavos *et al.*, 2011). This tool is applied only to weld a workpiece having a constant thickness as it has fix probe length. The flexible friction stir welding tool consists of two independent pieces of the separate shoulder and probe so as to make an adjustment of probe length during welding (Ding & Oelgoetz 2012; Ding, 2013). It is used for welding of variable and multiple gauge thickness workpieces. Also, implementation of filling the exit hole left at the end of the friction stir weld is performed with this type of tool. Both the fixed and the flexible tool often require a backing anvil. The self-retracting friction stir welding tool consists of three independent pieces, top shoulder, probe and bottom shoulder (Wayne *et al.,* 2003; Skinners & Edwards, 2003). It can have multiple gauge thickness joints due to the flexible probe length between the top and bottom shoulders (Sylva *et al.,* 2004; Marie *et al.,* 2004). The self-retracting tool can only work perpendicularly to the workpiece surface while the fixed and adjustable tools can be tilted longitudinally and laterally.

### 2.3.3   Characteristics of microstructural zones

The solid-state nature of the friction stir welding process, combined with its unusual welding tool, results in a microstructure with several distinct characteristic zones. The major zones concerning the microstructure are as follows:

**(i)      The stir zone or weld nuggets**

The stir zone which is also referred to as nugget, dynamically recrystallised zone is a region of heavily deformed material that roughly corresponds to the location of the pin during welding. The grains within the stir zone are roughly equiaxed and often an order of magnitude smaller than the grains in the parent material (Murr *et al*., 1997). A unique feature of the stir zone is the common occurrence of several concentric rings which has been referred to as an "onion-ring" structure (Khrishna, 2002). The precise origin of these rings has not been firmly established, although variations in particle number, density, grain size and texture have all been suggested.

**(ii)     The flow arms zone**

The flow arms zone is on the upper surface of the weld and consists of material that is dragged by the shoulder from the retreating side of the weld, around the rear of the tool, and deposited on the advancing side.

**(iii)     Thermo-mechanically affected zone**

The thermo-mechanically affected (TMAZ) occurs on either side of the stir zone. In this region the strain and temperature are lower and the effect of welding on the microstructure is correspondingly smaller. Unlike the stir zone the microstructure is recognizably that of the parent material, albeit significantly deformed and rotated. Although the term TMAZ technically refers to the entire deformed region it is often used to describe any region not already covered by the terms stir zone and flow arm.

**(iv)     The heat affected zone**

The heat affected zone (HAZ) is common to all welding processes. As indicated by the name, this region is subjected to a thermal cycle but is not deformed during welding. The temperatures are lower than those in the TMAZ but may still have a significant effect if

the microstructure is thermally unstable. In fact, in age-hardened aluminium alloys this region commonly exhibits the poorest mechanical properties. (Mahoney *et al.*1998).

**(v)     Defects in Friction Stir Welding**

The following defects are commonly found in the friction stir welding (Podrzaj *et al.* 2015; Bied-Charreton, 2016 and Abdulaziz, 2020).

a. Tunnel defects: This defect is formed due to improper stirring of the materials around the tool and improper material mixing

b. Lazy S / Zig Zag: This is a defect characterized by presence of zig-zag zone of the friction stir weld line pattern at the stir zone of the friction stir weld. It results from low heat input parameters

c. Kissing bond: This defect occurs when the tool pin stirring fails to make contact with weld bottom interface significant due to insufficient heat and material flow

d. Lack of Penetration: This is a type of defect that results from variation in sheet thickness and incorrect tool orientation/ pin length.

e. Flash: This is a defect in which materials are ejected to the surface due to softening of the materials. They are caused by excessive heat.

**2.3.4   Process parameters for welding**

Pankaj *et al.* (2014) conducted an experiment to study the welding of 6.35 mm thick plate of AA7075-T6 alloy using friction stir welding process. They used square butt joint in the experiments as it was found to have given better result. Process parameters were rotational speed which was varied between 1400 to 1600 rpm at 100 rpm interval, axial load of 8 to 9 kN, welding speed of 50-100 mm/min at 25 mm/min interval with tensile strength as output variable. There was a positive relationship between the load and tensile strength. If axial load increases tensile strength also increases. Tensile strength decreases with increase in welding speed up to 75 mm/min then begins to decrease. Tensile strength

increases with increase in spindle speed up to 1500 rpm, beyond that it decreases, the optimum spindle speed is 1500 rpm and 9 kN was optimum axial load.

Fereiduni *et al*. (2015) examined the friction stir spot welding between Al-5083 and aluminium/st-12 steel alloy sheets with the thicknesses of 3 and 1 mm, respectively. The effect of the rotational speed and dwell time on the joint interface microstructure and tensile shear strength of the weldment was investigated; temperature changes at the joint interface were measured. Rotational speeds of 900 and 1100 rpm were used with the dwell times of 5, 7, 10, 12 and 15 seconds to spot welding of the material. Average values of both tensile and shear test conducted on samples for each processing conditions were recorded. It was observed that dwell time of less than 5s was insufficient for welding to occur and that as dwell time increases with increase in joint strength up to certain limit and then starts declining, for instance, at 900 rpm, 5s dwell time, tensile strength was 2270 MPa and reached a maximum of 4020 MPa and as dwell time increased to 12 s and decreased to 2870 MPa as dwell time increased to 15 s. A similar pattern was followed 1100 rpm as weld strength of 1830 MPa at 5 s dwell time increased to a maximum of 3630 MPa with dwell time of 10 s and then begins to decrease at 12 and 15 s dwell time. Increase in dwell time from 5 to 15 seconds resulted in temperature increase from 310 to 410 ℃ at 900 rpm and respectively from 390 to 420 ℃ for 1100 rpm tool rotational speed.

Yoo *et al*. (2015) tested mechanical properties and macro structure of friction stir welded joint using radiography test for Al-Li alloy. Rotational and travel speeds were used as process parameters to compare the results. Tensile test was conducted to verify the strength and elongation of welded joint using defect free specimens. It was observed that highest tensile strength was obtained between 40 to 60 rpm tool rotational speed and 230 to 300 mm/min welding speed. Also, maximum ultimate tensile strength value was 73.9

% of the parent material and minimum was 63.3 % of the parent material and optimal process condition which shows highest tensile strength and elongation was 400 rpm and 300 mm/min. After welding, non-destructive tests by x-ray and macro observations of stir zone were conducted to verify the soundness of the weldment. Increasing travel speed causes irregular boundary shape in advancing side. Little defect formation started between advancing side and stir zone. From 300 mm/min, unstable boundary shape may be started. Increasing rotation speed also causes unstable boundary in advancing side. Defects formation started when there was insufficient time for mixing the material in high travel speed zone.

### 2.3.5  Friction stir welding of similar materials

Friction stir welding has been successfully used to weld similar materials. Research studies conducted on friction stir butt welds of similar aluminium alloys have been reported. (Lakshminarayanan *et al*., 2011; Xu *et al.,* 2012; Zhang, 2010) in which process windows were successfully established and are been applied in the industries. Similar copper plates have also been friction stir welded by Hwang *et al.* (2010), the appropriate processing parameters and temperature for joining copper plates were also achieved. Magnesium plates had also been joined using friction stir welding, good quality welds were produced and it was concluded that friction stir welding and its alloys has a good potential for the joining of magnesium and its alloys (Suhuddin *et al.,* 2009).

Lienert *et al.* (2013) conducted an experiment on the feasibility of joining mild steel by friction stir welding process. Welding was done on plates of hot rolled AISI 1018 steel in a butt weld configuration. The dimension of the workpiece was 203 mm x 110 mm x 6.35 mm. The process parameters used includes welding speeds ranging from 25.2 to 100.8 mm/min and tool rotational speeds ranging from 450- 650 rpm. Heat composition of the materials was determined by using LECO and x-ray flouresence method. Defect free

welds were produced by friction stir welding. It was observed that tool loads during friction stir welding of mild steel at 25.2 mm/min was approximately 18.7 kN while torques were in the range of 55 N/m$^2$, peak temperature obtained above the tool's shoulder diameter were in the neighbourhood of 1000 ℃, extrapolation of measured temperature and microstructural evidence suggest peak value of 1100 ℃. The EDS shows light etching features at the bottom centre of the stir zone.

### 2.3.5.1 Friction stir welding of aluminium alloys

Sajid *et al* (2012) studied the effect of friction stir welding parameters on mechanical properties and microstructure of 6061-T651. Chaitanya *et al.* (2013) studied the effect of post weld heat treatment on microstructure and mechanical properties of friction stir weld joins of AA 7039.

Bhatt and Pillai, (2012) examined the simulation of peak temperature and flow stress during friction stir welding of AA7050-T7451 aluminium alloy using hyperworks. The aim was to simulate the friction stir welding process to obtain temperature profiles and flow stresses using finite element analysis software known as hyperworks 9.0 to avoid difficulties of measuring directly. The process parameters include welding speeds of 51.0 and 76.2 mm/min and a constant rotational speed and tilt angles of 180 rpm and 2.5$^\circ$, respectively. The dimension of the workpieces was 381 x 127.5 x 6.4 mm. Simulation was performed by entering the following physical and thermal properties of AA7075 which are density of 2830 kg/ $m^3$ , melting point of 488-629 ℃, , modulus of elasticity of 7.17 $\times$ 10$^{10}$ Pa , poison's ratio of 0.33, thermal conductivity of 155 W/$m^{-K}$ , specific heat of 860 J/$kg^{-K}$, volumetric heat source of 0.0 w/ $m^3$ along with physical and thermal properties of default tool which are density of 2260 kg/ $m^3$, specific heat of 896 J/$kg^{-K}$, modulus of elasticity of 2.0 $\times$ 10$^{10}$ Pa, poison's ratio 0.35, X, Y and Z conductivities

18

198 W/$m^{-K}$ . The results obtained for temperature and flow stress distribution at constant rotational speed of 180 rpm and weld speeds of 51.0 and 70.2 mm/min indicates peak values of 340 and 360 and are maximum at centre of the tool pin.

It was concluded that at constant tool rotational speed and tool with the same geometry; variation in tool welding speed significantly affects temperature history & flow stresses developed during FSW of AA7050-T7451. The induced temperatures and flow stresses are in conformity with the results obtained in literature. The flow stresses at lower peak temperature of 340 ℃ are as high as 720 MPa but are as low as 680 MPa at higher peak temperature of 360 ℃ as the flow of material becomes easier at higher temperatures. It is also observed that at constant rotational speed the peak temperature has increased by increasing the welding speed (Bhatt & Pillai, 2012).

Kumar *et al.* (2008) examined the role of friction stir welding tool on material flow and weld formation. The system of friction stir welding and the function of the tool in forming welds in aluminium alloys 7020-T6 were studied. A frustum pin of H13 with 55 HRV hardness was used. In the experiments, consistent welding characteristics which are rotational speed of 140 rpm, 80 mm/min welding speed and the angle of tilt $2°$ were maintained. It was observed that while the contact surface of the tool advances, the defect of the weld gets reduced. It was also observed that in the initial part of welding, the shoulder of the tool does not come in contact with the metal to the full extent as a result of which the force around the axis will not be sufficient to generate heat. As such the joint becomes imperfect. The point is that when contact surface between shoulder and metal extends, the force of the axis also enhances which of the force of the metal will be confined to the cavity of the welds. It will generate enough heat and hydrostatic power.

Raza *et al.* (2015) used 3 mm thick AA 5052-O aluminum alloy plates in his experiment. Specimens were welded using constant tool traverse speed of 120 mm/min and by varying rotational speed from 800 to 3000 rpm. The physical appearance of the joints, microstructural and mechanical properties were investigated. It was observed that joints produced at 1000 rpm gave a maximum tensile strength which was 74% of the base material strength. The stir zone produced finer grain compared to base material. The average micro hardness of the nugget zone was lower than the base material hardness. The heating and extreme deformation due to tool rotation and axial pressure during friction stir welding process leads to diffusion of magnesium atom from the grain interiors to the grain boundaries to form more b-phase ( $Mg_2Al_3$ ) particles.

Jambulingam (2015) examined AA7075 and AA3014 joined by friction stir welding in order to optimize the process using Taguchi method, a total of nine experiments were conducted at different speed, feed rate, and axial force. The dimensions of the workpieces were 100 x 100 x 6 mm. The weldability and mechanical properties of these alloys were examined. The best parameters for the speed, feed and tool profile were chosen among 3 levels. For the best hardness of the welded area, the suitable parameters are 1200 rpm speed, 10 mm/min feed and cylindrical tool profile. The percentage contribution of speed was 36.51 %, feed was 16.69 %, and tool was 16.77 % for the hardness property using ANOVA. For the best UTS of the welded area, the suitable parameters are 1200 rpm speed, 20 mm/min feed and cylindrical tool profile. The percentage contribution of speed was 52.01 %, feed was 3.30 %, and tool was 24.4% for the hardness property using ANOVA. From the experiments, it was concluded that speed is the major factor influencing the mechanical properties like tensile strength and hardness.

Zhang *et al.* (2015) in their study used super high strength aluminum alloy with high zinc content as workpiece materials. Friction stir welding was conducted at tool rotational

speed of 350–950 rpm and welding speeds of 50–150 mm/min. It was observed that the grain size of the nugget zones decreased with increasing welding speed. The ultimate tensile strength and elongation decreased when rotational speed increased from 350 to 950 rpm at a constant welding speed of 100 mm/min.

The corrosion behavior of the parent alloy, the heat affected and weld nugget zones were studied in a 3.5% (mass fraction) aerated Nacl solution using potentiodynamic polarization and electrochemical impedance spectrometry by Kamran and Ferhad (2016). They used a non-heat treatable 5086 Al- alloy plate with dimensions 300 mm x 100 mm x 8 mm. The process parameters used were tool tilt angle of 3°, welding speed of 63 to 100 mm/min, rotational speed of 1000 rev/min, pin length of 7.5 cm, pin diameter of 8 mm and shoulder diameter of 20 mm.

Friction stir welding was adopted in a butt-welded configuration parallel to the rolling direction of the plate. Microstructural analysis and corrosion tests were performed on the weldment, corrosion test was carried out at the heat affected, weld nugget and the thermomechanically affected zones as well as the electrochemical impedance spectrometry test. They found out that: (i) The corrosion susceptibility of the weldment increases with increase in welding speed from 63 to 100 mm/mn (ii) corrosion rate in the weldment is higher than in the parent alloy (iii) corrosion current density increases with increasing the welding speed in the heat affected and the weld nugget zones (iv) corrosion potential in the weld nugget zone appears more positive than in the heat affected zone with decrease in the welding speed (v) the weld nugget zone exhibits higher resistance compared to heat affected zone and the parent alloy as the welding speed decreases. From the result of the electrochemical impedance spectrometry it can be concluded that: (i) the weld regions have higher corrosion resistance than the parent alloy (ii) with an increase in the welding speed, the distribution and extent of the corroded areas in the weld nugget

zone regions are lower than those of the heat affected zones region (iii) in the heat affected zone region, in addition to pits in the corroded area, some cracks can be seen in this area confirming the formation of intergranular corrosion in the area. (iv) alkaline localized corrosion and the pitting corrosion are the main corrosion mechanism in the corroded area within the weld region. Crystallographic pits are observed within the weld region.

Rusdi *et al.* (2017) studied the mechanical properties of friction stir welded aluminium alloy 5052. Their study focused on the analysis of mechanical properties and effects of welding parameters (tool geometry, welding speed, and rotational speed) in the friction stir welding of aluminium material AA5052. The tensile and bending strengths of the weldment were analysed, the result revealed that best mechanical properties were obtained with a tool of diameter 17.8 mm. The maximum tensile strength at 1300 rpm and a transverse speed of 50 mm/min was 222.1 MPa. The highest bending strength of 422.6 MPa was obtained at 1300 rpm rotational speed, 208 mm/min welding speed and 17.8 mm shoulder diametre while the lowest bending strength of 18.3 MPa was obtained at 1950 rpm rotational speed, 208 mm/min welding speed and 17.8 mm shoulder diametre.

Underwater friction stir welding is a variant of friction stir welding process which controls heat conduction and dissipation along the weld line improving the joint properties. The feasibility of underwater friction stir welding of AA 5052 H32 aluminum alloy to improve the joint performance than normal friction stir welding was addressed by Shanavas *et al.* (2018). The effects of tool rotational speed and welding speed on ultimate tensile strength by underwater and normal friction stir welding were analyzed and compared. They observed that the tensile strength of underwater welded joints was higher than normal friction stir welded joints except at 500 rpm. Maximum tensile strength of 208.9 MPa was obtained by underwater friction stir welding at rotational and welding speeds of 700 rpm

and 65 mm/min respectively. The optimum process parameters for achieving maximum tensile strength by normal friction stir welding were compared with underwater friction stir welding. The result showed that the ultimate tensile strength obtained by underwater friction stir welding was about 2% greater than that of the normal friction stir welding process. The joints with maximum tensile strength during underwater and normal welding fractured at the retreating side of the welded joint. Microstructural examination revealed that heat-affected region was not found in underwater welding. Microhardness was decreased slightly towards the stir zone. Fractography observation revealed that the welded joints exhibiting higher joint efficiency failed under ductile mode.

Amit *et al.* (2017) performed an experiment on the optimization of friction stir welding parameter for AA3003 aluminium alloy joints using response surface methodology. The study was focused on the influence of friction stir welding parameters on the ultimate tensile strength of AA3003 aluminium alloy joints. Trial experiments were performed to determine the process parameters affecting weld strength of AA3003 joints. Tool rotational speed (N), welding speed (S) and tool tilt angle (ɵ) were used for the investigation and the working range of selected parameters were chosen through primary trial runs based upon one factor at a time (OFAT) technique, where a factor is varied at different levels keeping other factors at some predefined fixed level. The range of the identified process parameters was selected to ensure the joints are free from any visible defects like blow holes and surface crack. The mechanical properties of AA 3003 aluminium alloys are: ultimate tensile strength (142 MPa), Yield stress (134 MPa), percentage elongation (12%), and hardness (35HV).

For experimental design building, Amit *et al*. (2017) used a 3-factor 5-level, rotatable central composite design matrix, having 20 combinations of different levels of selected parameters in the optimization. The upper and lower limit of a factor was coded as 1.682

and -1.682 respectively. The selected design is composed of $2^3=8$ full factorial, 6 centre and 6 star points. They showed a relationship between ultimate tensile strength and identified parameters that is tool rotational speed, welding speed and tilt angle ($\theta$)

Y (UTS) = F (N,S,$\theta$)

Design expert DX10 software package was used to determine the values of coefficients. The welding speed, rotational speed and tool tilt angle were optimised using the developed model and the values obtained were 74.64 mm/min, 971.77 rpm and 1.52°, respectively.

Rajesh *et al.* (2012) examined the influence of processing parameters on induced energy, mechanical and corrosion behaviours of AA7475 joints welded in butt configuration. The rotational speed was varied between 300 and 1000 rpm at constant welding speed of 50 mm/min. Energy calculation, metallographic, microhardness, tensile and corrosion tests were performed on the weldment. The results revealed that maximum induced energy of 87.2 J was obtained at 1000 rpm; microstructural observation revealed that with increase in tool rotational speed from 300 to 400 rpm the stir zone area first increased from 46 to 62 m$^2$ then decreased to 28 and 19 m$^2$ as the rotational speed increased from 400 to 700 and 1000 rpm respectively. Maximum UTS value of 355 MPa was obtained at 400 rpm and 50 mm/min. Maximum hardness at each point was obtained at 1000 rpm while maximum corrosion resistance property of the wed was obtained at 1000 rpm and 50 mm/min.

**2.3.5.2 Friction stir welding of other materials**

Olivier *et al*. (2010) examined the material flow path in friction stir welding using two geometries of tools. They stated that threaded pins are used in industrial application. In the initial stages there was a possibility of threaded tools becoming unthreaded. This happened due to the wear of the tool when the tool was used for alloys of a high melting

point as well as aluminum alloys that are strengthened. Friction stir welding tests were performed with two variant pin profiles. The two pins were unthreaded with or without level faces. The main idea of this experiment was to study the flow when unthreaded pins are used to weld plates that are thin. To examine the flow of the material, welds with cross and longitudinal sections were studied with or without using material marker. Both the threaded and unthreaded pins were observed to possess the same material flows. The material was placed in the advancing side in upper portion of the weld which in the retreating side it was placed in the lower portion of the weld with a rotating layer appearing around the tool. This study showed a very low vertical movement towards the weld's bottom due to the absence of threads. The force of the plunge and the speed of the rotation affected the size of the zone controlled by the shoulder. This can be diminished by the use of cylindrical frustum pin having flat surface. Numerous studies on transfer of heat and flow of material during friction stir welding were made.

Valero *et al.* (2008) made an attempt to identify the tensile characteristics of the joint performed in different conditions of welding. This study showed the least tensile strength and malleability at the lowest spindle speed for a specific traverse speed. When the speed of the spindle extended, there was increase in strength and elongation attaining the highest point before falling down due to high speed of rotation. In friction stir welding, the speed of rotation and the input of heat increase simultaneously. Therefore the speed of the tool rotation must be maximized to achieve the highest tensile of the joints. When the speed of welding rises, the width of the exerted area and the value of the maximum exertion go down. Then the area of the maximum exertion slowly moves to the retreating side of the joint from its advancing side. The tensile strength diminishes considerably as the speed of welding rises. The area which is softened is narrower for higher speeds of welding than

for lower speeds of welding. Therefore, the speed of welding must be maximized to obtain maximum tensile characteristics of the friction stir joints.

Pradeep and Muthukumaran (2013) conducted an experiment to analyze the friction stir welding of low alloy steel using Taguchi method. Three levels of process parameters specifically 900, 1120 and 1400 rpm; 0, 1 and $2°$ tilt angle and welding speed of 8, 15.75 and 20 mm/min were used. The aim was to optimize the process parameters for the welding of IS: 3039 grade II alloy steel which was done in butt arrangement. The dimension of the workpieces was 100 x 50 x 3 mm. Tensile strength was used as response. The predicted ultimate tensile strength value from ANOVA was 474 MPa while the confirmation test gave 472 MPa. The optimal process parameter was 1120 rpm rotational speed, $1°$ tilt angle and 8 mm/min welding speed.

### 2.3.6   Friction stir welding of dissimilar materials

Dissimilar metal welding refers to joining of two different alloy systems. Actually, all fusion welding are dissimilar welding because the metal been joined has a wrought structure while the welds have a cast structure. Frequently, the matching composition of the filler metal is deliberately altered from that of the base alloy.

Researchers have worked on the friction stir welding of dissimilar metals. Yoshikawa (2003) established a joining criterion for lap welding of dissimilar aluminium and stainless steel, Fukumoto *et al.* (2004) achieved good weld joint efficiency in dissimilar joints between normal carbon steel (S45C) and 6063 aluminium alloys. Dinaharan *et al.* (2012) examined the welding of dissimilar materials and reported that better weld efficiency is obtained when material with high strength is placed on the retrieving side and with material of low strength the advancing side.  Other successful dissimilar joining through friction stir welding includes aluminium and brass (Esmaeili *et al.,* 2011),

aluminium and titanium (Wei *et al.,* 2012), aluminium and magnessium (Yan *et al.,* 2010) and magnesium and Titanium (Aonuma & Nakata, 2012).

Vinayak and Bhatwadekar (2014) worked on AA6101 aluminium and pure copper plates of 5 mm thickness in butt joint configuration. Welding was done with at speed of 700 rpm and at 11 mm/min tool traverse speed and tool with cylindrical configuration. Welded joint shows onion ring structure in stir zone. They found that AA6101 and copper joint was brittle in nature, more downward force, higher welding speed and rotational speed produces strong butt joint.

**2.3.6.1 Friction stir welding of dissimilar aluminium alloys**

Elatharasan *et al*. (2012) used response surface methodology process to optimize the friction stir welding parameters for dissimilar aluminium alloys for ultimate tensile strength. Lee *et al*. (2008) studied the dissimilar lap joint friction stir welding  of AA5052-H112 and AA6061-T6 plates having thickness of 1 mm and 2 mm respectively, with various tool rotational speeds and tool traverse speeds according to the fixed location of each material on top or bottom sheet. They found that the interface morphologies were characterized by interface pull-up and pull-down in the advancing side and retreating side. The thickness of the thinner AA5052 sheet lessened due to the vertical movement of the materials. It was identified that the amount of vertical transport increased and consequently the thickness of AA5052 decreased when the heat input was increased either by increasing the tool rotation speeds or by decreasing the tool traverse speeds. Joint strengths mainly depended on the interface morphology and vertical movement of material.

Park and Kim (2010) investigated the effect of tool rotation speed and tool traverse speed on the stirring action and friction heat during FSW experiments on dissimilar Al alloys—

AA5052-O and AA6061-T6. The aim was to find optimum rotational and welding speeds for the two alloy pairs for shipbuilding application. They used a range of process parameters which are tool rotational speed of 800, 1250, 1600, 1800, 2500 rpm and welding speed of 15, 32, 124, 432 and 507 mm/min to determine the mechanical strength of weld nugget of the dissimilar materials. They concluded that the optimum conditions were a traveling speed of 61 mm/min and rotation speed of 1600 rpm. Their observations of the weld surface finish and plastic flow behavior showed that the stirring effect increased and number of defects decreased when the traverse speed was decreased.

Park *et al*. (2013) evaluated the effect of material locations on the properties of dissimilar friction stir welding joints of AA5052-H32 and AA6061-T6 which were both 2.0 mm thick. The process parameters used were tool rotational speed of 2000 rpm, welding speed of 10 mm/min, tilt angle of $3^{\circ}$, plunge depth of 1.9 mm, shoulder diameter of 10 mm, pin diameter of 4 mm and pin length of 1.7 mm while the position of the two alloys were varied during each welding operation, that is, material on advancing and retreating sides. It was observed that the material mixing patterns in friction stir welding joints vary depending on the location of base materials. For the given aluminium alloys, the materials were more properly mixed when AA5052-H32 was in the advancing side and AA6061-T6 was in the retreating side than the case of AA6061-T6 in the advancing side and AA5052-H32 aluminium alloy in the retreating side. It was found that for both combinations of material arrangement, AA5052-H32 showed the lowest value of microhardness in the heat-affected zone (HAZ), which clearly explained the reasons for the fracture of tensile test specimens at the 5052-H32 side.

Shaikh and Yagnesh (2015) conducted an experiment on optimization of friction stir welding of dissimilar aluminium alloys. The materials used were AA6061-T6 and AA2024 T6 and design of experiment using Taguchi method based on L9 orthogonal

array was employed. Hardness value, tensile stress and yield stress were measured. Optimization analysis was done using MINITAB software. It was observed that dissimilar metal joining process using friction stir welding was difficult to achieve because of different co-efficient of heat and the base metal chemical composition.

Nandan *et al,* (2013) examined the numerical simulation of three-dimensional heat transfer and plastic flow during friction stir welding of AA 6351 to AA 1200 aluminium alloys. The dimensions of the workpieces were 900 x 100 x 5 mm. The axial force was 4.7 kN with cylindrical tool having shoulder diametre of 20 mm, pin diametre of 10 mm, pin length of 4.8 mm, tilt angle of $2^{\circ}$ .

The equation of mass conservation, momentum and energy were numerically solved with appropriate boundary conditions to obtain 3D temperature and plastic flow fluids during friction stir welding. It was observed that significant plastic flow occurred in close proximity to the tool and heat plastic flow significantly affects heat transport within the workpieces (Nandan *et al*., 2013).

Dissimilar friction stir welding between Al5052 and Al 6061 alloys was investigated by Kumbhar and Bhanumurthy (2017). The dimensions of the workpieces were 300 mm $\times$ 50 mm $\times$ 5 mm. High speed steel tool, having a cylindrical shape with 4.8 mm pin length, 6 mm and 25mm pin and shoulder diameter, respectively. Several friction stir welding trials were carried out at 1120 and 1400 rpm with welding speeds ranging from 60 mm/min, 80 mm/min and 100 mm/min at constant tilt angle of $3^{\circ}$. They carried out optimization of process parameters by varying the normal and traverse loads, and spindle torque with respect to time during the experimental trials.

It was observed that the normal load experienced by the tool varied in the range of 3.5 to 7 kN at rotational speed of 1120 rpm. Whereas at a higher rotational speed of 1400 rpm,

the normal load was found to decrease and was in the range of 3.5 to 6 kN. Thus the normal load was less at higher rotational speed of 1400 rpm. However, no conclusive statement could be made for the normal load at rotational speed of 1120 rpm. The traverse load was in the range 0.6 to 1.2 kN and 0.7 to 1.3 kN for rotational speeds of 1120 and 1400 rpm, respectively. The spindle torque decreases with an increase in the rotational speed. Spindle torque values in the traversing phase were in the range of 33 to 38 Nm at 1120 rpm and 25 to 30 Nm at 1400 rpm. Further observations revealed that for a particular rotational speed, the spindle torque was not affected with the variation in traverse speeds (60, 80, and 100 mm/min) (Kumbhar & Bhanumurthy, 2017).

Microstructural Characterization showed the nature of the optical images of the cross-section of a FSW AA5052- AA6061 R1400F080 specimen. Kumbhar and Bhanumurthy, (2017) reported that the interface between the two alloy joints, which initially was linear prior to welding, later had a nonlinear, wavy, and distorted appearance. They concluded that the microstructural studies suggested that there was no rigorous mixing of both materials in the nugget, also that at higher rotational speeds, the normal load and the tensile properties of the FSW AA5052- AA6061 specimens were better than the properties of the softest of the similar friction-stir-welded systems (FSW AA6061).

Vinayak and Bhatwadekar (2015) conducted an experiment on dissimilar friction stir welding of AA1100 to AA6101-T6 aluminium alloys. The welding parameters used were feed rate of 3 mm/min, spindle or tool rotational speed of 1500 rpm, plate size of 100 mm x 50 mm x5 mm thickness, pin diameter of 6 mm. Trial welds were carried out in which a cylindrical profile tool of H13 was used. Tensile testing was done using a computerized UTM machine. The AA 6101 alloy was placed at the advancing side while the AA1100 was at the retreating side. Tensile test results can be seen in Table 2.1.

**Table 2.1: Comparison of Tensile Test**

| Material | Tensile Strength (N/mm$^2$) |
| --- | --- |
| Dissimilar joint | 153.33 |
| AA6101-T6 Aluminium | 284.4 |
| AA1100 Aluminium | 165.60 |

Source: Vinayak and Bhatwadekar (2015)

The results revealed that (i) AA1100 to AA6101-T6 aluminium alloys can be friction stir welded (ii) tunnel like defects are present in joint surface (iii) tensile strength of dissimilar joint is less than that of stronger base metal (AA6101-T6) but very nearer to weaker material (AA1100), this shows that tensile properties of aluminium alloys are retained after welding. Vinayak and Bhatwadekar (2015) concluded that extensive experimentation is required to study the effect of parameters on properties of dissimilar aluminium AA1100 to AA6101-T6 friction stir welded specimen.

Anil-kumar *et al*, (2007) examined the mechanical properties of dissimilar friction stir welding of the AA2024 T351 and AA 7075-T6 alloys. The objective was to assess the joint strength of the welds for the given set of process parameters. The welding was done under different feeds of 1000, 1100 and 1200 rpm. Two tool profiles (threaded cylindrical and triangle), 100 mm/min welding speed, tool rotational speed of 1200 rpm provided high joint strength. The micro-macro structural and mechanical properties were investigated using rotational speed of 1000 to 1200 rpm and welding speed of 80-100 mm/min as process parameters.

The micro and macro structural analysis revealed that at 1200 rpm, 100 mm/min and using triangular profile tool, there was proper mixing of the two alloys at the interface

resulting in good mechanical properties. The macro images showed no cavity and no shoulder fragmentation, but rather proper mixing of the alloys without defects. Micro-effective stirring by pin and heat generation resulted in good fusion at the interface of nugget zone and the parent metal. It was also revealed that finer grains were present at the nugget zone resulting from fragmentation and heat, tensile strength increases with increase in rotational speed. The result of the hardness test showed that hardness was enhanced in the weld region due to reduction in both grain size and residual work hardening as a result of severe deformation and increased frictional heat. This region contains low density of big grains and high density of fine grains. There is high hardness due to small grains. It was concluded that joints fabricated at the speed of 1200 rpm, feed rate of 100 mm/min showed the proper mixing of the two alloys and high tensile strength (Anil-kumar *et al*, 2007)

Ashish *et al.* (2017) examined the friction stir welding of aluminium alloys AA2014 welded to AA 5052. The process parameters were optimised using Taguchi method. Experiments were conducted to determine the effect of different controllable parameters on the hardness of the joint for the two alloys. The hardness of welding zone and base metal were determined. The result revealed that the maximum hardness was found at 1950 rpm tool rotational speed, 50 mm/min transverse speed, 2° tilt angle. The maximum and minimum hardness were, respectively, 79.9HB and 62.7HB found at 1200 rpm tool rotational speed, 40 mm/min transverse speeds, 0° tilt angle. It was observed that rotational speed has greater impact on hardness and tensile strength among all process parameters (ii) increase in transverse speed and tilt angle leads to increase in hardness but with increase in rotational speed firstly hardness increases then decreases (iii) increase in tilt angle – tensile strength increases but increase in rotational speed / transverse speed, tensile strength increases then decreases.

Dissimilar AA6061 and AA7075 alloy was friction stir welded with various process parameters by Guo *et al.* (2014). The effects of materials position and welding speed on the material flow, microstructure, microhardness distribution and tensile property of the joints were investigated. The machine has a capacity of generating 12 kN downward force. The dimensions of the workpiece were 300 mm x 50 mm x 6.3 mm and tool shoulder diameter was 15 mm. The process parameters are as shown in Table 2.2.

**Table 2.2: Friction Stir Welding Parameters**

| Condition | Material | Rotational speed(rpm) | Travel speed(mm/s) | Downward force(kN) | Tool tilt ($^\circ$) |
|-----------|----------|-----------------------|--------------------|--------------------|----------------------|
| D1 | 7075-6061 | 1200 | 2 | 6.6 | 2.5 |
| D2 | 7075-6061 | 1200 | 3 | 6.1 | 2.5 |
| D3 | 7075-6061 | 1200 | 5 | 7.0 | 2.5 |
| D4 | 6061-7075 | 1200 | 3 | 6.0 | 2.5 |
| D5 | 6061-7075 | 1200 | 5 | 6.7 | 2.5 |

*The materials on the left were located on advancing side during friction stir welding.

Source: (Guo *et al*, 2014)

It was observed that proper mixing is achieved when AA6061 alloy is placed on the advancing side and formation of multiple vortexes at the nugget zones. Three distinct zones with different extents of materials intercalations were identified. Refined grains were observed in these layers with 7075 having smaller grains. All the welded joints fractured at the heat affected zone on the AA6061 Al side during tensile testing, which corresponds to the minimum values in microhardness profiles. It was found that the tensile strength of the dissimilar joints increases with decreasing heat input. The highest joint strength was obtained when welding at highest welding speed and AA6061 on the advancing side (Guo *et al.,* 2014).

It was concluded that all the joints failed at positions in heat affected zone on the AA6061 side which is the softer material and exhibited very good tensile strengths and ductility. The highest ultimate tensile strength achieved in condition D5 reached 245 MPa which is 32 % higher than required in the American Welding Society standard for friction stir welding (Guo *et al.,* 2014).

Jitender and Hari (2016) evaluated the effect of friction stir welding process parameters on mechanical properties of aluminium alloys. In their study, two dissimilar alloys, AA5083 and AA5086 were friction stir welded. Different experiments to determine tensile strength, percentage elongation and joint efficiency were conducted while varying welding parameters such as welding speed, different pin profiles, and tool tilt angle at five levels each. One factor at a time principle was used as rotational speed was varied as 355, 710, 1000, 1400 and 2000 rpm with welding speed and tilt angle respectively fixed at 20 mm/min and 3° and level 2 both rotational and welding speeds were fixed with tilt angle varied between 0- 8° at 2° interval while for stage 3, welding speed was varied as 16, 20, 40, 50, 63 mm/min while keeping rotational speed and tilt angle fixed at 1000 and 3° respectively. At stage 4, welding and rotational speeds were respectively fixed at 20 mm/min and 1000 rpm, tilt angle of 3° and threaded, cylindrical, square, rectangular and tapered tools were used while dwell time was kept at 8 s and plunge depth was 0.12 mm. Tensile strength and percentage of elongation were tested and compared with the base metals to determine the joint efficiency. For level 1 of step 1 at 355 rpm, tensile strength was 195.5 MPa and increased to 213.3 MPa at level 2 of the same parameter. Tensile strength increased up to level 3 and started decreasing with increasing rotational speed. Frictional heat increased to a maximum load while tensile strength was 274.4 MPa at 1000 rpm. Tilt angle has inverse effect as tensile strength was 210.2 MPa at 0°, increasing tilt angle from 0 to 2° lead to reduction in tensile strength from 203.3 to 152.2 MPa. Feed

rate was varied between 16 to 63 mm/min at 5 levels; tensile strength reduced as feed rate increased from level 1 to 3 and then started to drop. It was observed that tool rotational speed, tilt angle and tool geometry made significant impact on welded joints. Tool rotational speed increases the tensile strength to an extent. Also, tool pin profile affects the stirring or plastic flow of material under tool shoulder. It was shown through visual and optical analysis that surface finish and weld quality of joints depends on tool tilt angle. It was concluded that rotational speed of the tool is strongly related to welding speed to achieve higher strength value. At very low feed rate higher heat is generated at nugget zone. Joint strength is also good at higher tensile strength at the optimum range of 1000 rpm, $2^\circ$ tool tilt angle and minimum value of welding speed.

Rajkumar *et al.* (2017) examined the friction stir welding of aluminium alloys, AA 2024-T4 (Al-Cu alloy), AA 5052 and AA 6061-T4 (Al-Mg-Si alloy) plates of dimensions 100 x 50 x 5 mm which were friction stir welded using a specially designed tool with D/d ratio (shoulder/pin) of 3, where shoulder diameter is 18 mm and pin diameter being 6 mm. AISI H13 steel tool was used. Tensile test was done in accordance with ASTM E8/E8M standards of sub size specimen at a strain rate of 0.5 mm/min. Microhardness test was carried out at a load of 100 g force with dwell time of 10 s and distance of 0.25 mm interval across the weldment. In order to analyze the constituents in thermo-mechanically affected zone (TMAZ) and weld nugget, scanning electron microscopy (SEM) with energy-dispersive spectroscopy (EDS) was used.

It was observed that sound welds were obtained with new stepped pin tool, at 710 rpm and 28 mm/min. Morphological studies shows reduction in grain size of weld nugget compared to parent metals. Maximum tensile strength of 297 MPa was achieved on samples welded using stepped pin tool which is higher compared to other pin profiles. They deduced that for cylindrical pin, D/d ratio of 3, rotational speed of 710 rpm, traverse

speed of 28 mm/min, were the best optimal parameters and gave better mechanical properties. Also, that squared pin and cylindrical threaded tool profiles gave better performance than the other tools. Cylindrical threaded pin gave excellent bonding between both alloys (AA 5052 and AA 6061) by effective friction stir joining. Both the samples exhibited nearly equal ultimate strength. In terms of ductility, Sample B (with 710 rpm and 28 mm/min feed rate) outperformed Sample A (with 710 rpm).

Chetan *et al.* (2016) reported an X-ray radiography testing conducted on similar friction stir welds between AA7075-T651 aluminium alloy and dissimilar friction stir weld between aluminium alloys AA7075-T651 and AA6061-T6. For the dissimilar alloys, the tool rotational and welding speed was varied from 800 to 1000 rpm at 100 rpm intervals, while the transverse speed was varied from 30 to 40 mm/min at 5 mm/min intervals. The visual inspection and the X-ray radiographic testing were employed to ascertain the joint integrity/quality before characterization. In visual defects, the lateral flash were seen in most of the welds, but the X-ray radiography technique revealed the presence of lack of penetration flaws in all weld samples and cracks, voids, wormhole defects in some of the welds. It was observed that weld defects occurrence increases with increase in transverse speed. An optimum rotational speed for producing defect-free welds of aluminium AA7075-T651 was found to be 900 rpm. They stated that in dissimilar welding joints, the base metal 6061 positioned on advancing side gives good material mixing, an optimum rotational speed for producing defect-free welds was found to be 650 rpm. It was observed that the occurrence of defects in dissimilar friction stir welding joints is fewer with respect to similar friction stir welding joints. It was concluded that X-ray radiographic testing technique successfully detected the defects present in the welds and can be said to be appropriate in this regard.

Elathrasan and Senthil-Kumar (2012) conducted an experiment on modeling and optimization of friction stir welding parameters for dissimilar aluminium alloys using response surface methodology. In their work, aluminium alloy AA 6061-T6 and AA7075-T6 were friction stir welded using single pass- butt welds which were produced in 6-mm thickness to fabricate dissimilar friction stir welded joints of 100 mm length. The experiments were conducted using parameters of design matrix. Tensile test specimens were produced using the ASTM-E8 Standard for the test.

It was observed that ultimate tensile strength of all the joints were lower than those of the base metal, lower rotational speed, higher welding speeds, and lower axial force produced inadequate heat due to lower friction which results in poor plastic flow and defects formation in the welded zones. It was also observed that ultimate tensile strength of friction stir welded joints increases with increase in tool rotational speed, ultimate tensile strength decreases with increase in axial force, the yield strength of friction stir welded joints decreases with increase in axial load and tool feed rate, while displacement of the joints decreases with increase in tool rotational and welding speeds (Elathrasan & Senthil-Kumar, 2012).

Vivekanandan *et al.* (2012) examined the analysis of friction stir welding on aluminium composites. The focus of the research was to study the influence of friction stir welding on the microstructure and hardness of aluminium 6035 and 8011. The parameters used were: rotational speed of 550 rpm and welding speed of 40-90 mm/min. From their result, 50 N/mm² was obtained as maximum tensile strength at 60 mm/min welding speed. The hardness test gave the maximum hardness as 91 HV at weld centre. The microstructure test results showed that the high tensile strength and hardness was obtained in the friction stir welded zone of aluminium 8011.

It was concluded that changing the feed rate of a friction stir welding of the butt joints between aluminium AA6035 and AA8011 had influence on the microstructure and hardness of aluminium 6035 and 8011 and that the weld zone was divided into three regions (centre of weld, AA6035, AA8011) based on the microstructure. The centre of weld had fine grains due to dynamic recrystallization with higher tensile strength and hardness.

Patil and Soman (2013) studied the effect of processing parameters on the mechanical and metallurgical properties of dissimilar joints of AA6082–AA6061. Friction stir welding samples were produced by varying the welding speeds of the tool as 50 and 62 mm/min and by varying the alloy positioned on the advancing side of the tool with a constant rotational speed of 1600 rpm. Weldments were produced perpendicularly to the rolling direction of the alloys. Microhardness (HV) and tensile tests were performed; microstructural evaluation was conducted on fractured surface. The corrosion tests for both base and welded joints were carried out in 3.5% NaCl solution at a room temperature. Corrosion current and potential were determined using potentiostatic polarization measurements. It was found that the corrosion rates of welded joints were higher than those of base alloy. The result of tensile test is shown in Table 2.3.

**Table 2.3: Result of Tensile Test**

| Material | YS ($N/mm^2$) | UTS ($N/mm^2$) | % Elongation | Joint efficiency (%) |
|---|---|---|---|---|
| 6082T6-6061T6 | 167 | 183 | 5.14 | 50.13-49.03 |
| 6082T6-6061T6 | 101 | 170 | 4 | 46.57-45.57 |
| 6061T6-6082T6 | 91 | 173 | 4.29 | 47.39-46.38 |
| 6061T6-6082T6 | 95 | 154 | 4.43 | 42.19-41.28 |
| AA6082-T6 | 117 | 365 | 14 | - |
| AA6061-T6 | 99.84 | 373.12 | 16.56 | - |

Source: Patil and Soman (2013)

The downward force was observed to be constant as the welding speed for all the joints increases. The tensile strength of the welded joint was lower than that of the parent metal. With the 6082 alloy positioned on the advancing side of the tool, the dissimilar joints exhibited good mechanical properties with respect to AA6061. Microstructural changes induced by the friction stir welding process were clearly identified in the study. Friction stir welding of dissimilar alloys AA6082T6- 6060T6 resulted in a dynamically recrystalized zone, TMAZ and HAZ. A softened region has clearly occurred in the friction stir welded joints, due to dissolution of strengthening precipitates. With AA6082 on the advancing side; the corrosion rate is higher with respect to increasing welding speed of the tool while corrosion rate decreased in case of AA6061 on advancing side. Best strength and ductility condition was obtained with AA 6062 on advancing side at welding speed of 50 mm/min at a value of 183 MPa. The best microhardness value was obtained in AA6061- AA6082 at welding seed of 50 mm/min while the lowest was when AA6061 was on advancing side at welding speed of 62 mm/min.

In a study, the friction stir welding technique was used in joining similar and dissimilar 5 mm aluminium alloy plates by Selamat *et al.* (2016). The butt-joint type of similar joints (AA5083-AA5083) and dissimilar joints (AA5083- AA6061) were welded under the same welding parameters; 1000 rpm (rotational speed) and 100 mm/min (transverse speed). The dimensions of the workpiece were 150 mm x 100 mm x 5 mm. Macro- and microstructural observations were acquired at the cross-section of the weld regions by stereo and optical microscopes. Onion ring structure was seen in the nugget zone of similar joints, while wavy and distorted patterns were present in dissimilar joints. All tensile specimens of similar welded joints fractured at the thermo-mechanically affected zone. However, tensile specimens of dissimilar welding joint failed at both the thermo-mechanically affected zone and AA6061 base material at the retreating side. The tensile

strength of similar joint and dissimilar joint were 22 % and 19 % lower compared to the base metal of Al 5083 and Al 6061.

Navaneethakrishna and Ganesh (2015) studied the effect of welding parameters on friction stir welding of dissimilar aluminium alloys 7075 and 8082. The study was focused on investigating the effect of different tool pin profiles on friction stir welding of dissimilar AA 6082 –T6 and AA 7075 – T6. Tool rotational speed, welding speed, tool pin profiles and number of passes were used as process parametres. The dimension of the workpiece was 100 mm x 70 mm x 6.35 mm. Microstructure examination, micro hardness, and tensile tests were performed as well as multi pass friction stir welding. The result revealed that the tensile strength for single pass is relatively higher than multi-pass friction stir welding, the process parameters which had the greater influence on the tensile strength of dissimilar friction stir welded joints were identified as rotational speed, welding speed and tool pin profile. The hardness profile reduces while increasing the number of passes and grain refinement was observed much in single pass friction stir welding than in the multi-pass friction stir welding. Other conclusions made are as follows:

1. The tensile properties were found to be decreasing in multi-pass friction stir welding when compared to single pass.

2. The hardness value was found to be decreasing in square pin in single pass friction stir welding. The hardness profile was found to decrease in multi-pass friction stir welding when compared to single pass at heat affected zone.

3. For cylindrical threaded tool pin and triangular pin profiles the microstructure consists of good flow of alloy and fragmented particles

Aby *et al.* (2016) conducted an experiment on the optimisation of process parameters of friction stir welding of dissimilar aluminium alloy. Three process parameters namely

rotational speed, welding speed and plunge depth were considered. Friction stir butt welding was carried out between dissimilar aluminium alloy plates (AA6063 and AA5052) with dimensions 200 mm x 75 mm x 6 mm. The analysis presented the effect of spindle speed, welding speed and plunge depth on weld quality. Tensile and yield strengths of friction stir welded dissimilar aluminium alloy were evaluated under different conditions using Taguchi experimental design. It was observed that plunge depth was the most dominant parameter which affects tensile strength. The other parameters which influence the tensile strength in order of ranking are spindle speed, welding speed. Optimum conditions for high tensile strength were found to be Spindle speed of 1400 rpm, welding speed of 100 mm/min, and plunge depth of 0.15mm.

Agus *et al.* (2017) examined the mechanical behavior of aluminium alloy tailor welded blank developed by using friction stir welding process. The objective was to investigate the mechanical properties and microstructure of tailor welded blank made from AA6061-T6 and AA1100. Mechanical properties of the two alloys differ; microhardness test was conducted to determine the hardness distribution across the weld nugget. The mixing of the two materials was influenced by tool rotational speed. Microstructure analysis was performed to investigate the grain size and shape. It was observed that the grain size of AA6061-T6 increased in the heat affected zone while that of AA1100 decreased. In the weld nugget, they found hook defects in the joining. Monotonic tensile loading revealed weld line directions with expansion in tool rotation. The joints failure was on the area of AA1100 series. Also, two specimens were investigated, one through the dissimilar aluminium and the other through similar material. Inspection of the weld nugget's hardness revealed that there was no homogenous material mixing during the stirring process as confirmed by microhardness measurement.

The tensile test gave the highest value of 78.07 MPa obtained by joining AA1100 to AA6061- T6 with the welding direction of $0°$ while at $45°$, 75.26 MPa was obtained Whereas, the strain value was 10.99% and 13.8% for the weld direction of $0°$ and $45°$, respectively. Therefore, in this research, the highest tensile strength was given by specimen of AA1100 x AA6061- T6. The highest value of hardness test was 55.1 HVN and the lowest was 31.9 HVN. This could be caused by many factors such as homogeneity and the defects or voids. In the investigation of micro structure, it can be said that there was grain size transformation during the welding process. In the heat affected zone of AA1100 material, it was smaller grain size compared to the base metal. Larger grain sizes were seen in the material of AA6061-T6. While in the weld nugget, it was grain refinement in both materials due to the influence of temperature and stirring action of the tool.

**2.3.6.2 Friction stir welding of dissimilar aluminium alloys to other metals**

Li *et al.* (2012), in a study on the microstructure and mechanical properties of dissimilar friction stir welded pure copper and 1350 aluminium alloy butt joints reported that complicated microstructure was formed in the nugget, they found that vortex-like and lamellar structure of aluminium and copper were formed at the nugget zone of the welds. They also concluded that the fracture surface shows that the joints failed with a ductile-brittle mixed fracture mode.

Wei *et al.* (2012) successfully joined dissimilar aluminium and titanium using the friction stir lap welding with cutting pin. Welding was done at welding speeds of 150 235 300 375 and 475 mm/min. The dimensions of the workpieces were 100 mm x 100 mm x 3 mm. Tensile test and mirostrutural analysis were performed. It was observed that failure load ranged from 1086 to 1910 N. Failure load increases with welding speed and reaches a maximum at 300 mm/min and then begins to decrease. This value is close to the ultimate

tensile strength of the base metal which is 1853 MPa, it can also be said that optimal value of UTS is equal to that of base metal and that at low rotational speed; fracture was at Al-Ti joint interface. Many titanium scrapings were seen in aluminum near the interface. A swirl-like structure with lighter and darker parts was observed in the SEM micrograph of the interface region.

Akinlabi (2012) examined the effect of shoulder size on weld properties of dissimilar friction stir welding between the two metals AA5754 and C11000 in butt configuration. The dimensions of the workpieces were 600 mm x 120 mm x 3.175 mm. The process parameters used were tool rotational speed of 600, 950, 1200 rpm, welding speed of 50, 150, 300 rpm with constant tilt angle and dwell time of $2°$ and 2 seconds respectively. Microstructural investigation, microhardness and tensile test were performed as well as XRD and electrical resistivity. It was observed that the weldment produced at 950 rpm, 50 mm/min and with tool of 18 mm shoulder diametre gave the highest value of joint efficiency; more ductile behaviour making them the optimal process parameters and that 18 mm shoulder diametre tool is more suitable for achieving good weld between aluminium and copper. The joint efficiencies of the weld group ranges from 73 to 86 %. Also the weldments have low percentage increase in electrical resistivities making it suitable for joints between Al and Cu.

The formation and distribution of brittle structures in friction stir welds of aluminium and copper and the influence of the shoulder geometry was reported by Galvao *et al*., (2012), it was reported that the shoulder geometries employed influenced the formation of intermetallics in the joints and the material flow mechanism during the welding process.

Sheikh and Dabade (2015) conducted an experiment on dissimilar friction stir welding between Al 6061-T6 and electrolytic tough pitch copper ETPC1000, they investigated the

effect of friction stir welding process parameters such as welding speed of 30, 40, 60 mm/min, tool rotational speed of 510 and 675 rpm and axial load of 1000, 1500 and 2000 N on tensile strength of friction lap joints. ensile test was conducted on the weldment and the result evaluated, ANOVA was used to determine the most significant factor affecting the tensile strength, It was observed that rotational speed of 675 rpm, welding speed of 40 mm/min and axial force of 1500N produced superior tensile strength of 224.62 N/mm² but the combination of welding speed 30 mm/min, rotational speed of 510 rpm and axial force 1000 N produced lesser tensile strength. The ultimate tensile strength of FSW lap weld reaches to 72.25 % of the base metal ultimate tensile strength. Also from the ANOVA, it was observed that rotational and welding speed has the most significant effect on the tensile strength.

### a.    Aluminium alloy steel

The effect of tool rotational speed, tilt angle on the mechanical properties, metallographic characteristics of the joints was investigated by Ramachandran *et al.* (2015). AA 5052 and HSLA steel IRS M -42-97 were joined by friction stir welding in a butt configuration. The process parameters used includes tool rotational speed which was varied between 400 to 600 rpm at 50 rpm intervals, tilt angle of  0.5° - 2.5° at 0.5° interval.   The microstructural investigation at joint interface using optical microscopy, scanning electron microscopy (SEM) and EDS analysis were performed.

The EDS suggests that intermetalic layer was formed at the joint interface. Their findings revealed that the ranges of tool rotational speed within which good tensile strength can be achieved is narrow, highest joint strength of 196 MPa which is 94 % of the ultimate tensile strength of base aluminium alloy was obtained at a tool rotational speed of 450 rpm, welding speed of 45 mm/min, axial load of 7 kN and tool tilt angle of  1.5°. It was observed that hardness at the joint interface was higher than that at rest of the joints, at

600 rpm, microhardness at steel side closer to the interface was higher in value compared to that of the base metal steel and may be attributed to higher temperature generated at that speed. Also, microhardness at stir zone of aluminium was higher in value than that of the aluminium base metal and may be due to presence of steel flakes but dropped at both 400 and 450 rpm in the stir zone of aluminium side away from the interface.

Sandeep and Sandeen (2016) stated that for joining of aluminium alloy to steel, the friction stir welding tool cannot be plunged symmetrically to the joint line because of excessive heating of steel which will cause melting of aluminium alloy resulting in defective welds necessitating the use of offset method. In the offset method, the centre of the tool is plunged towards the low melting temperature material. The process parameters used were rotational speed, welding speed, tilt angle and tool type. The experiments were performed in two phases. In the first phase (that is PHASE-1), the effect of six different reinforcement strategies was studied while in the second phase (i.e. PHASE-2), the effect of varying tool offset distance was investigated. To accomplish the first phase, direct pasting strategy was used. Then second (S2), third (S3) and fourth (S4) samples were based on groove technique, the fifth (S5) and sixth (S6) samples were based on hole technique. The process parameters were kept constant (at optimized level based upon trial experiments) during entire experimentation to observe the exclusive effect of reinforcement strategies. Levels of constant process parameters were kept at 1120 rpm tool rotational speed, 40 mm/min tool traverse speed, 2.5˚ tool tilt angle and 0.25 mm tool plunge depth.

The measured parameters includes ultimate tensile strength, micro- hardness and percentage elongation, they also stated that heat and material flow are important process phenomena. Material on advancing side mixed more vigorously than those of the retreating side.

### b. Aluminium Alloys and Copper Alloys

Yaduwanshi *et al.* (2016) conducted an experiment on the effect of tool offset in hybrid dissimilar friction stir welding of copper and aluminium Alloys. They underscored the importance of tool offset in dissimilar joining of metals. An investigation on tool offset towards thermal history, material flow pattern, mechanical properties, welding force and weld joint morphology was also carried out. The materials used were pure copper and aluminium alloy (1100) with dimensions of 200 mm x 100 mm x 6 mm, a total of 8 welds were produced using tool offsets of 0.0- 2.75 mm at an interval of 0.5 mm. Aluminium alloy was placed on retreating side and the plasma arc was placed with an offset of approximately 5 mm towards the copper side. The offsetting aids in temperature gain up to 420 to 470 K in copper side. With reference to tool axis, the welding torch was placed 23 mm ahead with angle of $60°$. The plasma current is optimized at 55A with the present geometric constraint and limitation of the system. In addition, the authors stated that from literature, good quality weld joint was obtained at tool rotational speed of 815 rpm and tool transverse speed of 98 mm/min.

Suriya *et al.* (2015) performed an experiment on friction stir welding of AA5052 and C1100 copper lap joint. The aim was to apply friction stir spot welding for producing lap joints between AA5052 aluminium and C1100 copper alloy. The welding parameters used were rotational speed of 2500 to 4000 rpm, pin insertion rate of 2 to 8 mm/min and holding time of 6 seconds. The mechanical tests and the microstructure investigation were performed to evaluate the joint quality. The results obtained revealed that the two alloys are weldable by friction spot welding. Increase in rotational speed and holding time leads to decrease in tensile shear strength of the lap joint. The optimum process parameters that gave the highest value of tensile strength of 864 MPa are rotational speed of 3500 rpm, pin insertion rate of 6 mm/min and holding time of 4s.

Akinlabi and Akinlabi (2012) conducted an experiment on the effect of heat input on properties of dissimilar friction stir welds of aluminium and copper of grades AA5754 and C11000, respectively with material thickness of 3.175 mm and copper on advancing side. The welding was done using three shoulder diameter tools of 15, 18 and 25 mm while varying the rotational and welding speeds as 600, 950 and 1200 rpm and 50, 150 and 300 mm/min, respectively with each set of parameters representing low, medium and high in order to vary the heat input to the welds. The parameters were combined as 15 mm shoulder diametre, 600 rpm rotational speed and 50 mm/min welding (travel) speed for the first set. For the second and third set it was 18 mm shoulder diametre, 950 rpm rotational speed and 150 mm/min welding speed and 25 mm shoulder diametre, 1200 rpm rotational speed and 300 mm/min welding speed respectively. The microstructures, the grain size and micro-hardness of the weldments were investigated as well as the electrical resistivity. The microstructural characterization revealed good metallurgical bonding at the joints. There was grain rerystalisation at the interfacial regions leading to reduction in grain size as compared to parent metals. They obtained higher microhardness values at the joint interface which resulted from strain hardening and presence of intermetallics. They stated that increase in heat input leads to increase in electrical resistivity.

Microstructural evaluation of joint interface revealed that good mixing was achieved as a result of sufficient heat input. 92 % reduction in the grain sizes at the stir zone was observed compared to the parent materials. Higher Vickers microhardness values were also measured at the joint interfaces resulting from the heat input into the welds. The electrical resistivity of the joints produced within the range of process parameter increased as the heat input to the welds increases. The maximum percentage increase in the resistivity compared to the average joint resistivity of the parent material was found to be 9.8% (Akinlabi & Akinlabi, 2012).

Akinlabi *et al.* (2012) reported the effect of transverse speed on joint properties of dissimilar metal friction stir welds between aluminium and copper sheets. AA5754 and C11000 were welded in butt arrangement at a constant rotational speed of 950 rpm with the traverse speed varied between 50 and 300 mm/min while other parameters were constant. The average ultimate tensile strength of the welds decreased with increase in welding speed. Higher microhardness values were obtained at the thermo-mechanically affected and stir zones of the welds due to dynamic recrystallization and presence of intermetallic compounds formed in the joint regions. They concluded that Microstructural evaluation revealed that at a constant rotational speed, improved metallurgical bonding and mixing were achieved at the lowest traverse speed due to low downward vertical force and high heat input.

Akinlabi and Akinlabi (2014) conducted an experiment on friction stir welding of aluminium alloy in which butt welds of both aluminium and copper alloys were produced by Friction Stir Welding. They varied the feed rate while keeping other parameters constant. The AA5754 and C1100 were used as base metals; the final weldment was comprised of welds produced by a constant rotational speed of 600 rpm and the feed rate varied between 50, 150 and 300 mm/min representing low, medium and high. The microstructure and fracture surfaces of the joint interface were investigated. The results revealed that the joint interface was characterized by mixed layers of both materials joined. The strongest weld was produced at the highest feed rate of 300 mm/min. Intermetallic compounds were present at the thin layer of the fractured surface and the weldment can be considered fit for practical applications.

Ewuola *et al.* (2016) studied the effects of plunge depth on the weld integrities of friction stir lap welds of aluminium and copper. Friction stir welding process was used to join 3 mm sheets of aluminium to copper. The tool rotational speed was 900 rpm while

transverse speed was varied from 50 to 250 at 100 mm/min interval and plunge depth for the first 3 samples were 4.5 mm each and 4.8 mm each from samples 4-6. The aim was to study the relationship between defects and process parameters. Visual inspection, microstructural evaluation and microhardness profiling was done on the samples. They found out that while all the typical friction stir welding microstructural zones were present in the welds, the void sizes observed in them were dependent on the plunge depth used. They concluded that microstructural analysis revealed grain refinement at the heat affected zones, thermo mechanically affected zone and weld zone of the copper while the aluminium grains showed little signs of grain refinements. However, the equiaxed grain structure was maintained for the copper grains in all the microstructural zones. Microhardness profiling suggested the absence of the formation of significant amounts of intermetallic compounds. The recommended that the range of the process parameters and the plunge depths considered in their research study need to be optimised to produce lap welds with sound integrity.

**c.      Aluminium and magnesium alloys**

Jagesver *et al.* (2017) studied the effect of friction stir welding process parameters on Mg-Az31B/Al- AA6061 joints. The two dissimilar alloys were friction stir welded in butt arrangement, the dimensions were 125 mm x 100 mm x 3.6 mm. The rotational speed was varied as 560, 710, 860 and 1000 rpm while the transverse speed was 16 and 25 mm/min respectively, metallographic studies was carried out by optical scanning electron microscope and the Energy dispersive spectrometry.

During the friction stir welding, Mg-AZ31B and Al-AA6061 plates were placed on the advancing and retreating side respectively, with an offset of 0.2 mm towards Mg. The result of their findings revealed that speed parameters affects the microstructural growth mechanism which further affects the mechanical properties and corrosion behavior (ii)

both rotational and welding speeds recrystallised and plasticized the material and produced an alternative lamellar shear band of aluminium and magnesium in the stir zone. (iii) peak temperature and high rotational speed formed an oxide on the top region and caused liquation and intermetallic formation (iv) tensile and hardness were increased as per the hall-petch (fine grain) effect (v) higher impact energy was formed at moderate rotational speed and low transverse speed due to presence of more soft aluminium patches (vi) tensile fractographs revealed a river like pattern which indicated the brittle nature of the joints (vii) high rotational and transverse speeds showed higher tensile strength , while better corrosion resistance was observed in high rotational speed and transverse speed. They concluded that higher rotational and welding speeds results in intense plastic deformation and dynamic recrystallization between Al and Mg alloys and promoted the fine equiaxed grains in the stir zone along with some Mg-reach intermetallics leading to increase in strength and hardness. Coarse grains improved the toughness formed by high rotational speed and low welding speed.

Paradiso *et al.* (2017) studied the process of dissimilar joining of magnesium and aluminium alloys by friction stir welding. The ZE41A Mg alloy and AA2024-T3 Al alloys both of 4mm plate thickness were welded in the butt joint configuration with a tool offset of 1 mm towards the magnesium side using a machining center (MCX 600 ECO). A scheme of the experimental welding configuration and parameters are shown in Plate I and Table 2.4. The process parameters used were tool rotational speed ranging from 1000 to 1400 rpm, feed rates of 20 to 80 mm/min, tilt angle of $2^{°}$, plunge of depth 0.48 mm. The parameters were chosen based on available literature and also in consideration of the works of Carlone *et al.* (2015) and Carlone *et al.* (2016).
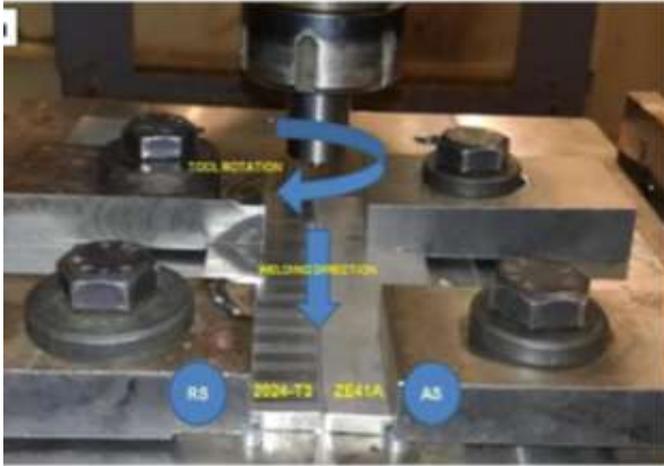
**Plate I: Experimental welding configuration**
**Source: (Paradiso *et al.* 2017)**

**Table 2.4: Welding process parameters**

| Test No | Rotating speed (mm/min) | Feed Rate (mm/min) |
|---------|-------------------------|--------------------|
| 1       | 1000                    | 20                 |
| 2       | 1000                    | 50                 |
| 3       | 1000                    | 80                 |
| 4       | 1200                    | 20                 |
| 5       | 1200                    | 50                 |
| 6       | 1200                    | 80                 |
| 7       | 1400                    | 20                 |
| 8       | 1400                    | 50                 |
| 9       | 1400                    | 80                 |

Source: (Paradiso *et al.* 2017)

Sound joints were obtained with 1200 rpm of tool rotational speed and 20 mm/min of welding speed. Microstructure and microhardness of the sound joints were examined. Microstructural observations revealed that a complex vortex flow occurred in the stirred zone. Mixing of both alloys occurred at the stir zone but the fraction of Al 2024-T3 alloy appeared to be more compared to ZE41A alloy. Also, very fine dispersed interetallic compounds in aluminium highly rich matrix were observed in the stir zone. Presence of intermetallic compounds and fine grain structure affects the hardness distribution at the stir zone. The investigation shows great prospects for improved joining of the two alloy

pairs. The feasibility of the process was assessed by means of microstructure and mechanical analysis. The formation of brittle intermetallic compounds was investigated as well. This preliminary investigation showed the feasibility of joining the aluminium alloy 2024-T3 to ZE41A magnesium alloy offsetting the tool towards the Magnesium side and fixing the Aluminium in the retreating side. Several difficulties were encountered during welding process due to the different behavior of the alloy with regards to mode of plastic deformation and thermal conductivity. Hot cracks and poor joints were obtained in some processing conditions (Paradiso et al., 2017).

Heena et al. (2016) performed an experimental analysis on friction stir welding of dissimilar alloys AA6061 and Mg Az 31. The two dissimilar alloy plates of 6 mm thickness were welded in circular butt arrangement by friction stir welding. In the experimental work, welding was carried out at welding speed varying from 10 to 40 mm/min and tool rotational speed from 800 to 2000 rpm. Effects of process parameters on butt welded circular joint were investigated for weld strength. They found out that the two dissimilar metals can be friction stir welded by good selection of welding parameters and tool geometry. They stated that friction stir welding of aluminium and magnesium alloys with circular butt joint geometry has great potential for automobile applications by harnessing the properties from each material in a functional way (Heena et al, 2016).

It was concluded that:

1. With good parameter settings and appropriate tool geometry, Al 6061 and Mg AZ31 can be friction stir welded.

2. Circular welding paths are more difficult to weld than linear paths; tool design affects appearance and properties of welded joints.

4. Tool rotational speed of 1200 rpm and welding speed of 10 mm/min were found to be the most influential parameters, affecting mechanical properties of circular butt weld joint

between AA6061 and AZ31 when welded by using cylindrical threaded pin tool of HCHCr material.

**d.   Aluminium Alloy AA6111 and Thermoplastic**

Ratanathavorn and Melinder (2015) performed a dissimilar joining between aluminium alloy AA6111 and thermoplastic. Friction stir welding was used to produce shear overlap joints between aluminium and a thermoplastic (AA 6111 to polyphenylene sulphide). The process used the friction stir welding tool to create metallic chips which merge with the molten thermoplastic to form a joint. No special surface pretreatment was required before joining. Cross-sections show mechanical locking between the chipped polymers filled zone and the surrounding aluminium sheet. The effects of joining parameters such as rotational speed, translational speed and distance to backing were investigated in relation to the joint strength and failure mode. The joint strength is dominated by mechanical interlocking between the chip and polymer filled zone and aluminium sheets. They observed the following:

1. The weld zone contains a mixture of aluminium fragments and chips, surrounded by PPS  matrix generating a composite stir zone. The stir zone creates a trench in the aluminium sheet after the process.

2. Defects such as voids can be detected at the boundary interfaces between resolidified polymer and the aluminium

3. Mechanical interlocking of the stir zone trench to the aluminium sheet is the main factor contributing to tensile strength of the joints.

4. Fracture took place in two mechanisms, namely initial fracture along the boundary between the aluminium and the stir zone and fracture through polymer sheet

**e.       AA6061-T6 and ultrafine grained 1050**

Yufeng *et al.* (2016) examined the microstructure and mechanical properties of dissimilar friction stir welding between 2 mm thick ultrafined grained 1050 and 6061-T6 aluminium alloy plates which were joined in butt arrangement at different revolutionary pitch that varied from 0.5 to 1.25 mm/rev. The rotational speed was 800 rpm and welding speeds were varied from 400-600 mm/min at 200 mm/min intervals.

 In the stir zone, the initial nano-sized lamellar structure of the UFGed 1050 Al alloy plate transformed into an equiaxial grain structure with a larger average grain size due to the dynamic recrystallization and  grain growth. However, an equiaxial grain structure with a much smaller grain size was simultaneously formed in the 6061 Al alloy plates, together with coarsening of the precipitates. Tensile tests of the welds obtained at different welding speeds revealed that two kinds of fracture modes (ductile and brittle) occurred for the specimens depending on their revolutionary pitches. The maximum tensile strength was about 110 MPa and the fractures were all located in the stir zone close to the 1050 aluminium side. However, dissimilar welding was difficult between the two alloys they both have different deformation characteristics.

They concluded that in the stir zone, the two dissimilar Al alloys could still be distinguished. The nano-sized lamellar structure of the UFGed 1050 Al alloy could not be distinguished any more. Finally, dynamic recrystallization was seen at the 1050 Al side with larger grain size when compared to the 6061 Al alloy and that all the dissimilar joints fractured in the stir zone during the tensile tests. For the joints produced at 1.25 and 1 mm/rev, the fracture strength was low and showed the brittle fracture mode. In contrast, the joints produced at 0.75 and 0.5 mm/rev, both tensile strength and plastic elongations were higher.

**f.      AA3003-H24 and 2124/ SiC/25P-T4**

Aluminum alloy AA 3003-H24 and 2124/SiC/25p-T4 composite plates was successfully friction stir butt joined by Bozkurt and Duman (2011) by offsetting the high strength plate to retreating side of the tool under tool rotational speed of 900 to 1400 rpm and traversing speed of 40 to 125 mm/min, keeping other parameters constant. Ultimate tensile strength, percentage elongation and joint efficiency values of the welded joints and hardness variations across the weld interface were determined. The integrity of the joints was investigated using optical microscopy, scanning electron microscopy and energy dispersive spectroscopy. Results indicated that the high quality welded joints could be obtained when a tool rotational speed of 900 rpm and a traverse speed of 125 mm/min were employed. The maximum tensile strength value obtained was about 182 MPa, which corresponds to a joint efficiency of 104 % of that of the aluminum alloy base metal. It was concluded that AA 3003 H24 and 2124/SiC/25-T4 dissimilar alloys plates were successfully joined by FSW without any visible superficial porosity or macroscopic defects on the top and bottom regions of welded samples, except the one produced with a traverse speed of 40 mm/min.

In the SEM examination, no evidence of porosity and article cracking or tool wear was observed in the stir zones of the welds. All the microhardness profiles of the dissimilar Al/MMCs FSW joints exhibited a lower hardness in the stir zone. The hardness in the advancing side of AA3003- H24 Al side of the HAZ region is higher than TMAZ because of thermal softening and frictional heating apart (Bozkurt & Duman, 2011).

### 2.3.7 Applications of friction stir welding in industries

Industries have adopted the use of friction stir welding for structurally demanding applications; this is because the process is devoid of severe distortion. Currently, the process is being used for joining similar and dissimilar alloys in ship building, marine industries, aerospace, rail industries container and fuel tank industries. The replacement

of fastened joints with friction stir welded lap joints has been observed to lead to significant weight reduction and cost savings for many industries and the weight savings can be achieved as a result of the elimination of fasteners. The cost savings can be realized by a decrease in design, manufacturing, assembly and maintenance times, and improved corrosion performance by eliminating the fasteners as a source of dissimilar metal contact (Khaled, 2005). Also, the technology provides significant advantage to the aluminium industry: automotive suppliers are already using the technique for wheel rims and suspension arms. It is also applicable to the railway industries with the rapid development in high-speed rail cars. The friction stir welding process has been used in the manufacturing of high quality joints in the rail car body, window, side walls and coupling gears (Wang *et al*., 2009).

Friction stir welding finds its application in various industries ranging from electrical, aerospace, rail and automobile industries. Table 2.4 shows typical applications of friction stir welding and the advantages of friction stir welding over other others methods.

**Table 2.5: Typical applications of friction stir welding**

| Industry Categories | Specific Application | Present process | Advantages of using friction stir welding |
|---|---|---|---|
| Electrical | Heat sink- welded laminations | Gas metal arc welding | High density of fins, better conductivity |
| Electrical | Cabinets and enclosures | GMAW | Reduced cost, welds through corrosion coatings |
| Batteries | Leads | Solder | Light quality |
| Military | Shipping pallets | GMAW | Reduced cost |
| Extrusion | Customized extrusions | Not done today | Can be customized to reduce need for large presses |
| Boats and ship building | Keel, tanks and the hull | Rivets and GMAW | Stronger, less distortion |

| | | | |
|---|---|---|---|
| Golfcars, snowmobiles | Chassis, suspension | GMAW | Less distortion, better fatigue life properties |
| Tanks and cylinders | Fittings, long and circumferential seams | GMAW | Higher quality-less leaks, higher uptime |
| Aerospace | Floors, wings and fuselage | Rivets | Higher quality, cheap (no rivets and holes) |
| Automotive | Wheel rims and suspension arms | GMAW, MIG | Better joint integrity |
| Rail industry | Rail car body, window, side wall and coupling gears | GMAC | High quality joints |

Source: (Smith *et al*, 2012).

## 2.4 Joint Efficiency of Welded joints

Joint efficiency refers to the strength of a welded joint with respect to the strength of the base metal. A joint efficiency of 1.00 indicates that the weld has same strength as the base metal (Record *et al.,* 2004). Joint efficiency is expressed by a numerical value or equivalently a percentage referred to as joint efficiency factor. It is the ratio of the strength of a joint (riveted, welded or brazed) over the strength of the base material (Robert *et al.,* 2019).

Joint efficiency (ŋ) that is ratio of joint strength compared to strength of parent material usually expressed in percentage varies from 100 % for perfect weld down to 75 % for an acceptable weld (Akinlabi, 2010).

## 2.5 Modelling and Optimisation

A modeling technique is a mathematical equation based model developed based on input parameters relationship to get optimum conditions. While in optimization technique, an

objective function is formulated with or without mathematical model to get optimum condition (Sunil *et al,* 2018).

Modeling and optimization was classified by (Sunil *et al.,* 2018) as:
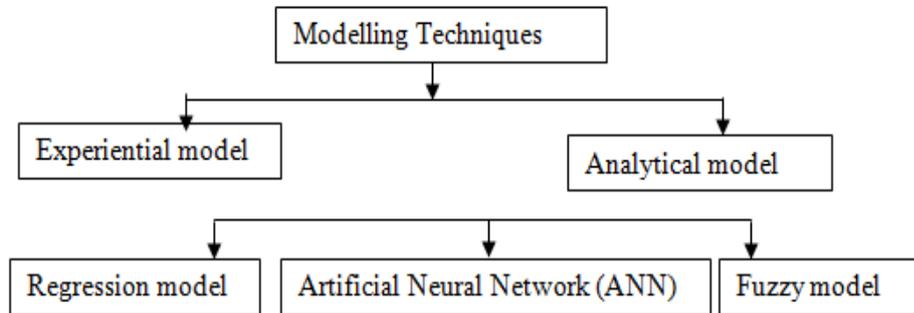


Figure 2.3: Modelling Techniques
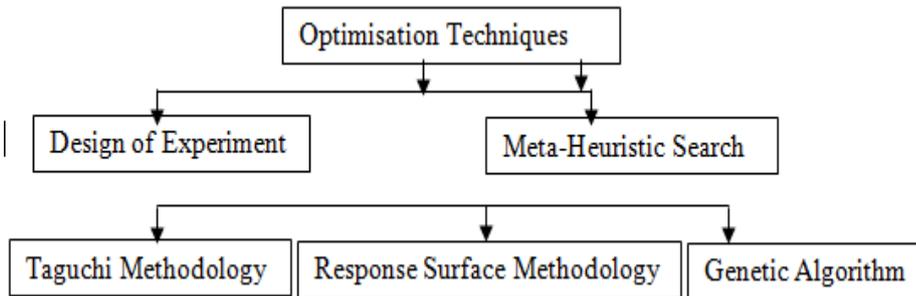


Figure 2.4: Optimisation Techniques

Regression based modeling is a modeling technique in which a functional relationship between independent variables and dependent variables are established. Regression method helps to know how dependent variables changes with the change of the independent variables. A regression based modeling technique was used with N-N method to optimize surface roughness and flank wear for turning of die steel material by (Ozel *et al*, 2005). A regression model for cutting forces as a function of speed, feed and depth of cut (doc) was developed by (Uthaya-Kumar *et al.,* 2012)

## 2.6    Existing Gap

The literature review highlighted welding in general and basic background of friction stir welding with key interest in dissimilar welding of alloys of aluminium and other metals.

The AA7075-T651 and AA1200-H19 aluminium alloys were chosen in this research work as AA7075 is a high strength alloy while AA1200 is a high purity alloy with high resistance to corrosion. They are both used for structural (wings and fuselage) and non structural (fuel tank and fuel supply lines) applications on the aircraft.

Dissimilar welding of the two alloy pairs has not been reported. The 1200 being a high purity alloy is also widely used as cladding (alclad7050) of aircraft body frame and with this research work this corrosion resistant property can be further harnessed in reducing corrosion at the crevices of the aircraft wing-fuel tank interface. Also, suitable joining parameters have to be determined so as to obtain optimum properties of friction stir weldment of the two alloys.

## CHAPTER THREE

## 3.0          MATERIALS AND METHODS

## 3.1    Materials

## 3.1.1   Welding materials

The materials used for welding are discussed below

## a.      Base materials

The base materials (a; milled sample, b; un-milled plates) used during the study are AA7075 and AA 1200 Aluminium alloys. These materials were obtained from Bharat Aerospace alloys, Gulalwadi- Mombai, India- 400:004. Plate II shows the aluminium alloy plates before and after milling.

(a) Milled pairs base materials       (b) Unmilled base materials
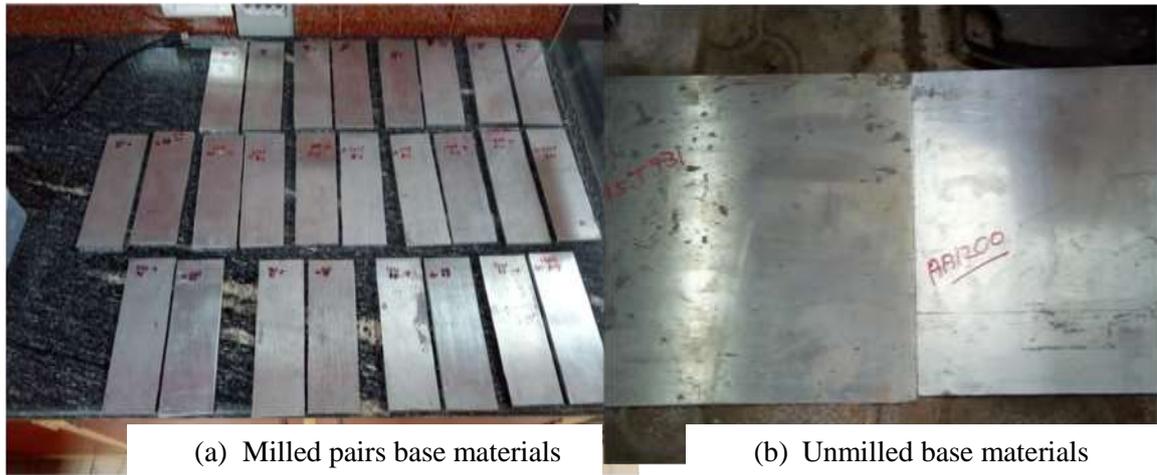
Plate II: Base materials

**b.      Other Materials**

The materials used for sample preparation are 320 grit silicon carbide paper and acetone obtained from Metallurgical and Materials Engineering Department of Indian Institute of Technology, Kharagpur, India.

**c.      Friction stir welding equipment**

The equipment used during the welding process are listed in Table 3.1 and presented in Plates III.

**Table 3.1: Welding Equipment**

| S/N | Equipment | Manufacturer | Model No | Country of Manufacture |
|-----|-----------|--------------|----------|------------------------|
| 1 | Stir Welding Equipment | ETA Technology PVT LTD | WS004 | Bangalore India |
| 2 | Backing Plate and Clamping System | ETA Technology PVT LTD | - | Bangalore India |

| 3 | Friction Stir Welding Tools | V3 Instruments | - | Kharagpur India |
| 4 | Digital Vernier Calipper | - | - | |
| 5 | Wired Electrical Discharge Machine | Reliable EDM | ED350/200SP | USA |
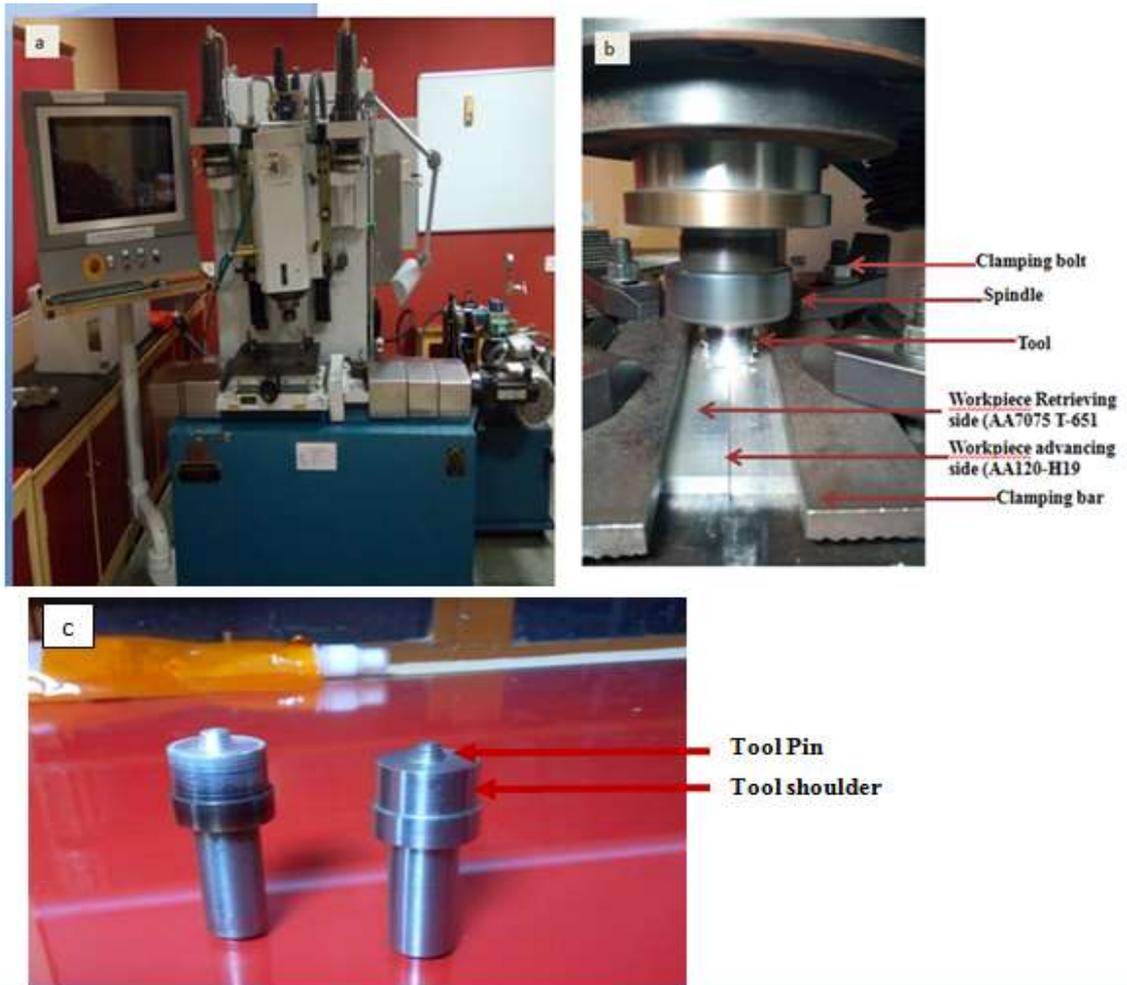


Plate III:  (a) Stir welding Equipment (b) Backing plate and clamping system (c)

Friction stir welding tools (Tapered and Tapered Threaded Tools)

### 3.1.2   Equipment for Chemical Analysis

Spectroscopy machine (model No 8113, serial No 45767-5450-TV5-5028) shown in Plate IV and situated at the Central Research Facility (CRF) of Indian Institute of Technology, Kharagpur, India was used to conduct chemical composition analysis.



**Plate IV: Spectroscopy Machine**

### 3.1.3   Testing Equipment

**a.      Hardness**

The hardness test was carried out using Vickers hardness tester (MHVD-10 IS) shown in plate V and situated at the Steel Technology Centre of Indian Institute of Technology Kharagpur India.



**Plate V: Hardness tester**

**b.**     **Tensile Testing Machine**

The tensile test was performed using Instron 8862 tensile machine shown in plate VI and situated at the Steel Technology Centre of Indian Institute of Technology Kharagpur India.



**Plate VI:**     **Instron 8862 tensile machine**

**c.**     **Impact Test**

The Charpy impact test was done using the Galdabini impact 450 testing machine (Model: V92Q) shown in plate VII. It is situated at the Pipe Factory of SCC laboratory Abuja

**Plate VII: Impact testing machine**

**d.     Corrosion Test**

The corrosion test was conducted using the Metrohm potentiostat / galvanostat (Autolab

PGSTAT 101) which was interfaced with NOVA software of version 2.1.2 situated at the

Faculty of Engineering and Built Environment University of Johannesburg South Africa.

It is shown in Plate VIII



**Plate VIII: Metrohm potentiostat/galvanostat**

**e.     Scanning Electron Microscopy**

The scanning electron microscopy test was conducted using the TESCAN VEGA 3 LMH optical microscope shown in Plate IX and situated at the Faculty of Engineering and Built Environment University of Johannesburg South Africa.



**Plate IX: Scanning Electron Microscope**

**f.      Optical Microscopy**

The optical microscopy test was performed using the Olympus 82X16 optical microscope shown in Plate X and situated at the Faculty of Engineering and Built Environment University of Johannesburg South Africa.



**Plate X: Optical Microscope**

## 3.2 Methods

### 3.2.1 Chemical composition

The samples used for chemical composition determination were cut into small piece measuring 10 mm x 10 mm using band saw and the chemical composition analysis was done using the spectroscopy machine. The samples were polished using 1000 grade grit paper and were thoroughly washed using acetone to remove dirts, they were inserted into the machine and the machine was allowed to run for about 20 minutes and results were generated.

### 3.2.2 Preparation of base materials

After chemical composition analysis was done using the spectroscopy machine, the workpieces for the welding process were cut in small piece using the band saw (Plate XI). They were cut to required dimensions for welding and the two interfaces were milled

using the milling machine such that when placed side by side one is unable to see through as shown in Figure 3.1.



**Plate XI: Cutting of workpiece using band saw**
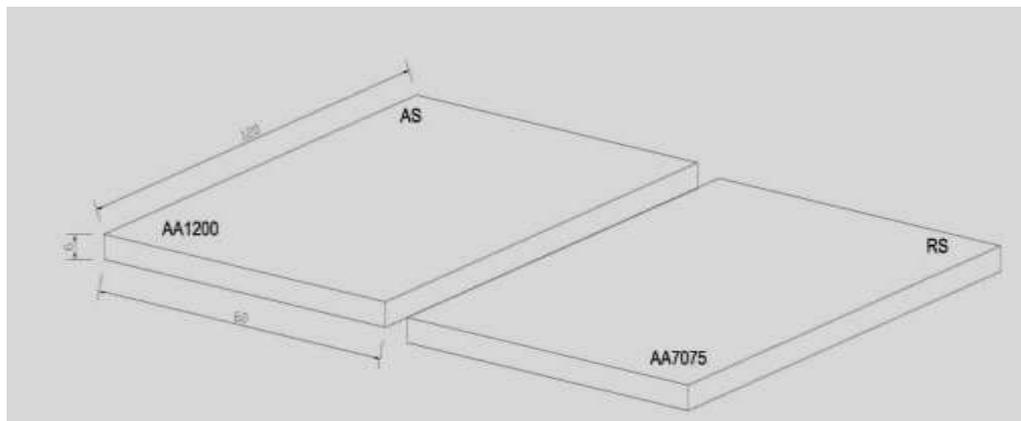


**Figure 3.1: Dimensions of work piece material**

### 3.2.3 Experimental trials for process window

Based on available literature (Elangovan *et al.*, 2009; Guvir *et al.*, 2016), trial welds were made with the following weld parameters namely: rotational speed, welding speed and tilt angle of tool. The plunge force (downward force) was fixed at 7 kN. The experimental trials design for process window is shown in Table 3.2.

**Table 3:2      Experimental Trials for process window**

| Experiment No | Rotational speed(rpm) | Welding speed( mm/min) | Tilt angle ( ˚) |
|---|---|---|---|
| 1 | 800 | 50 | 1 |
| 2 | 1600 | 50 | 1 |
| 3 | 800 | 150 | 1 |

| | | | |
|---|---|---|---|
| 4 | 1600 | 50 | 2 |
| 5 | 1600 | 25 | 2 |
| 6 | 1000 | 50 | 2 |
| 7 | 1000 | 30 | 2 |
| 8 | 1500 | 30 | 2 |

## 3.3 Design of Experiment

Experimental design was conducted using Minitab 17 software. Response Surface Methodology (RSM), specifically central composite design (CCD) approach was employed in this design. The CCD was selected in preference to Box Benhken's Design (BBD) because it consists of 2-level full factorial design, axial points ($\alpha$) and centre points. The three critical factors used in this study include, rotational speed, transverse speed and tool tilt angle as input variables as shown in Table 3.3, the plunge force (downward force) was fixed at 7 kN. A total of twenty (20) experiments were obtained using Minitab 17 software as shown in Table 3.4. This design consisting of six (6) centre points, eight (8) cubic points and six (6) axial points was applied for the welding process using tapered tool (TT) and tapered threaded tool (TTT). Based on the results obtained from preliminary investigation, the values presented in the factor level of welding parameter shown Table 3.3 were selected. The experimental design matrix is shown in Table 3.4.

**Table 3.3 Factor levels of Process Parameters**

| Parameters | - $\alpha$ | -1 | 0 | +1 | $\alpha$ |
|---|---|---|---|---|---|
| Rotational speed | 900 | 1150 | 1500 | 1850 | 2100 |
| Transverse speed | 30 | 45 | 60 | 75 | 90 |
| Tool tilt angle | 1 | 1.5 | 2 | 2.5 | 3 |

**Table 3.4: Experimental matrix**

| Standard order | Experimental Runs | Rotational speed (rpm) | Transverse speed (mm/min) | Tool Tilt Angle ( ˚ ) |
|---|---|---|---|---|
| 10 | 1 | 1150 | 45 | 1.5 |
| 1 | 2 | 1850 | 45 | 1.5 |
| 3 | 3 | 1150 | 75 | 1.5 |
| 6 | 4 | 1850 | 75 | 1.5 |
| 19 | 5 | 1150 | 45 | 2.5 |
| 16 | 6 | 1850 | 45 | 2.5 |
| 4 | 7 | 1150 | 75 | 2.5 |
| 15 | 8 | 1850 | 75 | 2.5 |
| 9 | 9 | 900 | 60 | 2 |
| 2 | 10 | 2100 | 60 | 2 |
| 14 | 11 | 1500 | 30 | 2 |
| 12 | 12 | 1500 | 90 | 2 |
| 5 | 13 | 1500 | 60 | 1 |
| 8 | 14 | 1500 | 60 | 3 |
| 11 | 15 | 1500 | 60 | 2 |
| 13 | 16 | 1500 | 60 | 2 |
| 7 | 17 | 1500 | 60 | 2 |
| 20 | 18 | 1500 | 60 | 2 |
| 17 | 19 | 1500 | 60 | 2 |
| 18 | 20 | 1500 | 60 | 2 |

## 3.4 Friction Stir Welding

### i. Tool configuration

Tool design is an important factor for consideration in friction stir welding as the tool is responsible for heat generation, plastic deformation and flow, joint integrity as well as microstructure and mechanical properties of the welds. A shoulder to pin ratio of 3:1 was used in the tool design based on available literature (Daswes *et al.*, 2007: Hua, 2006) and Akinlabi *et al.*, 2012). The tool must be suitable for every material to be welded based on the strength and thickness of the material. The two tools used are shown in Plate II. The dimensions of the tool are given in Table 3.5.

**Table 3.5    Friction Stir Welding Tool Dimensions and Features**

| Dimensions | Tool | (mm) |
| --- | --- | --- |
| | Dimensions | |
| | A | B |
| Pin diameter(mm) | 7.3 | 7.3 |
| Pin length(mm) | 5.6 | 5.6 |
| Shoulder diameter(mm) | 22 | 22 |
| Features/Geometry | Tapered    threaded cylindrical | Tapered  cylindrical |

**ii. Welding process**

The workpieces were cut to the required dimensions of 120 mm x 60 mm x 6 mm representing length, breath and thickness respectively. The proposed joint edges were milled to allow for proper lapping. The samples were clamped on the friction stir welding machine in a butt configuration. An offset of 2 mm was given towards the AA 1200-H19 aluminium alloy (softer material) to encourage better plastic deformation and bonding. The surface area of the proposed weld region was cleaned with emery paper to remove oxide layers that may have been formed and washed with acetone to remove dirts or grease. The welding parameters were fed manually into the friction stir machine and welding was done automatically. A constantly rotating non consumable cylindrical-shouldered tool with a pin length of 5.65 mm was transversely fed into a butt joint between the two clamped pieces of butted materials at varied feed rate and rotational speed with the pin length slightly shorter than the weld depth required. Frictional heat was generated between the wear resistant welding components and the workpieces by the ridding action of the tool shoulder on top of the workpieces. This heat along with that generated by the mechanical mixing process and the adiabatic heat within the materials caused the stirred materials to soften without melting. As the pin moves forward, a special

profile on its leading face forced the plasticized materials to the rear where clamping force assisted in a forged consolidation of the weld. The weldment was allowed to cool and then unclamped from the platform. This procedure was applied for the two tool geometries used in form of tapered and tapered threaded tools. Figure 3.2 shows the schematic representation of friction stir butt welding process.
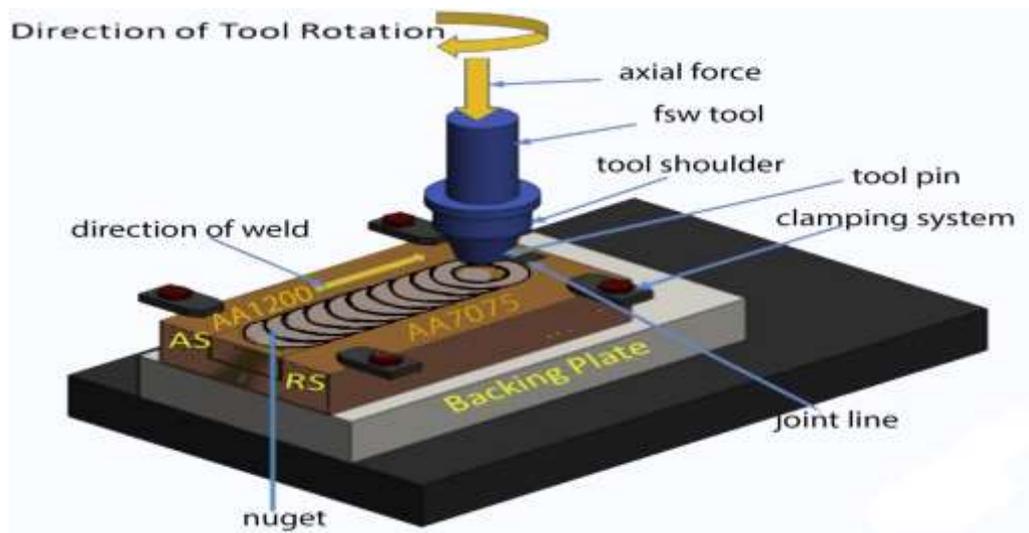


**Figure 3.2: Schematic Representation of Friction stir butt welding process**

## 3.5     Machining Process

The test piece for hardness, impact and tensile tests were cut using the wired-cut EDM machine. The dimensions of these specimens were programmed into the machine and the machine was allowed to run with the electrolyte serving as dielectric material and coolant until the cutting was completed. The cutting process is shown in Plate XII.

**Plate XII: Cutting with Wired EDM**

## 3.6    Testing Procedure

The procedures followed to determine the properties of the weldment were in accordance with the ASTM testing standards (ASTM-E10, ASTM-D8 sub-size, ASTM-E23 reduced specimen) for hardness, tensile and impact tests, respectively and the testing machine specification. The procedures are highlighted below. The mechanical tests performed are those of the tree responses (hardness, impact and tensile test). The locations of the specimens are as shown in the weldment in Figure 3.3.
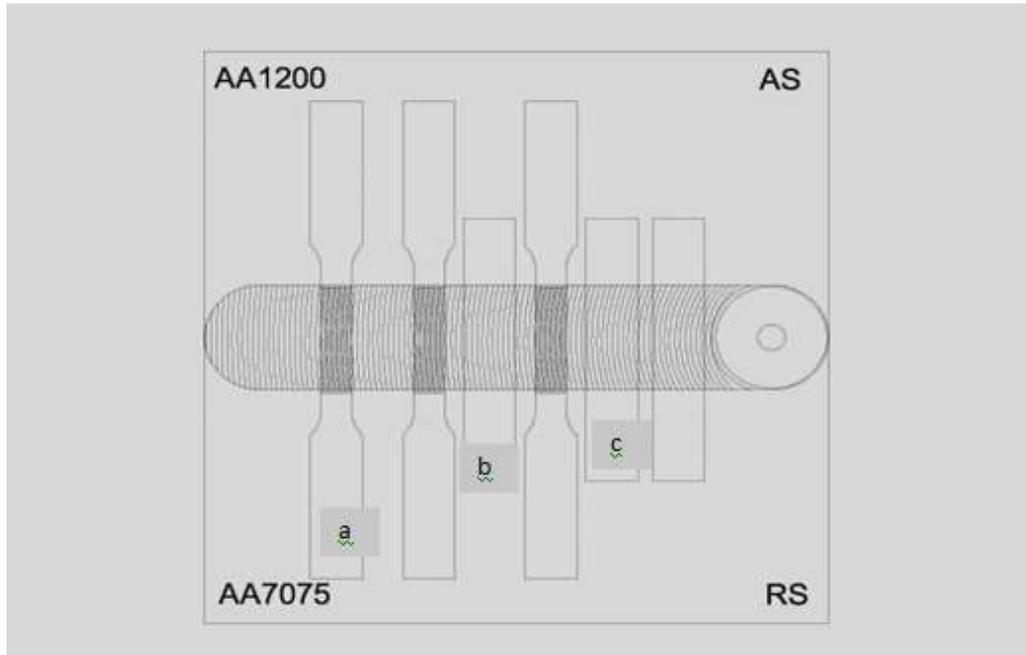
**Figure 3.3: Samples (a) Tensile (b) hardness (c) impact specimen**

### 3.6.1 Hardness

A surface hardness test was conducted on each sample using the Vickers Hardness Tester (MHVD-10IS) to determine the resistance of each weldment to indentation according to ASTM-E10 standard. The prepared specimens from the sample of different process parameters were subjected to pressure which was applied by a spring (calibrated) to a spherical shaped indenter and an indicator which measures the indentation depth. A 5 kg load was applied at a dwell time of 15 seconds and 29 indentations were made at 1 mm interval on each sample. The values of the hardness measurements at the nugget zone were recorded as the average hardness of each sample. The test specimens (Plate XIII (a and b)) obtained from different samples at varied process parameters represents hardness values of tapered tool (TT) and tapered threaded tool (TTT) . The Dimensions (mm) of microhardness specimen is shown in Figure 3.4
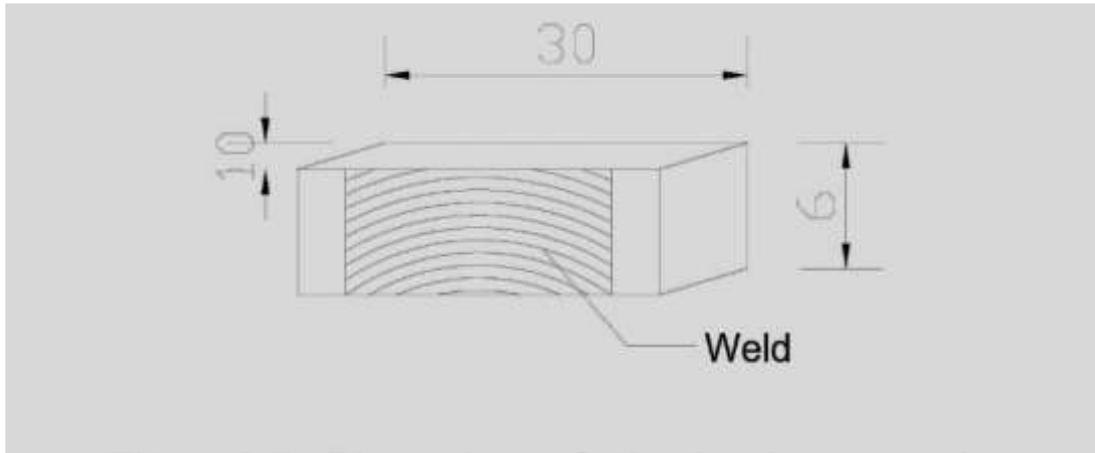
**Figure 3.4    Dimensions of microhardness specimen in mm**



(a) TT                                                                    (b) TTT

**Plate XIII: Microhardness  specimen**

### 3.6.2    Tensile strength

The tensile test was conducted using the 100kN Instron 8862 tensile testing machine on each specimen from the different experimental runs. The test specimens were prepared and labelled in compliance with ASTM D8 standard for sub-size specimen. Specimen dimension was measured using a vernier calliper of accuracy 0.01cm. With the machine reading set at 0.00N, the test was performed by clamping each prepared specimen from required sets of process parameter into a hole in the fixture; the machine was used to pull until failure occurred. The results obtained were used to calculate the tensile strength

expressed in megapascal. Ultimate tensile strength was determined by dividing the maximum load at break by the cross-sectional area. This cross-sectional area was calculated by multiplying the width of specimen by the thickness of the specimen. The mathematical equations are shown in equations 3.1 and 3.2. Figure 3.5 shows the tensile specimen dimensions in mm. Tensile tests specimen is shown in plate XIV.

Cross sectional Area = width (b) x thickness (t)     (3.1)

$$\text{Ultimate tensile Stress } (\sigma) = \frac{\text{Maximum Force (Pmax)}}{\text{cross−sectional area (A)}}$$     (3.2)
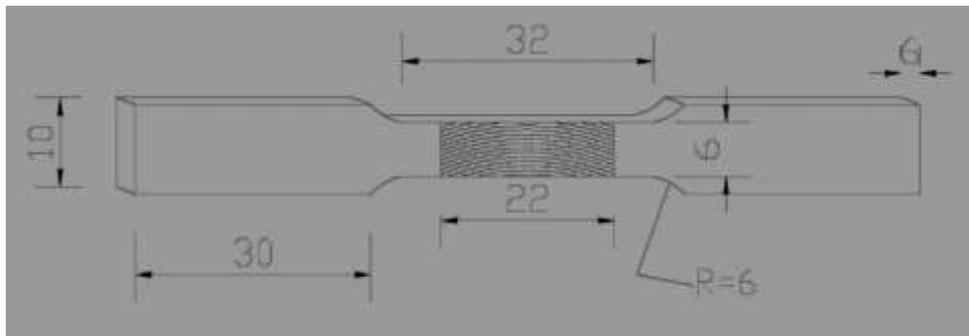


**Figure 3.5: Tensile specimen dimensions**

As adopted by Ilangovan *et al.* (2015), the joint efficiency was calculated by dividing the UTS of the weldment by the UTS of softer base material whose UTS value is 180 MPa and expressed in percentage. It can be expressed as;

Joint efficiency n $= \frac{UTS\ joint}{UTS\ soft}$ x 100 %     (3.3)

Joint efficiency varies from 100% for perfect weld down to 75% for acceptable weld (Akinlabi, 2010).

**Plate XIV: Tensile test specimens**

### 3.6.3 Impact test

Test specimens with a V notch in the fusion zone for impact test fracture were prepared according to ASTM E-23 standard (reduced specimen). The test was carried out on specially prepared specimens in the form of a notched bar as shown in Figure 3.6. For the purpose of this research, 6 mm thick dissimilar welded AA7075 and AA1200 aluminium alloys. The Charpy impact test was carried out on the test pieces. The bar of the material was 55 mm long, and a V-notch 2 mm deep with a notch tip radius of 0.25 mm (using a notching machine) and a notching angle of $45°$ was made at the centre of the specimens as shown in Figure 3.6. The specimen was supported at its two ends on an anvil and was struck on its opposite face to the notch by a pendulum hammer set at a predetermined operating position and which stores up 162.725 J at a velocity of 3.8 m/s. The impact from the knife edge mounted to the pendulum hammer bends or fractures the specimen at the notch which acts as the point of stress concentration for the high velocity impact blow. The reading is then taken which represents the impact energy of the specimen. The Charpy test shows whether a metal can be classified as ductile or brittle. The impact

specimen dimensions and impact specimens are shown in Figure 3.6 and Plate XV respectively
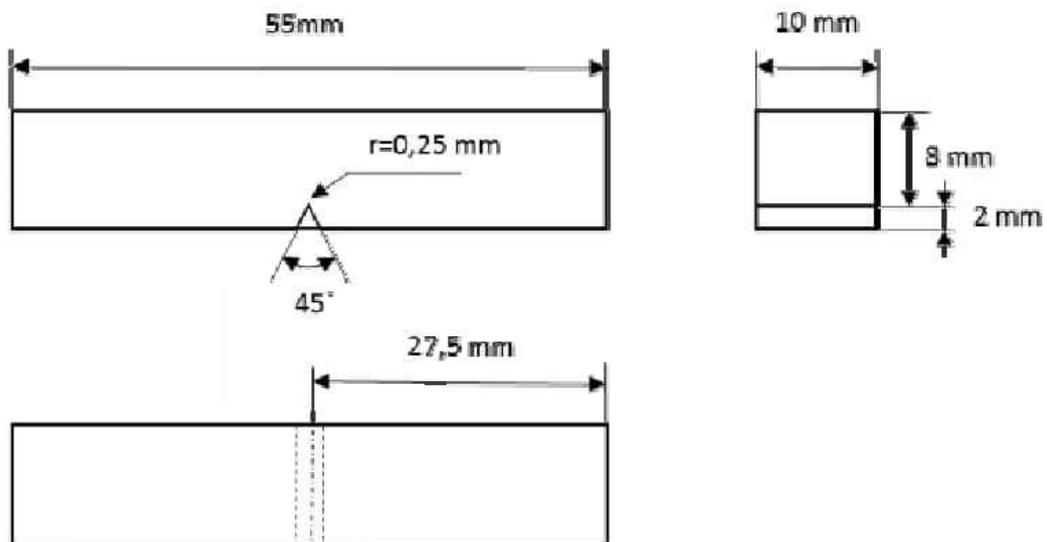


**Figure 3.6: Impact specimen dimensions**



**Plate XV: Impact specimen**

## 3.7    Analysis of Experimental Result

### 3.7.1   Signal to noise (SN) ratio analysis

SN ratio analysis was carried out to obtain the optimal welding parameters using experimental results. This analysis was conducted using larger-the better quality characteristics as per Equation 3.4.

$$SN = -10\log\frac{1}{n}(\sum\frac{1}{y_i^2})$$ (3.4)

Where, n= number of experimental runs and y = experimental response

## 3.7.2 Analysis of Variance (ANOVA)

The analysis of variance (ANOVA) was conducted to determine the percentage contribution of process parameters (rotational speed, transverse speed and tool tilt angle) on the three responses (hardness, tensile and impact energy) of the weldment using the two tool geometries. It was done at confidence level of 95 % and significance level α = 0.05. The sum of squares (SS), Degree of freedom, mean square (MS), F-values and percentage contribution P were calculated using equations 3.5- 3.10.

The $sum\ of\ square\ SS_T = \sum_{i=1}^{n}(y_i)^2 = -\frac{1}{n}\ \sum_{i=1}^{n}y_i^2$ (3.4)

DOF = number of level – 1 (3.6)

$MS = \frac{SS(individual)}{DOF}$ (3.7)

$F - value = \frac{SS(individual)}{MS_{(error)}}$ (3.8)

$P - value = \frac{SS(individual)}{SS_{T'}}$ (3.9)

Error = Total - $\sum DOF$ (3.10)

Where, y= response value

## 3.7.3 Empirical regression model

Empirical model was developed via Minitab 17 software using empirical experimental results, in order to predict the values of the investigated responses (hardness, UTS and

impact energy). These equations were used to study and understand how the values of the responses (dependent variables) changes when one of the independent variables (rotational speed, transverse speed and tool tilt angle) is varied while the others are kept constant. The equations developed were also used to calculate the mechanical properties of the weldment based on values of independent variables.

## 3.8    Grey Relational Analysis (GRA)

GRA was conducted using larger the better attribute as adopted by Abutu *et al.* (2018) with the aim of obtaining the multi-response optimal welding parameters that provide the optimal performance. The first stage of GRA optimization involved selection of an appropriate design technique (RSM, Taguchi, factorial and mixture). This was followed by calculation of signal-to-noise ratio (S∕N ratio, $\eta$) of individual responses using larger-the better quality characteristics as per Equation 3.4. The next stage of GRA was the calculation of grey relational generation (GRG) which involves processing all performance values for every alternative into a comparability sequence using Equation 3.8 (larger-the-better attributes). This Linear normalization of the S/N ratio is normally carried out in the range between 0 and 1.

The grey relational generation (GRG) procedure was followed by Grey relational coefficient (GRC) which involves scaling all performance values into 0, 1. If the value $x_{ij}$ is 1, or closer to 1 than the value for any other alternative, the performance of alternative $i$ is the best one for attribute $j$ (Equation 3.8). Therefore, an alternative will be the best choice if all of its values are closest to or equal to 1. This type of alternative does not usually exist as a result, it is better to define reference sequence like $x_0$ as ($x_{01}, x_{02}, \ldots, x_{0j}, \ldots, x_{0n}$) and then aims to find the alternative whose comparability sequence is the

closest to the reference sequence. The calculation of grey relational coefficient $\gamma\ (x_{0j},\ x_{ij})$ is followed by the grey relational grade computation using Equation 3.9.

Larger-the-better attributes $(x_{ij}) = \dfrac{y_{ij} - \underline{y_i}}{\overline{y_i} - \underline{y_j}}$ (3.11)

$(i = 1, 2, 3…. m$ and $j = 1, 2, 3…. n)$

Where, $y_i = (y_{i1}, y_{i2}, . . . , y_{ij} , . . . , y_{in})$, $y_{ij}$ is the performance value of attribute j of alternative i and $\overline{y_j} = \max\{y_{ij}, i = 1, 2, . . . , m\}$ and $\underline{y_j} = \min\{y_{ij}, i = 1, 2, . . . , m\}$.

$$\gamma(x_{0j}, x_{ij}) = \frac{\Delta_{min} + \beta\Delta_{max}}{\Delta_{ij} + \beta\Delta_{max}} \qquad (i = 1, 2, . . . , m \text{ and } j = 1, 2, . . . , n) \qquad (3.12)$$

Where, $\gamma\ (x_{0j}, x_{ij}\ )$ is the grey relational coefficient between $x_{ij}$ and $x_{0j}$ ,

$\Delta_{ij} = x_{0j} - x_{ij}$ , $\Delta_{min} = \min (\Delta_{ij}, i = 1, 2, . . . , m; j = 1, 2, . . . , n)$,

$\Delta_{max} = \max (\Delta_{ij}, i = 1, 2, . . . , m; j = 1, 2, . . . , n)$ and $\beta$ is the distinguishing coefficient, $\beta \in [0, 1]$.

The aim of the distinguishing coefficient ($\beta$) is to compress or expand the range of the grey relational coefficient and 0.5 is the widely accepted value. Abutu *et al.* (2018) reported that after grey relational generating, $\Delta_{max}$ will be equal to 1 and $\Delta_{min}$ will be equal to 0.

$$\varphi\ (x_0, x_i) = \sum_{j=1}^{n} w_j \beta(x_{oj}, x_{ij}) ; \ (i = 1, 2, 3……. m) \qquad (3.13)$$

$w_j$ represents the weight of attribute *j* which is usually dependent on the judgments of the decision maker or the structure of the proposed problem. Abutu *et al.* (2018) reported

that $\sum_{j=1}^{n} w_j$ is equal 1. The final process of GRA was the determination of optimal factors for the single response.

## 3.9    Characterisation of GRA-Optimised Weldment

### 3.9.1    Corrosion test of the base-metals and friction stir welded samples

Corrosion tests were performed on specimens from AA1200-H19 and AA7075-T651 base metal as well as those from the produced friction stir welding of dissimilar AA1200-H19 and AA7075-T651 materials with each specimen having 22 mm x 10 mm x 6 mm dimensions. To act as control experiments the corrosion analysis for as-received materials was studied. In order to minimize any foreign objects and in accordance with the ASTM G1-03 standard (Ikumapayi *et al.* 2020), the outer layer of each specimen was treated with grades 1000 and 1200 grit of silicon carbide emery papers and afterwards flushed in reasonable distilled water. A 3.5 percent NaCl corrosive medium was prepared and this was accomplished by measuring 35 g of sodium chloride salt (NaCl). A corrosive test medium was prepared with 35 g of NaCl and one liter of distilled water which resulted in a 3.5 % NaCl solution after complete dissolution was achieved. During preparation, the electrolyte temperature was held at room temperature. The electrochemical test was separately conducted for the base metals AA1200-H19 and AA7075-T651 and the friction stir welded samples. Investigations aimed to examine open circuit potential (OCP) and potentiodynamic polarization (PDP), using the 3-electrode links which are reference electrode (RE), working electrode (WE), and counter electrode (CE). OCP refers to the potential produced between the working and the reference electrodes in the electrochemical system for the cathodic and anodic reactions. The OCP shows the material's behaviours or integrity in a certain electrolyte, although it does not give

information about electrochemical kinetics. The evaluation was carried with AutoLab PGSTAT 101 Metrohm potentiostat / galvanostat which was interfaced with NOVA software version 2.1.2. The Potentiostat corrosion experiment helped to expose the corrosion levels of the base metals as well as the Tafel plots for the welded samples; this helps us to hopefully determine when corrosion can attack the material and to recognize that the transformations are of vital importance for the protection of the material. The base metal and friction stir welded materials were used as working electrodes, whereas the counter-electrode was graphite rod, while the reference electrode used in this research was the potassium chloride electrode (PCE). The anodic potential was (1.5 V) in this test, and the cathodic potential was (-1.5 V) and the scan rate was used at 0.005 V / s. In a 3.5 percent NaCl solution electrolyte medium, the base metals (AA1200-H19 and AA7075-T651) and friction stir welded samples of dissimilar materials were used as working electrodes and were separately soaked for 10 minutes before OCP was measured, enabling the achievement of stable-state potential and the recording of potentiodynamic polarization (PDP) values immediately after OCP values were taken. To maintain reproducibility, the test was conducted three times on each corrosion sample and the average of the result of the tests was calculated and used. The polarization potential values ($E_{corr}$) and the current density ($j_{corr}$) were generated from the Tafel curves which were drawn from the data obtained in linear sweep voltammetry (*LSV*) data sheet. The IE percentage (percentage inhibition efficiency) was evaluated using equation 3.10. The following values were also obtained from corrosion resistance alloys (CRA) data sheet after the experiments, corrosion rate (CR), anodic slope (ba), corrosion current density ($j_{corr}$), polarization resistance (PR), cathodic slope (bc), and corrosion potential($E_{corr}$). The polarization method shows the possible transformation of a component from a stable state. In order to further improve the material corrosion rate, the Tafel obtained from the

potentiostat polarisation test was obtained through the linear sweep voltammetry (*LSV*). Based on this information one can also infer the essence of the prevalent reactions and the anodic arms against the cathodic arms, whether it is anodic or cathodic protection.

$$IE\ \% = 1 - \frac{j_{corr}}{j_{0corr}}\ x\ 100 \tag{3.14}$$

In this case, $j_{ocorr}$ = uninhibited corrosion current density and $j_{corr}$ = inhibited corrosion current densities.

## 3.10    Microstructural Analysis

### a.        Scanning Electron Microcopy (SEM)

Microstructure of the weldment was examined using a scanning electron microscope. Samples were cut to the required dimensions 6 mm x 6mm x 6mm), they were cold mounted with Phenolic thermosetting, they were grinded using a Melkon Forciol grinder and 1000 grade grit paper and was etched using Weck's reagent (100 ml water + 4 g KMnO4 ml HCl + 1g ml NaOH +) at room temperature for 30 s and successively washed in deionised water, ethanol and dried in a hot air stream prior to observations and thereafter microstructural images were taken

### b.        Optical Microscopy

Microstructural characterizations was performed by optical microscopy (OM) - Samples cut to 5 mm x 5mm x 6 mm and were grinded with Melkon Forcipol gringer and 1000 grade emery paper, polished with alumina down to 1 μm, thoroughly washed with ethanol, acetone and then dried in a hot-air stream. The samples were etched in Weck's reagent (100 ml water + 4 g KMnO4 ml HCl + 1g ml NaOH +) at room temperature for 30 s and successively washed in deionized water, ethanol and dried in a hot air stream prior to observations and thereafter microstructural images were taken

## CHAPTER FOUR

**4.0**                          **RESULTS AND DISCUSSION**

**4.1     Preliminary Results**

**4.1.1   Chemical composition**

The chemical composition of the base materials from spectroscopy analysis are shown in

Tables 4.1 and 4.2.

**Table 4.1:     Chemical Composition of AA1200 aluminium alloy**

| Element | Al | Fe | Si | Cu | Mn | S | As | Ta |
|---|---|---|---|---|---|---|---|---|
| Composition (%) | 99.27 | 0.43 | 0.24 | 0.04 | 0.02 | 0.01 | 0.01 | 0.01 |

**Table 4.2:     Chemical Composition of AA7075 aluminium alloy**

| Element | Al | Zn | Cu | Cr | Fe | Si | Ti | Mn | P | S | As | Ta |
|---|---|---|---|---|---|---|---|---|---|---|---|---|
| Composition (%) | 93.99 | 4.52 | 1.04 | 0.17 | 0.12 | 0.11 | 0.03 | 0.03 | 0.01 | 0.01 | 0.01 | 0.01 |

The results shown in Tables 4.1 and 4.2 indicate that the AA1200 and AA7075

Aluminium alloy base materials are composed of 99.27 and 93.99 % aluminium metal,

respectively with little percentages of trace metals.

**4.1.2   Trial welds**

During the process window development process, the following observations were made

from the weldment produced which aided in the establishment of workable process

parameter from which the experimental design matrix was drawn. These are as itemised

in Table 4.3 and presented in Plate XVI.

**Table 4.3: Nature of Weldment**

| S/N | Trial No | Observations | Remarks |
|---|---|---|---|

84

| 1 | Trial 1 | Specimen has surface gelling, no proper mixing, Insufficient heat | Defective |
|---|---------|------------------------------------------------------------------|-----------|
| 2 | Trial 2 | Tunnel defect/ wormhole | Defective |
| 3 | Trial 3 | Tunnel defect, no mixing due to insufficient heat and fast travel speed | Defective |
| 4 | Trial 4 | Tunnel and wormhole present | No mixing |
| 5 | Trial 5 | Tunnel/wormhole defect | No mixing |
| 6 | Trial 6 | Tunnel/wormhole defect | No mixing |
| 7 | Trial 7 | Little defect, offset giving room for mixing | Mixing occurred |
| 8 | Trial 8 | No defect- sufficient heat for plasticity time for mixing | Good weld |



**Plate XVI:    Trial welds**

In friction stir welding of dissimilar materials, the direction of rotation is important due to directional flow of the materials as it indicates which material should be on either advancing or retreating sides. (Divya *et al.,* 2014).

Trial 1 was based on the findings of Divya *et al.,* 2014, in which the softer material was placed on the advancing side. In this study, the AA1200 (softer material) was placed on the advancing side while the AA7075 was placed on the retreating side without tool offset, there was however no good weld, the same outcome was also observed in Trial 2. This may be due to insufficient heat for homogenous mix. Also, the defect in trial 3 was due to higher welding speed which resulted in tunnel defect. Trial 4 and 5 followed a similar trend as trial 1 and 2, but as the positioning was changed for trial 6, 7 and 8, there was continuous improvement in weld quality based on visual inspection. In addition, tool offset of 2 mm towards the advancing side (softer material) was introduced for trial 8 and it gave a good weld with better surface quality which is in conformity with the findings of Akinlabi *et al.* (2011) and Ramachandran *et al,* (2015). Hence for the main experiment the positioning was adopted. i.e AA1200 on advancing side while AA 7075 on the retreating side with 2 mm tool offset towards the advancing side. Therefore, from the results obtained from the preliminary welds produced, the final welds comprised 40 welds (20 welds with each tool geometry) that is tapered tool (TT) and tapered threaded tool (TTT). The weld settings were selected to represent the widest range of possible combinations within the friction stir welding platform's limits, thereby avoiding excessive machine vibration. The rotational speeds of 900, 1150, 1500, 1850 and 2100 rpm and welding speeds of 30,45,60,75 and 90 mm/min and tilt angles of 1,1.5,2,2.5 and 3° were chosen to represent five levels .Figure 4.1 shows the configuration of the final weldment.
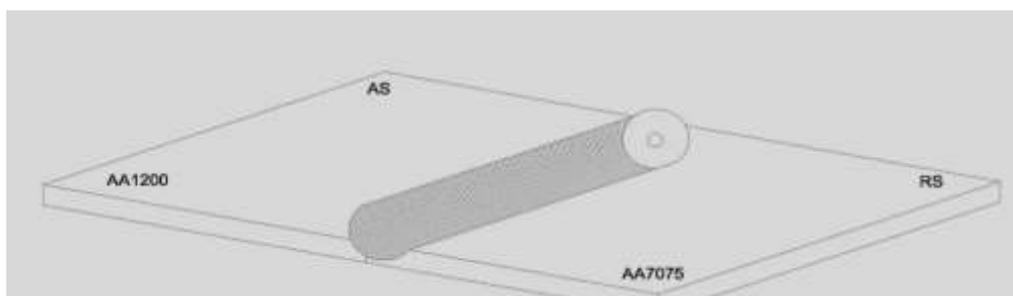
**Figure 4.1:  Final weldment**

## 4.2     Welded Samples

The weldment produced using tapered tools (TT) and tapered threaded tools (TTT) are shown in Plates XVI and Plate XVII, respectively. From plate XVI, it was observed that welding was possible at the selected range of process parameters but surface quality differs from sample to sample (different parameters) for both TT and TTT Weldments



**Plate XVII: TT-weldment**



**Plate XVIII: TTT-weldment**

## 4.3     Evaluation of Mechanical Properties of the Weldment

The experimental results obtained for TT and TTT are shown in Table 4.4 and 4.5, respectively.

**Table 4.4       Experimental Runs and Response for Tapered Tool (TT)**

| Experimental Runs | Rotational speed (rpm) | Transverse speed (mm/min) | Tool Tilt Angle (°) | Hardness (Vickers) | UTS (MPa) | Impact Energy (J) | Joint efficiency (%) |
|---|---|---|---|---|---|---|---|
| 1 | 1150 | 45 | 1.5 | 73.78 | 128.79 | 8.9 | 71.55 |
| 2 | 1850 | 45 | 1.5 | 74 | 122.47 | 10.9 | 68.04 |
| 3 | 1150 | 75 | 1.5 | 76.21 | 122.53 | 0.6 | 68.07 |
| 4 | 1850 | 75 | 1.5 | 85.5 | 126.81 | 6 | 70.45 |
| 5 | 1150 | 45 | 2.5 | 72.25 | 111.81 | 2.9 | 62.12 |
| 6 | 1850 | 45 | 2.5 | 84.65 | 125.5 | 10.1 | 69.72 |
| 7 | 1150 | 75 | 2.5 | 77.01 | 123.76 | 5.2 | 68.76 |
| 8 | 1850 | 75 | 2.5 | 64.26 | 122.68 | 4.1 | 68.16 |
| 9 | 900 | 60 | 2 | 66.85 | 111.51 | 3.4 | 61.95 |
| 10 | 2100 | 60 | 2 | 75.68 | 117.09 | 5.7 | 65.05 |
| 11 | 1500 | 30 | 2 | 81.99 | 126.04 | 12.9 | 70.02 |
| 12 | 1500 | 90 | 2 | 77 | 128.37 | 5.4 | 71.32 |
| 13 | 1500 | 60 | 1 | 70.22 | 123.32 | 6.4 | 68.51 |
| 14 | 1500 | 60 | 3 | 66 | 112.2 | 4.7 | 62.33 |
| 15 | 1500 | 60 | 2 | 98.58 | 151.54 | 21.4 | 84.19 |
| 16 | 1500 | 60 | 2 | 99.72 | 151.3 | 11.4 | 84.06 |
| 17 | 1500 | 60 | 2 | 97.91 | 150.51 | 10.7 | 83.62 |
| 18 | 1500 | 60 | 2 | 98.8 | 151.88 | 10.8 | 84.38 |
| 19 | 1500 | 60 | 2 | 98.87 | 151.99 | 11.4 | 84..44 |
| 20 | 1500 | 60 | 2 | 99.19 | 154.48 | 11.3 | 84.71 |

**Table 4.5      Experimental Runs and Response for Tapered Threaded Tool (TTT)**

| Experimental Runs | Rotational speed (rpm) | Transverse speed (mm/min) | Tool Tilt Angle (°) | Hardness (Vickers) | UTS (MPa) | Impact Energy (J) | Joint efficiency (%) |
|---|---|---|---|---|---|---|---|
| 1 | 1150 | 45 | 1.5 | 86.5 | 138.35 | 9.9 | 76.86 |

| 2 | 1850 | 45 | 1.5 | 86.04 | 138.42 | 10.2 | 76.90 |
|---|------|----|-----|-------|--------|------|-------|
| 3 | 1150 | 75 | 1.5 | 85.5 | 136.81 | 8.8 | 76.01 |
| 4 | 1850 | 75 | 1.5 | 88.28 | 141.08 | 9.1 | 78.38 |
| 5 | 1150 | 45 | 2.5 | 83.76 | 144.13 | 1.5 | 80.07 |
| 6 | 1850 | 45 | 2.5 | 84.91 | 130.53 | 10.4 | 72.52 |
| 7 | 1150 | 75 | 2.5 | 84.82 | 141.14 | 6.9 | 78.41 |
| 8 | 1850 | 75 | 2.5 | 83.28 | 158.77 | 12.6 | 88.21 |
| 9 | 900 | 60 | 2 | 81.21 | 135.59 | 0.7 | 75.33 |
| 10 | 2100 | 60 | 2 | 79.82 | 143.45 | 10.7 | 79.69 |
| 11 | 1500 | 30 | 2 | 77.8 | 162.66 | 16.9 | 90.37 |
| 12 | 1500 | 90 | 2 | 81.77 | 126.45 | 14.7 | 70.25 |
| 13 | 1500 | 60 | 1 | 88.8 | 136.51 | 8.7 | 75.84 |
| 14 | 1500 | 60 | 3 | 85.15 | 140.27 | 18.41 | 77.93 |
| 15 | 1500 | 60 | 2 | 105.25 | 161.8 | 23.4 | 89.89 |
| 16 | 1500 | 60 | 2 | 104.85 | 161.18 | 12 | 89.54 |
| 17 | 1500 | 60 | 2 | 105.52 | 162.21 | 11.8 | 90.12 |
| 18 | 1500 | 60 | 2 | 105.28 | 161.84 | 10.6 | 89.91 |
| 19 | 1500 | 60 | 2 | 105.75 | 162.57 | 11 | 90.32 |
| 20 | 1500 | 60 | 2 | 104.91 | 161.27 | 12.7 | 89.59 |

## 4.3.1 Tapered tool weldment

The mechanical properties of the tapered tool (TT) weldment were evaluated as discussed

in 4.3.1.1-4.3.1.3

**4.3.1.1 Hardness analysis**

a.      **Hardness at different welding speed**

The hardness test performed on the two base metals gave hardness values of 50 HV and 175 HV for AA1200-H19 and AA7075-T651, respectively. The hardness profile of the weldment is shown in Figure 4.2. The average hardness increased from 81.99 to 98.58 HV. This can be attributed to better grain refinement and mixing at 60 mm/min welding speed. Also, at the 60 mm/min welding speed precipitation of hardening precipitates was encouraged (Abolusoro & Akinlabi, 2020).

At 30 mm/min welding speed, the average hardness of 81.99 HV obtained was higher than that of the AA 1200 H-19 aluminium alloy but below that of 7075-T651 indicating occurrence of mixing of both alloys at the nugget zone (NZ). At 90 mm/min welding speed (high speed) the average hardness decreased from 98.58 to 77 HV, this can be attributed to dissolution of strengthening precipitates. Also, at 90 mm/min welding speed, the tool traversed faster on the material (dwelling time was low) not giving sufficient time for material coalescence to occur.

The hardness values obtained at the HAZ of the advancing side was lower than the hardness value of the base metal AA 1200 H-19 aluminium alloys. This may be attributed to subjection of the alloy to thermal cycle during welding resulting in dissolution of the alloy's precipitates and leading to reduction in hardness. On the retreating side, the hardness values were lower than that of the base metal AA7075-T651.

The average hardness values obtained at the NZ were higher than those of the base metal AA1200- H19 but lower than the base metal AA7075- T651. This is due to mixing of both alloys at this region. Also, the average hardness at the NZ is higher than those of the HAZ of both the advancing and retreating sides. This can be attributed to presence of inter-metallic compounds formed during the welding (Raju *et al,* 2016).
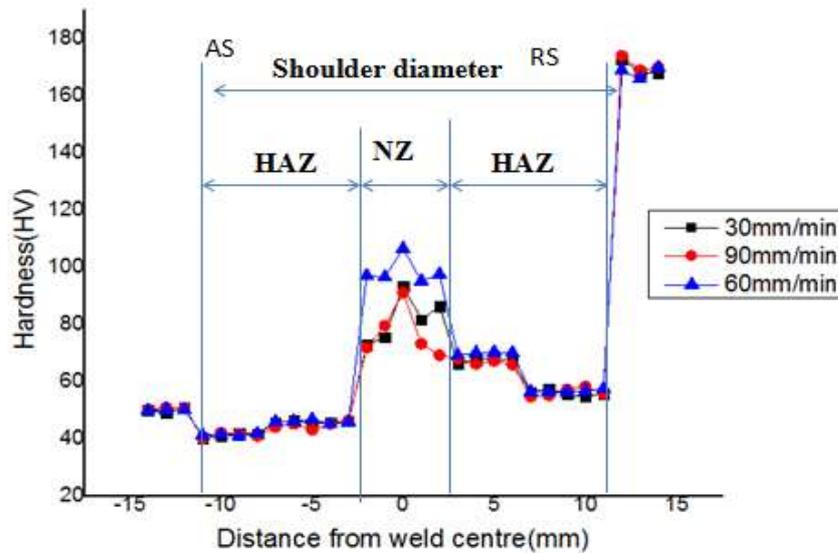
**Figure 4.2: Hardness profile at different welding speed for TT**

**b.      Effect of tilt angle on hardness**

The average hardness value at constant tool rotational and welding speeds of 1500 rpm

and 60 mm/min, respectively is seen to increase from 70.22 HV to 98.58 HV with increase

in tool tilt angle from 1 to 2 ˚ due to formation of intermetalics resulting from temperature

rise in stir zone. Also, this is because the tilt angle prevents spreading of material on the

surface of the weldment which may result in flash defects. The tilt angle encourages

material flow which results in good metallurgical bonding between the two alloys. A

further increase in tilt angle from 2 to 3 ˚ resulted in reduction in hardness from 98.58 HV

to 66 HV. Hardness values at varying tilt angle are shown in Figure 4.3.
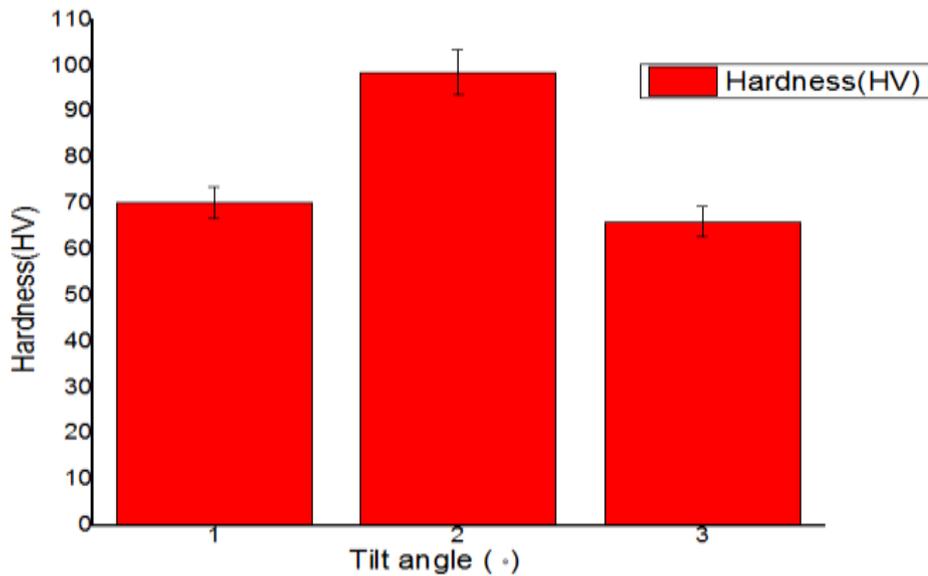
**Figure 4.3: Hardness values at varying tilt angle**

### c. Effect of rotational speed on hardness

The hardness (HV) of the weldment increased slightly from 73.78 HV at 1150 rpm to 74.0 HV at 1850 tool rotational speed, higher values of hardness can be achieved between the range of rotational speed this is an indication that there little or no difference in Hardness at low and very high values of tool rotational speed. This is because mechanical properties increases up to a certain limit and then begins to decrease as reported by Divya *et al,* (2014). Hardness values at varying rotational speed is shown in Figure 4.4.
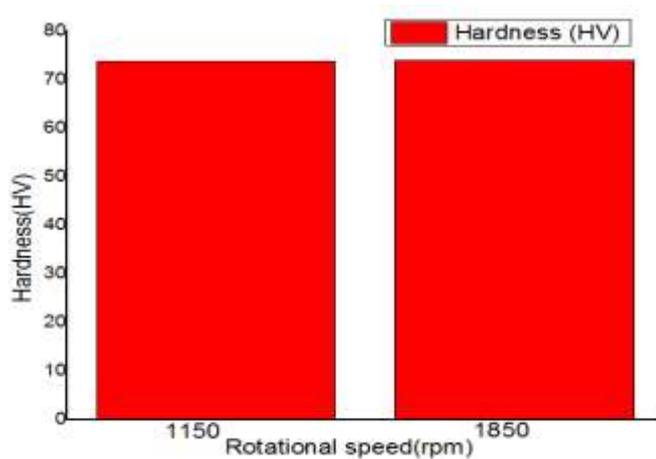


**Figure 4.4: Hardness at varying rotational**

92

## 4.3.1.2 Tensile analysis

The stress strain relationship obtained for the parameter combinations are shown in Figure 4.4 and the effect of welding speed on ultimate tensile strength is shown in Figure 4.5. The detailed analyses of the results are discussed in this section.
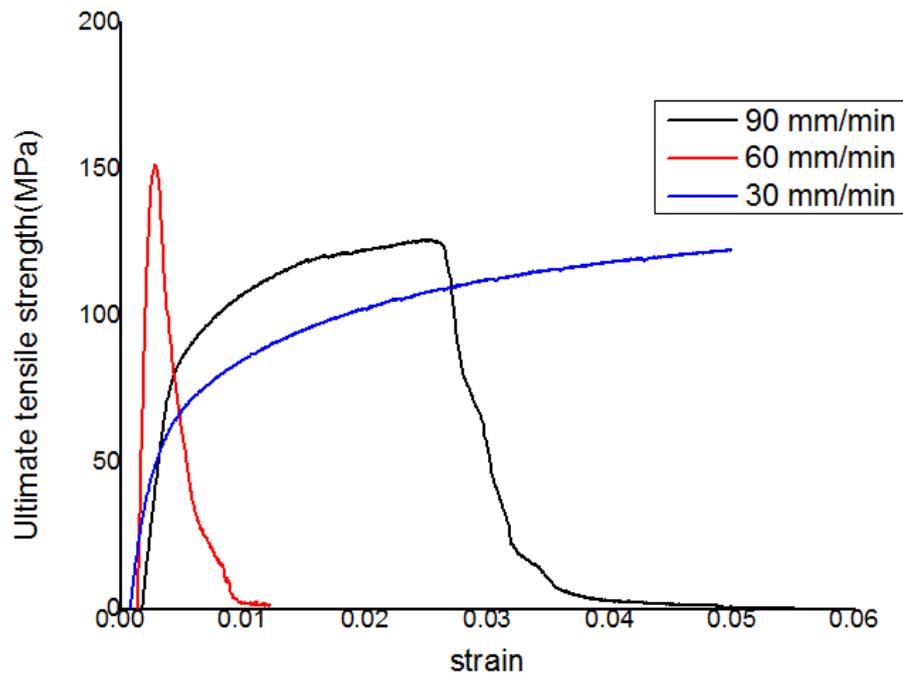


**Figure 4.5: Graph of stress against strain at different welding speeds**

**a.      Effect of welding speed on Ultimate tensile strength**

The UTS increased from 126.04 to 151.54 MPa with increase in welding speed from 30 mm/min to 60 mm/min. The UTS obtained was below that of the parent alloys. Although the UTS obtained at the three welding speeds as expected are lower than those of the base metals, however, their joint efficiencies which are significant enough is an indication of good bonding between the two alloys. Also it can be added that welding speed of 60 mm/min promotes better material mixing and bonding for the tapered tool weldment. At 90 mm/min welding speed, the speed was high not giving enough time for material mixing

and coalescence to occur as compared to the UTS value obtained at 60 mm/min welding speed. UTS at varying welding speeds are shown in Figure 4.6.
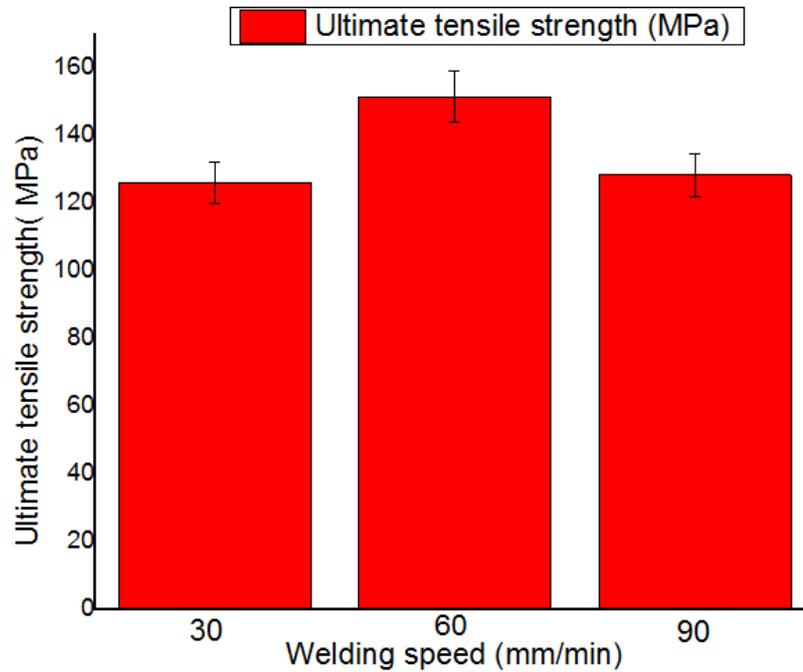


**Figure 4.6: UTS at varying welding speed**

**b.       Effect of Rotational speed on Ultimate tensile strength**

The ultimate tensile strength of the weldment at tool rotational speed of 1150 rpm is slightly higher than those of 1850 rpm. This may be due to high amount of heat generated by the tool at higher rotational speed as overheating leads to coarse grain size. This indicates that lower rotational speed of UTS was higher at 1150 rpm and but lower at 1850 rpm. UTS at varying rotational speed are shown in Figure 4.7.
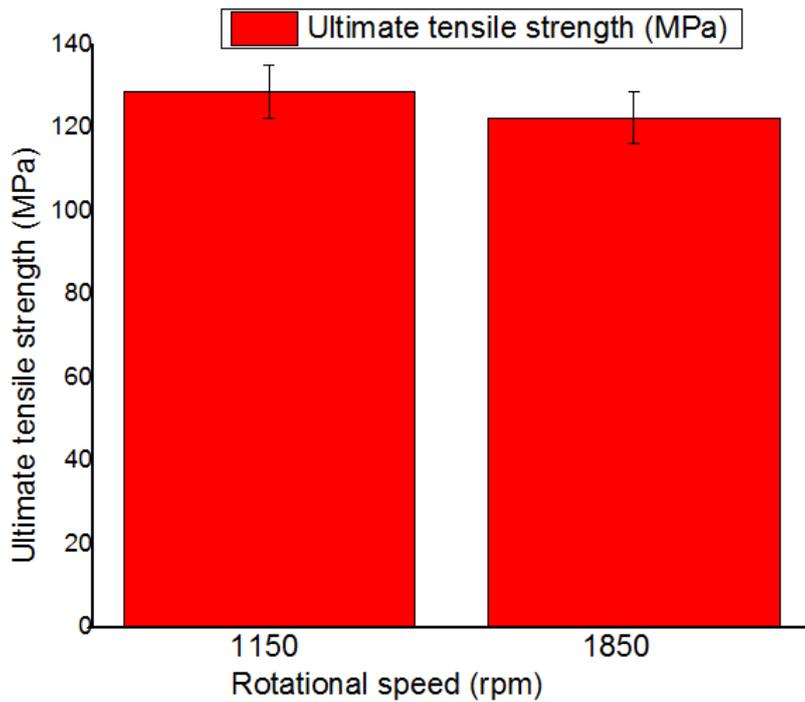
**Figure 4.7: UTS at varying rotational speed**

### c.  Effect of Tilt angle on UTS

The UTS is seen in Figure 4.7 to have increased from 123.32 MPa to 151.54 MPa as the tilt angle was increased from 1 to 2˚ and then decreased to 122.2 MPa with an increase in tilt angle from 2 to 3˚. This is an indication that tool tilt angle of $2^o$ favours better material transport leading to a better mixing of the alloys and proper metallurgical bonding as well as formation of void free joints which results in increased tensile strength of the weldment. UTS at varying tilt angle are shown in Figure 4.8.
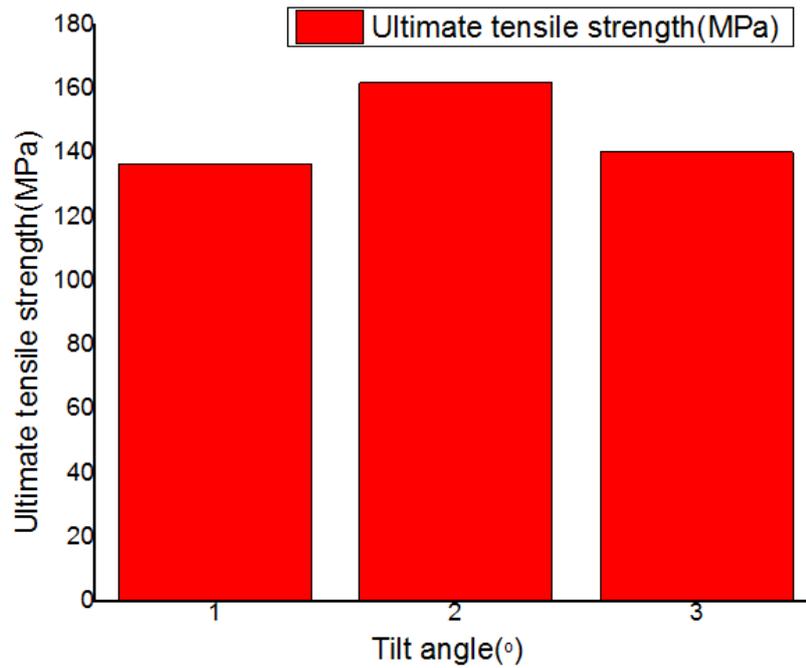
**Figure 4.8: UTS values at varying tilt angle**

### 4.3.1.3 Impact energy analysis

**a.** **Impact energy at different weld speed**

The impact energy increased from 12.9 to 21.4 J when the welding speed was increased from 30 mm/min to 60 mm/min. This can be attributed to proper bonding at medium welding speed of 60 mm/min as compared to low welding speed of 30 mm/min, an indication that welding speed of 60 mm/min encourages proper mixing and bonding.
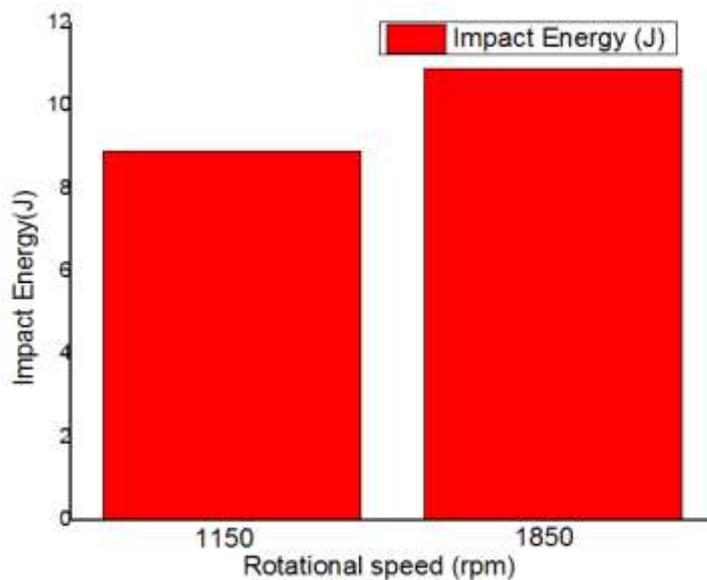
Also, at 90 mm/min welding speed, the impact energy decreased from 21.4 to 5.4 J, this may be because at 90 mm/min (higher welding speed) the tool traverses faster and not giving sufficient room for material coalescence to occur. Impact energy at varying welding speed is shown in Figure 4.9.
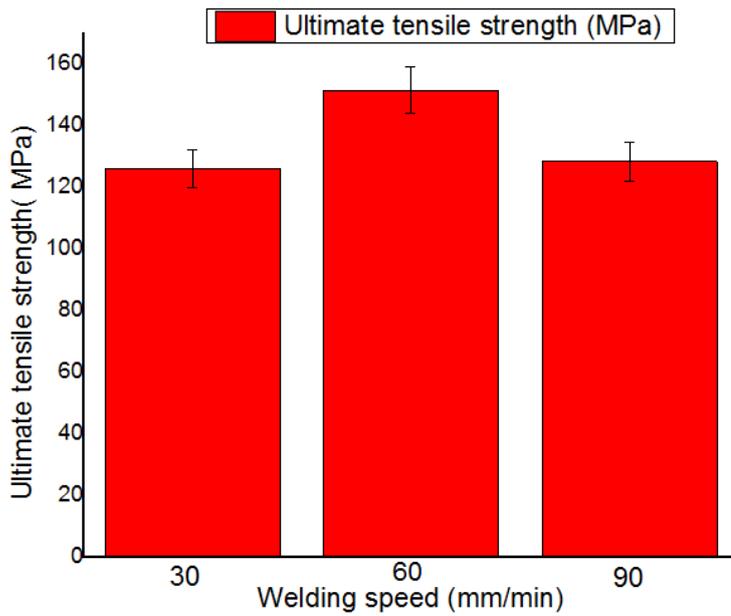
**Figure 4.9: Impact energy at varying weld speed**

### b. Effect of rotational speed on impact energy

The impact energy increased from 8.9 J to 10.9 J as rotational speed increased from 1150 rpm to 1850 rpm. This may be due of better material coalescence at higher heat input supplied with the higher rotational speed of the tool. Impact energy at varying rotational speed is shown in Figure 4.10.



**Figure 4.10: Impact energy at varying rotational speed**

### c. Effect of tilt angle on impact Energy

At constant rotational and welding speeds of 1500 rpm and 60 mm/min, respectively and varying the tool tilt angle, the impact energy increased as the tilt angle increased up to a certain limit and then began to decrease. As illustrated in Figure 4.9, the tilt angle of 2 $^\circ$ gave the highest average impact energy value of 21.4 J; this is because at this angle, there is better tool shoulder and workpiece surface interaction resulting in better plastic deformation and mixing of the alloys. Effect of tilt angle on impact energy is shown in Figure 4.11.
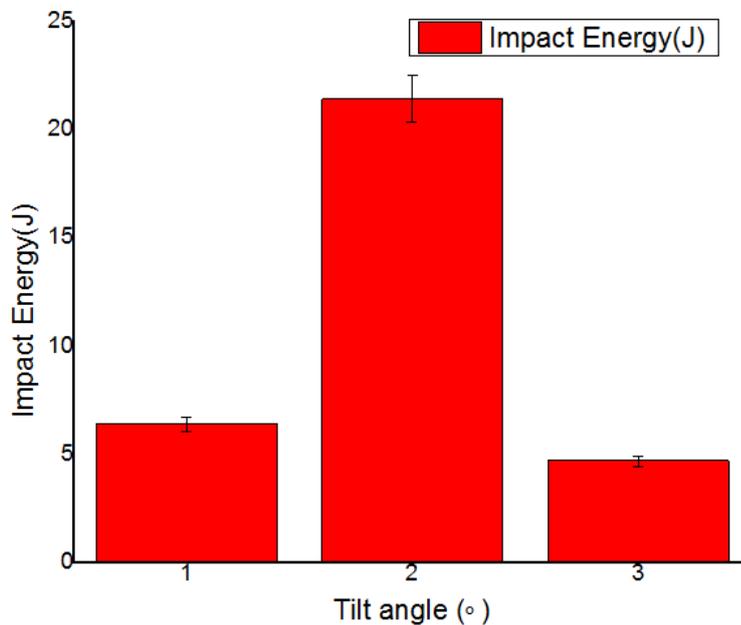


**Figure 4.11: Effect of tilt angle on impact energy**

### 4.3.2 Tapered Threaded Tool weldment (TTT)

### 4.3.2.1 Hardness analysis

### a. Hardness at different welding speed

The hardness test performed on the two base metals gave hardness values of 50 HV and 175 HV for AA1200-H19 and AA7075-T651, respectively. The hardness profile is shown in Figure 4.12. The average hardness increased from 77.8 to 105.25 HV. This can be

attributed to better grain refinement and mixing at 60 mm/min welding speed. Also, at the 60 mm/min welding speed precipitation of hardening precipitates was encouraged.

At 30 mm/min welding speed, the average hardness of 77.8 HV obtained was higher than that of the AA 1200 H-19 aluminium alloy and below that of 7075-T651 indicating occurrence of mixing of both alloys at the nugget zone. At 90 mm/min welding speed (high speed), the average hardness decreased from 105.25 to 81.77 HV, this can be attributed to dissolution of strengthening precipitates. Also, at 90 mm/min welding speed, the tool traversed faster on the material (dwelling time was low) not giving sufficient time for material coalescence to occur.

The hardness values obtained at the HAZ of the advancing side was lower than the hardness value of the base metal AA 1200 H-19 aluminium alloys. This may be attributed to subjection of the alloy to thermal cycle during welding resulting in dissolution of the alloy's precipitates and leading to reduction in hardness (Abolusoro & Akinlabi, 2020). On the retreating side, the hardness values were lower than that of the base metal AA7075-T651.

The average hardness values obtained at the NZ were higher than those of the base metal AA1200- H19 but lower than the base metal AA7075- T651. This is due to mixing of both alloys at this region. Also, the average hardness at the NZ is higher than those of the HAZ of both the advancing and retreating sides. This can be attributed to presence of inter-metallic compounds formed during the welding (Raju *et al,* 2016).
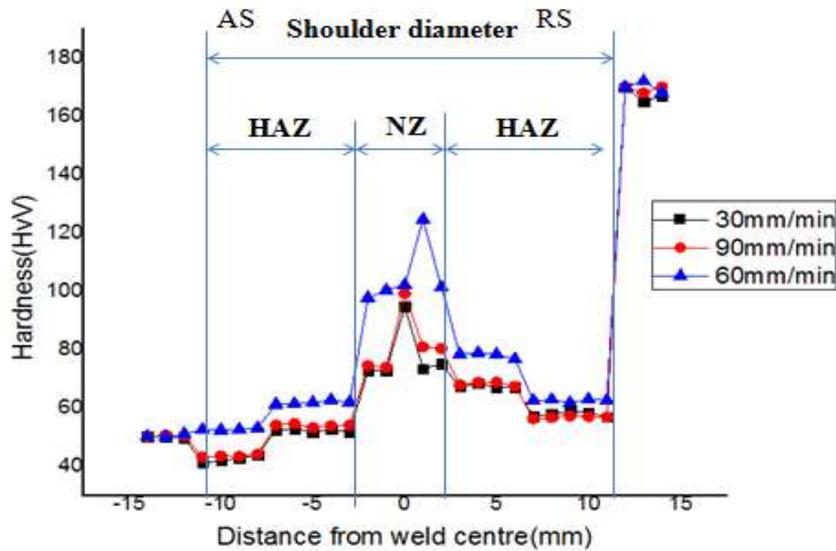
**Figure 4.12: Hardness profile for tapered threaded tool**

**b.      Effect of tilt angle on hardness**

The average hardness value at constant tool rotational and welding speeds of 1500 rpm and 60 mm/min respectively is seen to increase from 88.8 HV to 105.25 HV with increase in tool tilt angle from 1 to $2^{\circ}$ due to formation of intermetalics resulting from temperature rise in stir zone. Also, this is because the tilt angle prevents spreading of material on the surface of the weldment which may result in flash defects. The tilt angle encourages material flow which results in good metallurgical bonding between the two alloys. A further increase in tilt angle from 2 to $3^{\circ}$ resulted in reduction in hardness from 105.25 HV to 85.15 HV. Hardness values at varying tilt angle is shown in Figure 4.13
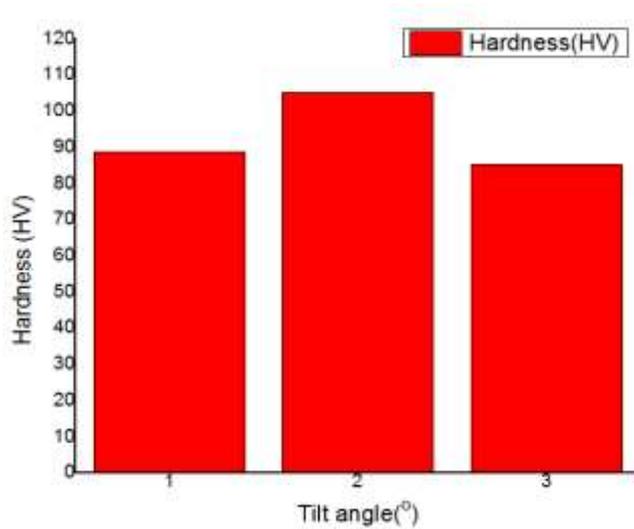
**Figure 4.13: Hardness values at varying tilt angle**

c        **Effect of rotational speed on hardness**

There is no significant difference in the values of hardness at both levels of parameters as they are close to extreme conditions. The hardness value at 1150 rpm was 86.5 and dropped to 86.04 at 1850 rpm. However, higher values of hardness can be obtained in between the range of parameters. This conforms to the findings of Divya *et al.*, (2014). A hardness value at varying rotational speed is shown in Figure 4.14.
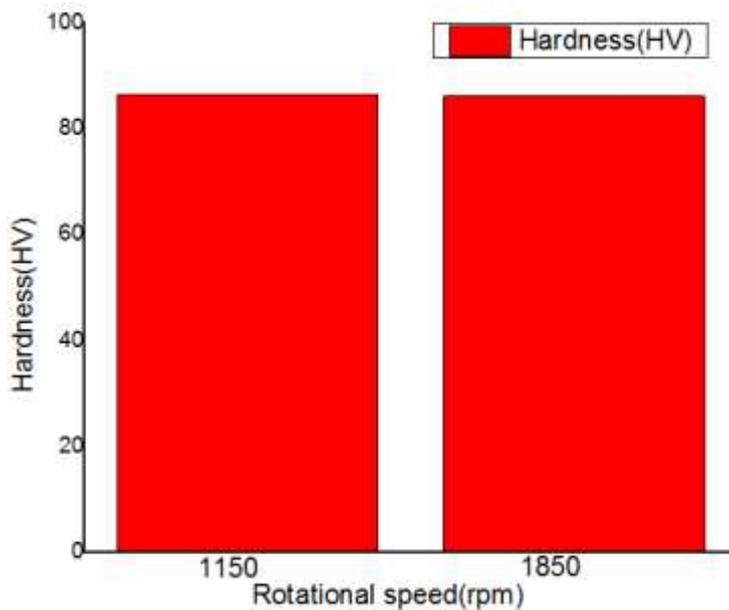


**Figure 4.14: Hardness at varying rotational speed**

### 4.3.2.2 Tensile analysis

The stress strain relationship obtained for the parameter combination are shown in Figure 4.12 and the effect of welding spe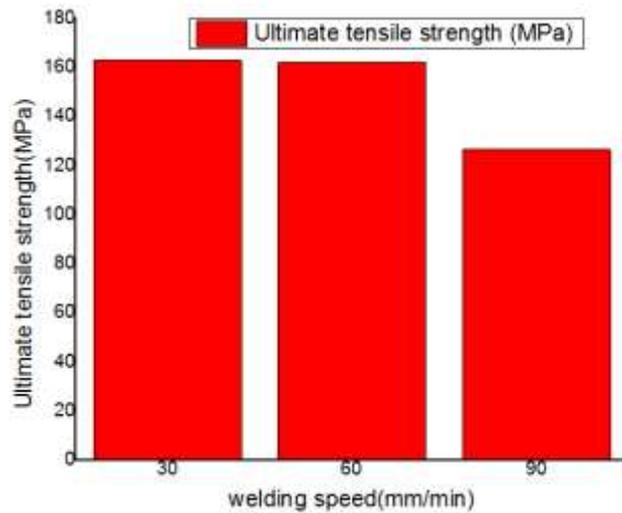ed on ultimate tensile strength is shown in Figure 4.13. The detailed analyses of the results are discussed in this section.
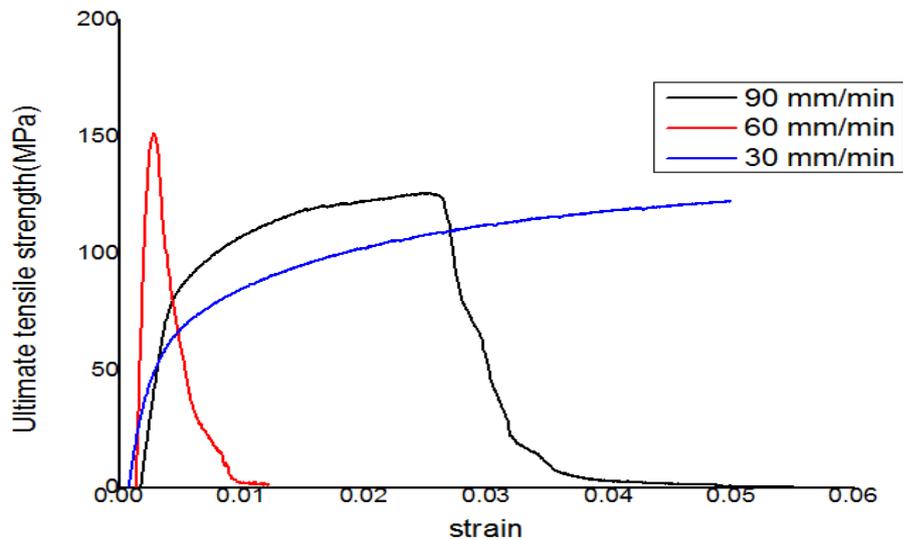


**Figure 4.15: Graph of stress against strain at different welding speeds**

### a. Effect of welding speed on ultimate tensile strength

The values 162.66 MPa and 161.8 MPa were respectively obtained as UTS values when the welding speed was increased from 30 to 60 mm/min, respectively indicating that there was little or no change in UTS values at the varied speed range. The two values were lower than those of the two base alloys. However, the UTS values dropped to 126.45 MPa at 90 mm/min welding speed, an indication that the speed was high and not giving room for material coalescence to occur. UTS values at varying welding speed are shown in Figure 4.16.

**Figure 4.16: UTS at varying welding speed**

**b.        Effect of Rotational speed on Ultimate tensile strength**

The ultimate tensile strength of the weldment at tool rotational speed of 1150 rpm is slightly higher than those of 1850 rpm. This may be due to high amount of heat generated by the tool at higher rotational speed as overheating leads to coarse grain size. This indicates that lower rotational speed of 1150 rpm favours higher UTS value. UTS values at varying rotational speed are shown in Figure 4.17.
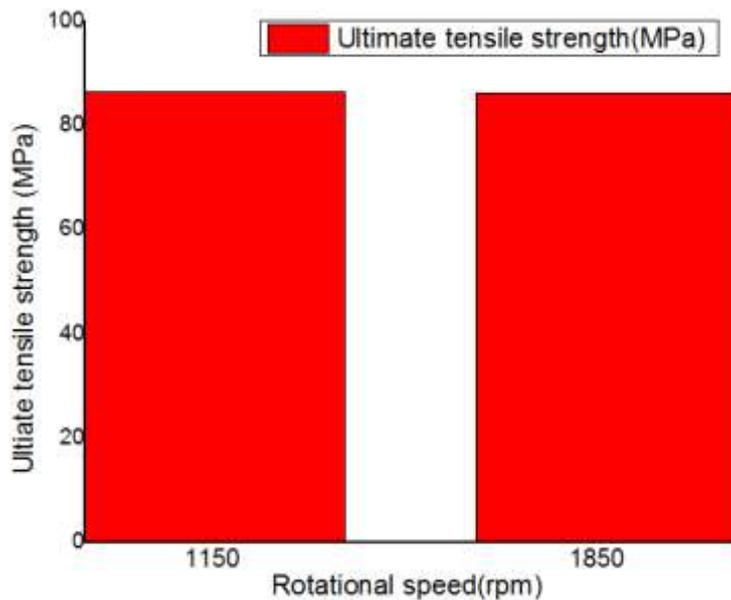


**Figure 4.17: UTS at varying rotational speed**

### c. Effect of Tilt angle on UTS

The UTS is seen in Figure 4.15 to have increased from 136.51 MPa to 161.8 MPa as the tilt angle was increased from 1 to 2 ° and then decreased to 140.27 MPa with an increase in tilt angle from 2 to 3 °. This is an indication that tool tilt angle of 2 ° favours better material transport leading to a better mixing of the alloys and proper metallurgical bonding as well as formation of void free joints which results in increased tensile strength of the weldment. UTS values at varying tilt angle are shown in Figure 4.18.
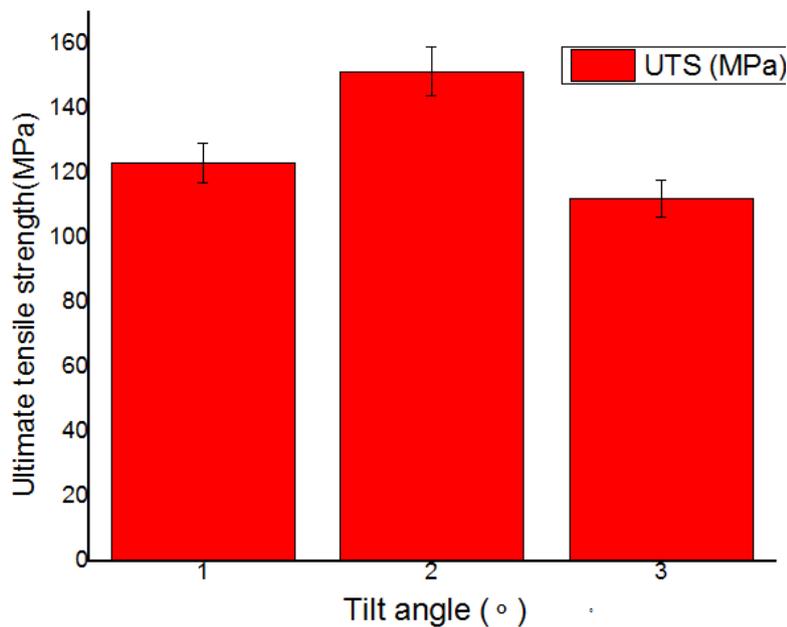


**Figure 4.18: UTS values at varying tilt angle**

### 4.3.2.3 Impact energy analysis

### a. Impact Energy at Different Weld Speed

The impact energy increased from 16.9 to 23.4 J when the welding speed was increased from 30 mm/min to 60 mm/min. This can be attributed to proper bonding at medium welding speed of 60 mm/min as compared to low welding speed of 30 mm/min, an indication that welding speed of 60 mm/min encourages proper mixing and bonding.
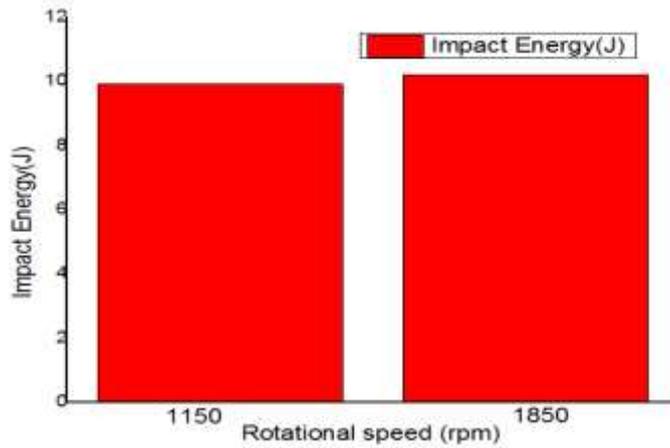
Also, at 90 mm/min welding speed, the impact energy decreased from 23.4 to 14.7 J, this may be because at 90 mm/min (higher welding speed) the tool traverses faster and not giving sufficient room for material coalescence to occur. Impact energy at varying welding speed is shown in Figure 4.19.
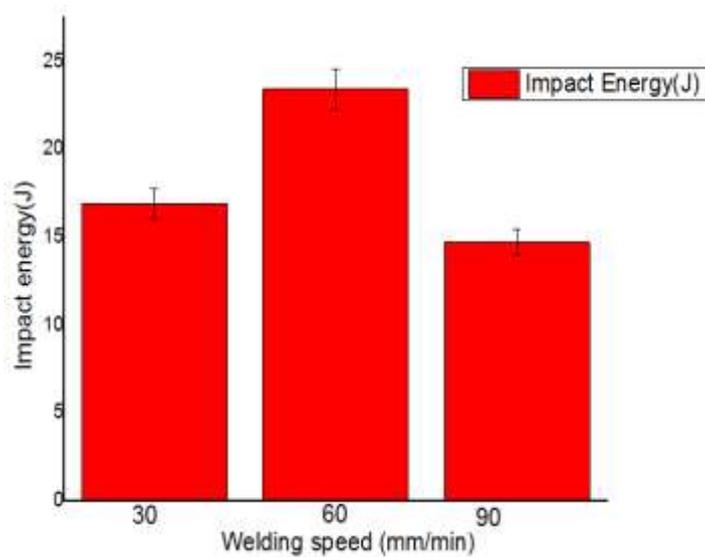


**Figure 4.19: Impact energy at varying weld speed**
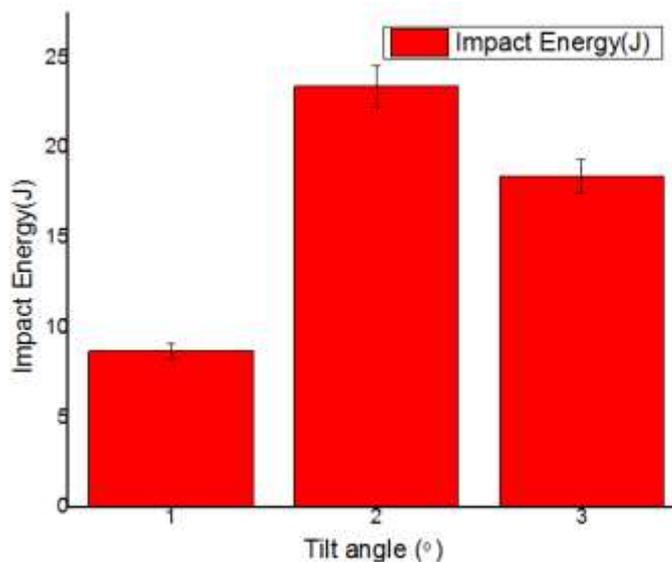
**b        Effect of rotational speed on impact energy**

There is little or no difference in impact energy values as both are very close to extreme conditions of the process parameters. The impact energy at 1150 rpm was 9.9 J and at 1850 rpm it was 10.2 J, however higher impact energy values can be obtained it between the ranges of parameters. Impact energy at varying rotational speed s shown in Figure 4.20

**Figure 4.20: Impact energy at varying rotational speed**

**c.  Effect of tilt angle on impact Energy**

At constant rotational and welding speeds of 1500 rpm and 60 mm/min, respectively and varying the tool tilt angle, the impact energy increased as the tilt angle increased up to a certain limit and then began to decrease. As illustrated in Figure 4.17, the tilt angle of 2˚ gave the highest average impact energy value of 23.4 J; this is because at this angle, there is better tool shoulder and workpiece surface interaction resulting in better plastic deformation and mixing of the alloys. Effect of tilt angle on impact energy is shown in Figure 4.21.



**Figure 4.21: Effect of tilt angle on impact energy**

c. Impact Energy at different rotational speed

## 4.4 Statistical Analysis and Model Fitting

### 4.4.1 ANOVA for tapered tool (TT) weldment

The ANOVA results for TT are presented in Tables 4.6 – 4.8

### 4.4.1.1 ANOVA for hardness

**Table 4.6: ANOVA for hardness**

| Factor | DOF | SS | MS | F | P |
|--------|-----|------|--------|-------|-------|
| Rotational speed | 4 | 1038 | 259.5 | 14.01 | 34.45 |
| Transverse speed | 4 | 585.9 | 146.47 | 7.91 | 19.44 |
| Tool Tilt Angle | 4 | 1259 | 314.75 | 16.99 | 41.79 |
| Error | 7 | 129.60 | 18.51 | | 4.30 |
| Total | 19 | 3012.50 | 158.55 | | 100 |

As shown in Table 4.6, it can be observed that the tool tilt angle (41.79 %) has the highest contribution to the hardness, followed by rotational speed (34.46 %) and finally the transverse speed (19.44 %). The percentage error recorded during this analysis was 4.3 %.

### 4.4.1.2 ANOVA for UTS

**Table 4.7: ANOVA for UTS**

| Factor | DOF | SS | MS | F | P |
|--------|-----|----------|---------|-------|-------|
| Rotational speed | 4 | 6894 | 1723.5 | 60.57 | 35.03 |
| Transverse speed | 4 | 5949 | 1487.25 | 52.27 | 30.23 |
| Tool Tilt Angle | 4 | 6636 | 1659 | 58.31 | 33.72 |
| Error | 7 | 199.15 | 28.450 | | 1.01 |
| Total | 19 | 19678.15 | 1035.69 | | 100 |

As shown in Table 4.7, it can be observed that the tool rotational speed (35.03 %) has the highest contribution to the UTS, followed by tilt angle (33.72 %) and finally the transverse speed (30.23 %). The percentage error recorded during this analysis was 1.01 %.

### 4.4.1.3 ANOVA for impact energy

**Table 4.8: ANOVA for Impact**

| Factor | DOF | SS | MS | F | P |
|---|---|---|---|---|---|
| Rotational speed | 4 | 157.3 | 39.32 | 18.67 | 37.45 |
| Transverse speed | 4 | 134.4 | 33.6 | 15.95 | 32.00 |
| Tool Tilt Angle | 4 | 113.5 | 28.37 | 13.47 | 27.02 |
| Error | 7 | 14.73 | 2.10 | | 3.50 |
| Total | 19 | 419.93 | 22.10 | | 100 |

As shown in Table 4.8, it can be observed that the tool rotational speed (37.45 %) has the highest contribution to the impact energy, followed by transverse speed (32.00 %) and finally the tilt angle (27.02 %). The percentage error recorded during this analysis was 3.5 %.

### 4.4.2   Analysis of variance (ANOVA) for tapered threaded tool (TTT)

The ANOVA results for TT are presented in Tables 4.9 – 4.11

### 4.4.2.1 ANOVA for hardness

**Table 4.9: ANOVA for hardness**

| Factor | DOF | SS | MS | F | P |
|---|---|---|---|---|---|
| Rotational speed | 4 | 741 | 185.25 | 56.18 | 36.97 |
| Transverse speed | 4 | 795.4 | 198.85 | 60.30 | 39.69 |
| Tool Tilt Angle | 4 | 444.5 | 111.125 | 33.70 | 22.18 |
| Error | 7 | 23.08 | 3.297 | | 1.15 |
| Total | 19 | 2003.98 | 105.47 | | 100 |

As shown in Table 4.9, it can be observed that the tool transverse speed (39.69 %) has the highest contribution to the hardness, followed by rotational speed (36.97 %) and finally the tilt angle (22.18 %). The percentage error recorded during this analysis was 1.15 %.

### 4.4.2.2 ANOVA for UTS

**Table 4.10: ANOVA for UTS**

| Factor | DOF | SS | MS | F | P |
|---|---|---|---|---|---|
| Rotational speed | 4 | 769.4 | 192.3 | 8.91 | 25.46 |
| Transverse speed | 4 | 1248 | 312 | 14.46 | 41.29 |
| Tool Tilt Angle | 4 | 853.4 | 213.35 | 9.88 | 28.24 |
| Error | 7 | 151.02 | 21.57 | | 4.99 |
| Total | 19 | 3021.82 | 159.04 | | 100 |

As shown in Table 4.10, it can be observed that the tool transverse speed (41.29 %) has the highest contribution to the UTS, followed by tilt angle (28.24 %) and finally the transverse speed (25.46 %). The percentage error recorded during this analysis was 4.99 %.

### 4.4.2.3 ANOVA for impact energy

**Table 4.11: ANOVA for impact**

| Factor | DOF | SS | MS | F | P |
|---|---|---|---|---|---|
| Rotational speed | 4 | 259.5 | 64.87 | 24.21 | 52.57 |
| Transverse speed | 4 | 95.4 | 23.85 | 8.90 | 19.32 |
| Tool Tilt Angle | 4 | 119.9 | 29.97 | 11.19 | 24.29 |
| Error | 7 | 18.75 | 2.67 | | 3.80 |
| Total | 19 | 493.55 | 25.97 | | 100 |

As shown in Table 4.11, it can be observed that the tool rotational speed (52.57 %) has the highest significant effect on the UTS, followed by tilt angle (24.29 %) and finally the transverse speed (19.32 %). The percentage error recorded during this analysis was 3.80 %.

### 4.4.3   Regression equations for tapered tool weldment

The empirical model for the responses along with their corresponding regression correlation coefficients (R-sq) are shown in equation 4.7-4.9. The RS, TS and TTA in the equations represent rotational speed, transverse speed and tool tilt angles, respectively. The regression equation for each property (response) was obtained using the Minitab 17 software. The optimal parameters were obtained from the gray relational analysis (GRA) and used to validate the equations. The R-square values for an ideal condition ranges between 80 and 100% (Montgomery *et al.*, 1998).

### 4.4.3.1 Regression equation for harness

Hardness (Vickers) = -394.9 + 0.2766 RS + 4.143 TS + 162.1 TTA - 0.000078 RS*RS- 0.02193 TS*TS - 31.12 TTA*TTA - 0.000383 RS*TS - 0.00704 RS*TTA- 0.493 TS*TTA           (4.1)
 R-sq = 94.56 %, R-sq (adj) = 89.67 %

Hardness = 99.102 HV

The full quadratic equation was used and it was not transformed. The R-sq values are as presented. The R-sq and R-sq (Adj) are suitable as they both fell within the range of ideal condition (80-100 %) despite experimental uncertainties

### 4.4.3.1 Regression equation for UTS

UTS (MPa) = -278.5 + 0.3064 RS + 3.154 TS + 105.9 TTA - 0.000106 RS*RS - 34.37 TTA*TTA - 0.000099 RS*TS + 0.01046 RS*TTA + 0.184 TS*TTA           (4.2)
R-sq = 97.83%     R-sq (Adj) = 95.89%

UTS = 150 MPa

The full quadratic equation was used and it was not transformed. The R-Sq values obtained are as presented. The R-sq and R-sq (Adj) are suitable as they both fell within the range of ideal condition (80-100 %) despite experimental uncertainties

### 4.4.3.3     Regression equation for impact energy

Impact Energy (J)^0.5  =  -11.44 + 0.01577 RS - 0.0017 TS + 3.45 TTA -
0.000004 RS*RS- 0.000779 TS*TS - 1.310 TTA*TTA - 0.000009 RS*TS
- 0.00055 RS*TTA+ 0.0414 TS*TTA

$$(4.3)$$

R-sq = 76.99%          R-sq (adj) = 56.29 %

Impact Energy (I.E) = 20.0399 J

The full quadratic equation was used and it was transformed using square root. R-sq and

R-sq (Adj) values obtained are as shown. The R-sq values are below 80 %, this is due to

uncontrollable noise effect.

### 4.4.4   Empirical regression equations for tapered threaded tool weldment

The empirical model equation for the responses along with its corresponding regression

correlation coefficients (R-sq) are shown in equations 4.10-4.12. The RS, TS and TTA in

the equations represent rotational speed, transverse speed and tool tilt angles,

respectively.

### 4.4.4.1       Regression equation for hardness

Hardness (Vickers) = -234.0 + 0.21166 RS + 3.500 TS + 76.56 TTA
- 0.000070 RS*RS - 0.028530 TS*TS - 18.487 TTA*TTA + 0.000013 RS*TS
- 0.00194 RS*TTA- 0.0302 TS*TTA                                                             (4.4)


R-sq = 99.45 %        R-sq (adj) = 98.95 %

Hardness = 104.18 HV

The full quadratic equation was used and it was not transformed. R-sq values as shown

were obtained. The R-sq and R-sq (Adj) are suitable as they both fell within the range of

ideal condition (80-100 %) despite experimental uncertainties

### 4.4.4.2       Regression equation for UTS

UTS (MPa) =  -39 + 0.1540 RS + 0.19 TS + 77.9 TTA - 0.000067 RS*RS
- 0.02045 TS*TS - 24.57 TTA*TTA + 0.000844 RS*TS - 0.0002 RS*TTA
+ 0.402 TS*TTA                                                                                          (4.5)
R-sq = 75.14 %    R-sq ( adj) = 52.76 %

UTS = 161.2 MPa

The linear square equation was used and it was not transformed. R-sq values as shown were obtained and are less than 80 % due to uncontrollable noise

### 4.4.4.3 Regression equation for impact energy

Impact Energy (J) = -8.6 + 0.0702 RS - 0.358 TS - 18.7 TTA
- 0.000026 RS*RS+ 0.00125 TS*TS - 1.12 TTA*TTA - 0.000076 RS*TS
+ 0.01000 RS*TTA+ 0.163 TS*TTA                                    (4.6)

R-sq = 69.01 %      R-sq (Adj) = 52.12 %

Impact Energy (I.E) = 22.15 J

The full quadratic equation was used and it was not transformed. R-sq values as shown were obtained. The R-sq (adj) is below 80 % due to uncontrollable noise effect.

## 4.5      Interactive Effects of Process Parameters on Mechanical Properties

### 4.5.1    Interactive effects of process parameters for tapered tool weldment

The interaction plot for the hardness response of tapered tool weldment is shown in Figure 4.30.
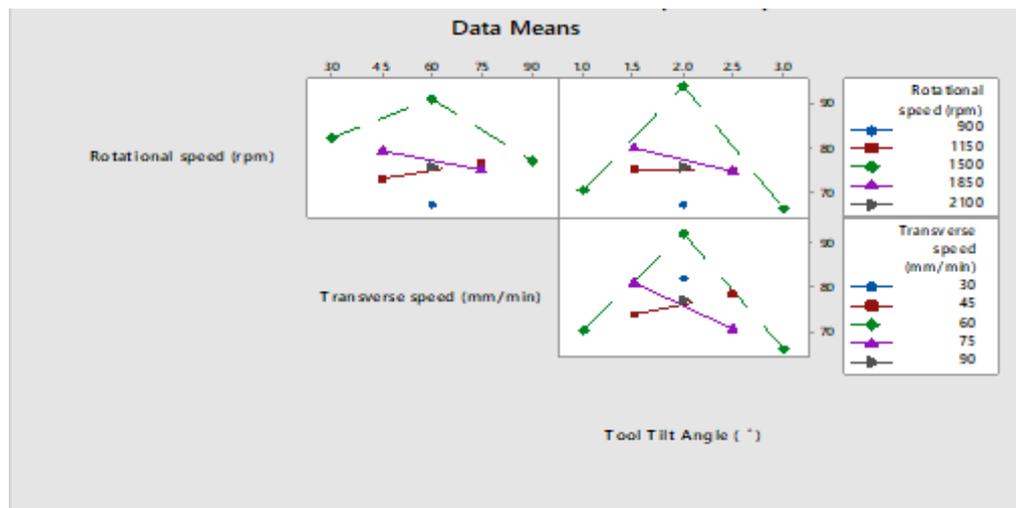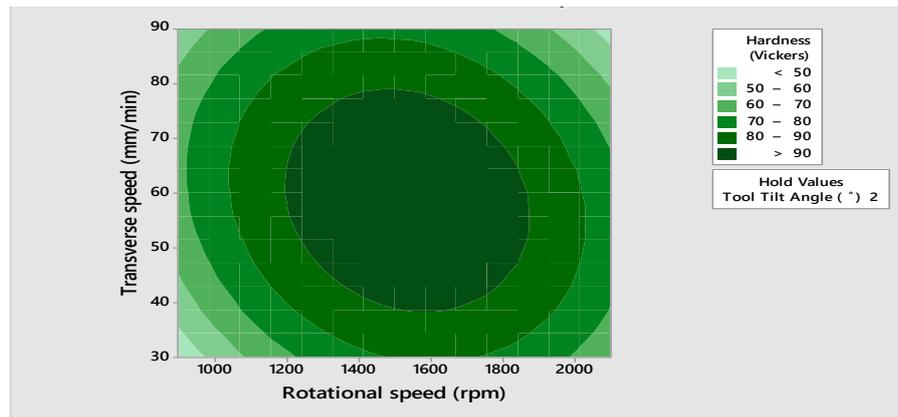


**Figure 4.22: Interaction plot for hardness (Vickers)**

The interaction plot obtained in Figure 4.22 shows that there is interaction between the three process parameters used. The interaction plots for other responses are shown in appendix A.

### 4.5.1.1 Hardness at various constant process parameters using contour plots

### i      hardness at constant tilt angle

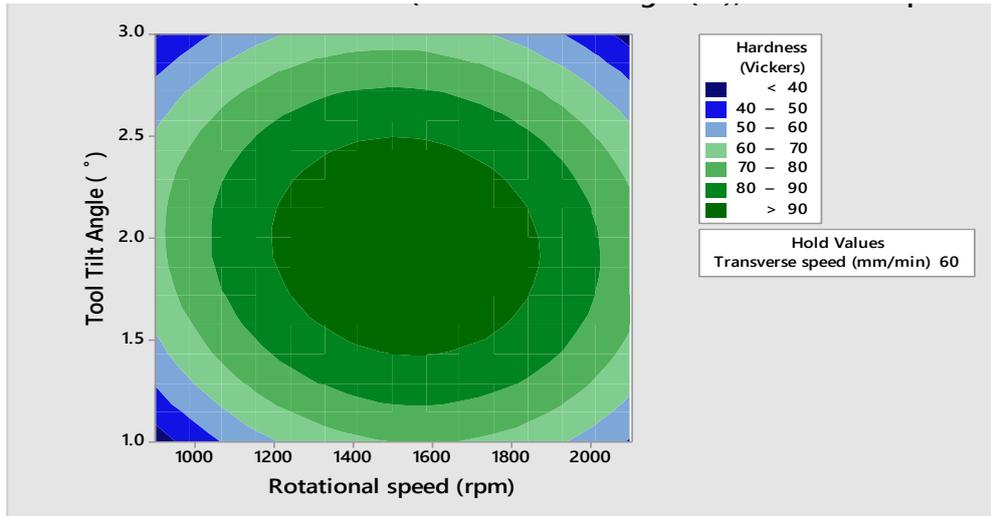The contour plot for the hardness of the weldment at constant tilt angle is shown in Figure 4.23



**Figure 4.23: Contour plot for hardness at constant tilt angle**

The contour plot indicates how change in tool rotational speed (rpm) and transverse speed (mm/min) affects the hardness (Vickers) of the weldment while keeping the tool tilt angle constant at $2^\circ$. The result indicates that a hardness of 80-90 HV can be achieved using TS of 45 mm/min and RS of 1150 rpm. The 3D surface plot is presented in Appendix B.

### ii.      Hardness at constant transverse speed

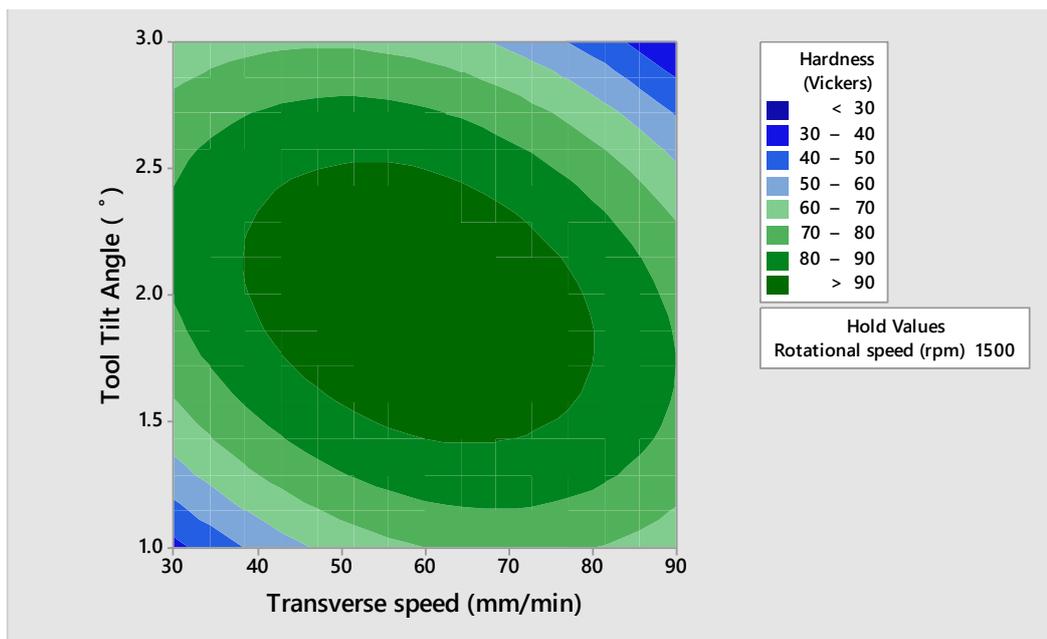The contour plot for the hardness of the weldment at constant transverse speed is shown in Figure 4.24.

**Figure 4.24: Contour plot for hardness at constant traverse speed**

The contour plot indicates how change in tool tilt angle ($^{\circ}$) and rotational speed (rpm) affects the hardness (Vickers) of the weldment while keeping the transverse speed constant at 60 mm/min The result indicates that a hardness of 80-90 HV can be achieved using tilt angle of 2.4 $^{\circ}$ and RS of 1900 rpm. The 3D surface plots is presented in Appendix C.

**iii.  Hardness at constant rotational speed**

The contour plot for the hardness of weldment at constant rotational speed is shown in Figure 4.25



**Figure 4.25: Contour plot of hardness at constant rotational speed**

The contour plot indicates how change in tool tilt angle ( $^0$ ) and transverse speed (mm/min) affects the hardness (Vickers) of the weldment while keeping the tool rotational speed (rpm) constant at 1500 rpm. The result indicates that a hardness of 80-90 HV can be achieved using tilt angle of 1.5 $^o$ and TS of 45 mm/min. The 3D surface plots are presented in Appendix D.

### 4.5.1.2 UTS at various constant process parameters

**i.        UTS at constant tilt angle**

The contour plot for UTS of the weldment at constant tilt angle of the tool is shown in Figure 4.26
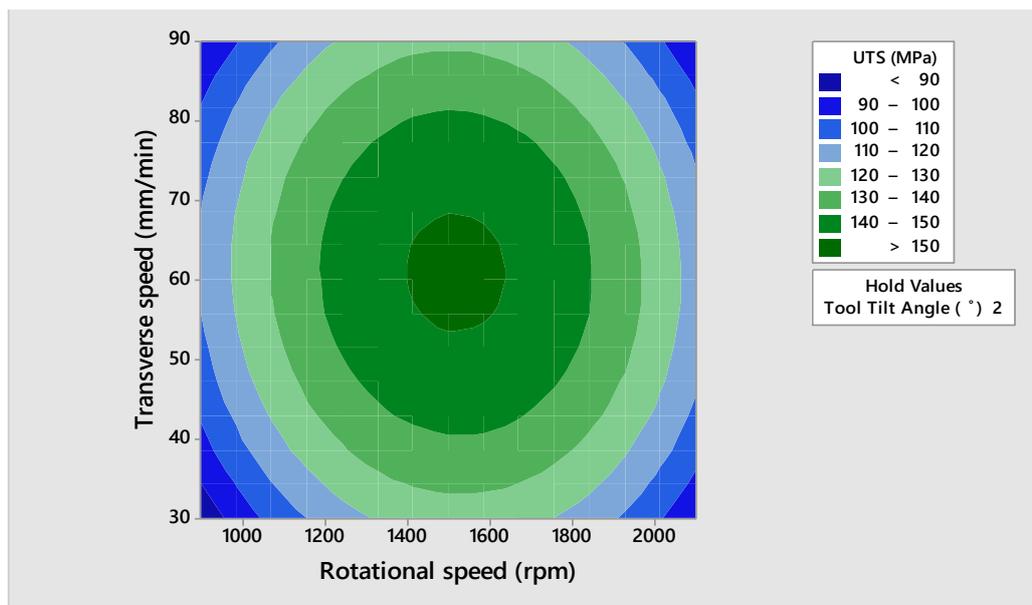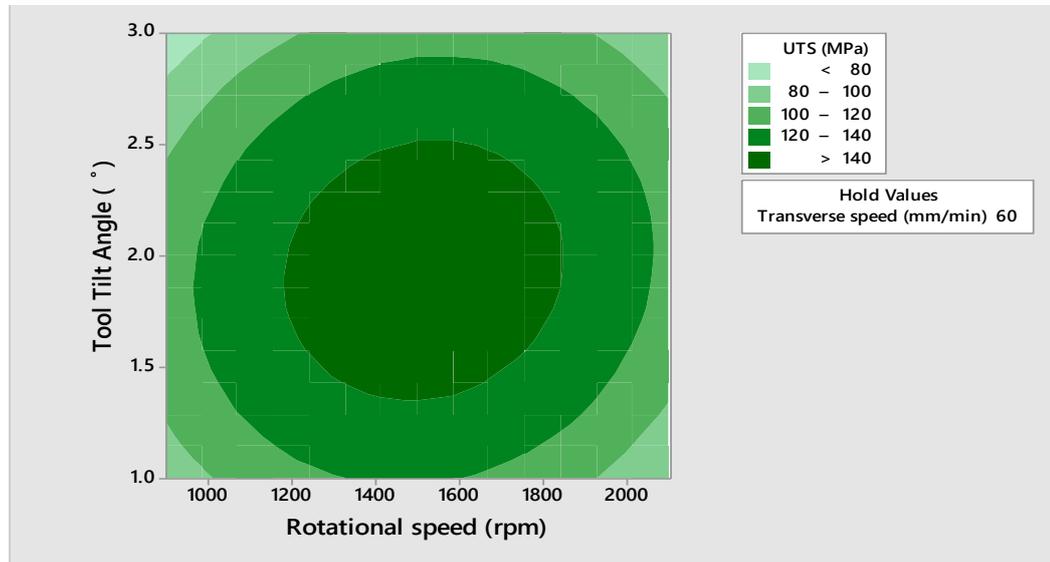


**Figure 4.26: Contour plot for UTS at constant tilt angle**

The contour plot indicates how change in tool rotational speed (rpm) and transverse speed (mm/min) affects the UTS values of the weldment while keeping the tool tilt angle constant at 2 $^°$. The result indicates that UTS values of 140-150 MPa can be achieved using TS of 75 mm/min and RS of 1300 rpm. The 3D surface plot is presented in Appendix E.

## ii.    UTS at constant transverse speed

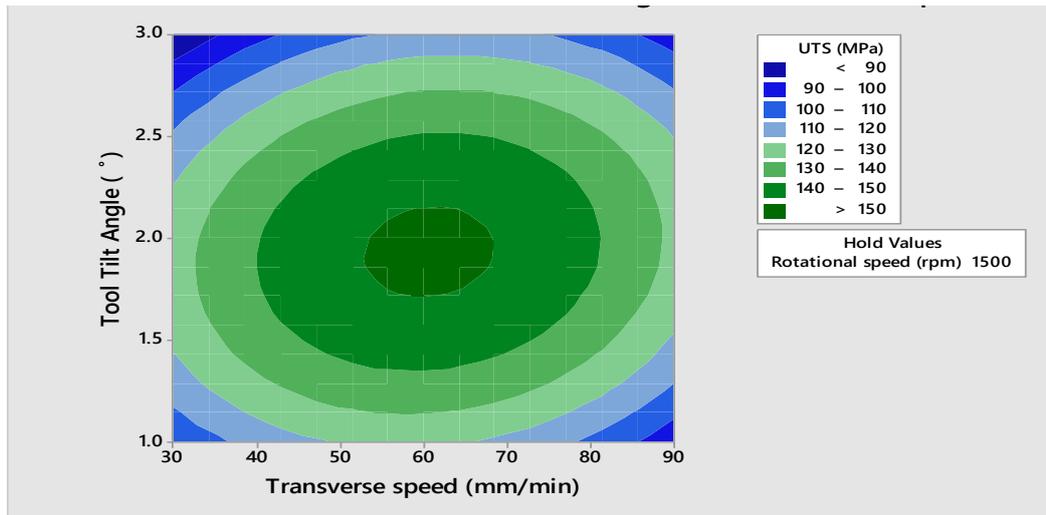Contour plot for UTS at constant transverse speed is shown in Figure 4.27.



**Figure 4.27: Contour plot for UTS at constant transverse speed**

The contour plot indicates how change in tool tilt angle (˚) and tool rotational speed (rpm) affects the UTS values of the weldment while keeping transverse speed (mm/min) constant at 60 mm/min. The result indicates that UTS values of 120-140 MPa can be achieved using tilt angle of 1.52 ˚ and RS of 1000 rpm. The 3D surface plot is presented in Appendix F.

## iii.    UTS at constant rotational speed

The contour plot for UTS of the weldment at constant rotational speed is shown in Figure 4.28.
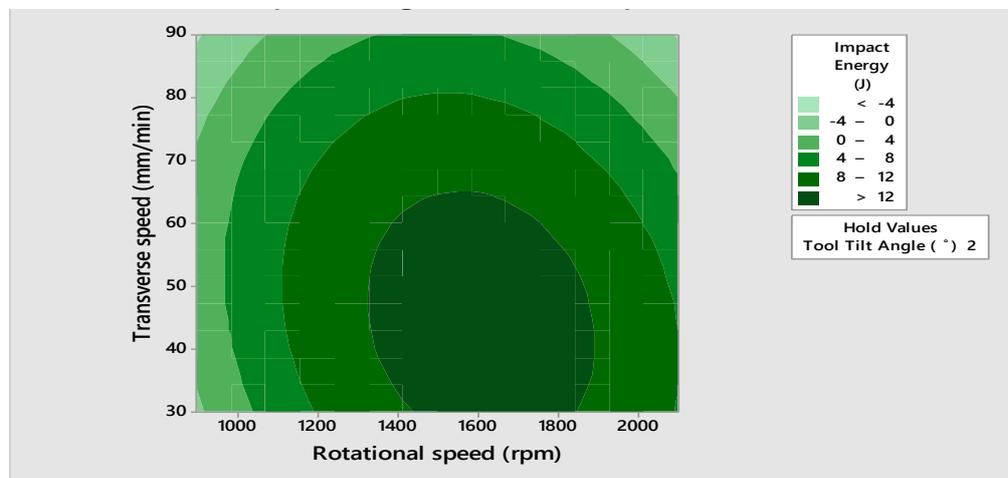
**Figure 4.28: Contour plot for UTS at constant rotational speed**

The contour plot indicates how change in tool tilt angle and transverse speed (mm/min) affects the UTS values of the weldment while keeping the tool rotational speed (rpm) constant at 1500 rpm. The result indicates that UTS values of 140-150 MPa can be achieved using tilt angle 1.75° and TS of 55 mm/min. The 3D surface plots are presented in Appendix G.

**4.5.1.3 Impact energy at various constant process parameters**

**i        Contour plot for impact energy at constant tilt angle**

The contour plot for the impact energy of the weldment at constant tilt angle is shown in Figure 4.29



**Figure 4.29: Contour plot for impact energy at constant tilt angle**

The contour plot indicates how change in tool rotational speed (rpm) and transverse speed (mm/min) affects the impact energy of the weldment while keeping the tool tilt angle constant at 2˚. The result indicates that impact energy values of 8-12 J can be achieved using TS of 50 mm/min and RS of 1150 rpm or 4-8 J at 1000 rpm, 40 mm/min or 1000 rpm, 50 mm/min.

**ii.      Impact Energy at constant transverse speed**

Contour plot for the impact energy of the at constant transverse speed is shown in Figure 4.30



**Figure 4.30: Contour plot for UTS at constant transverse speed**

The contour plot indicates how change in tool tilt angle and tool rotational speed (rpm) affects the impact energy of the weldment while keeping the transverse speed constant at 60 mm/min.  The result indicates that impact energy values of 5-10 J can be achieved using tilt angle 2˚ and rotational speed of 1050 rpm.

### iii. Impact energy at constant rotational speed
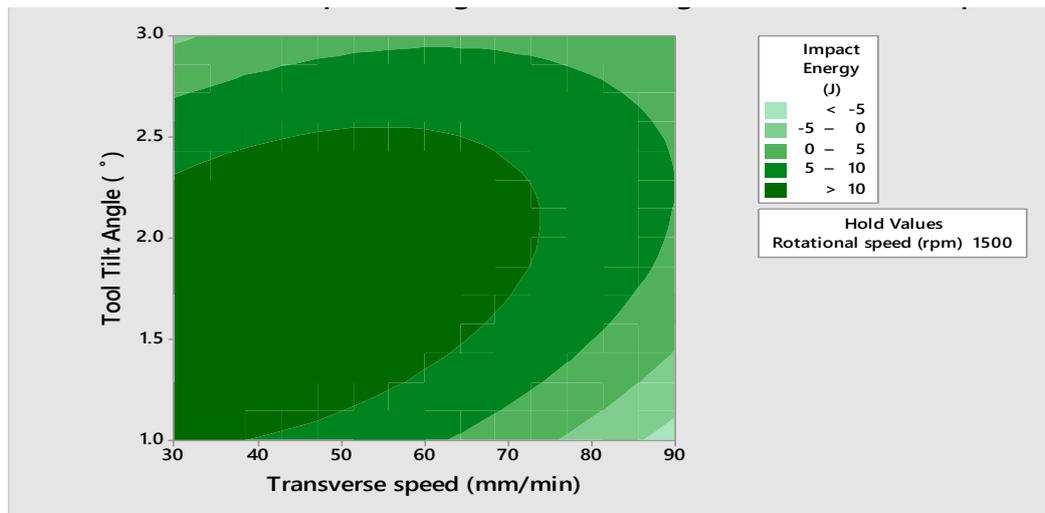


**Figure 4.31: Contour plots for impact energy at constant rotational speed**

The contour plot indicates how change in tool tilt angle and tool transverse speed (mm/min) affects the impact energy of the weldment while keeping the rotational speed constant at 1500 rpm. The result indicates that impact energy values of 5-10 J can be achieved using tilt angle 1.5° and transverse speed of 75 mm/min.

## 4.5.2 Interactive effects of process parameters on mechanical properties for tapered threaded tool weldment

The interaction plot for the hardness of the tapered threaded tool weldment is shown in Figure 4.44
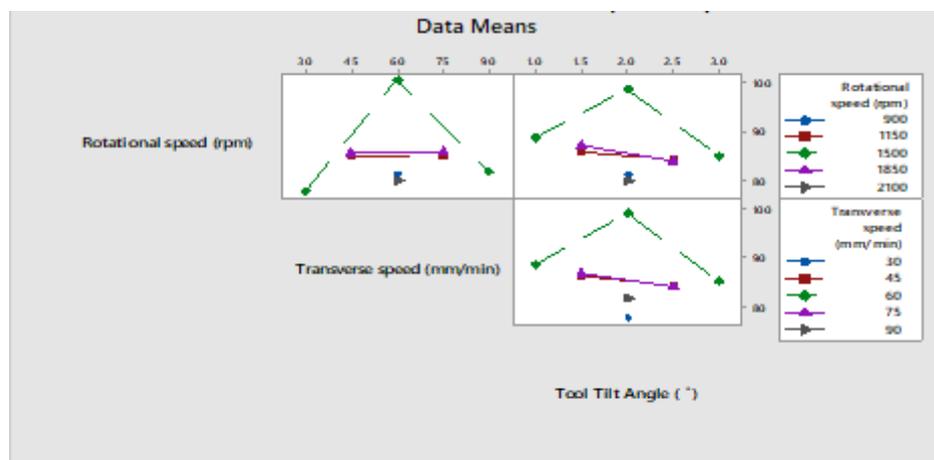


**Figure 4.32: Interaction plot for hardness (Vickers)**

The interaction plot obtained in figure 4.32 shows that there is an interaction between the three process parameters. The interaction plots for the other responses are shown in appendix H.

### 4.5.2.1 Hardness at various constant process parameters

i.      hardness at constant tilt angle

The contour plot for hardness at constant tilt angle is shown in Figure 4.33



**Figure 4.33: Contour plot for hardness at constant tilt angle**

The contour plot indicates how change in tool rotational speed (rpm) and transverse speed (mm/min) affects the hardness (Vickers) of the weldment while keeping the tool tilt angle constant at $2^{\circ}$. The result indicates that a hardness of 90-100 HV can be achieved using TS of 60 mm/min and RS of 1200 rpm or hardness of 100 HV and above at 1250 rpm, 65 mm/min welding speed and tilt angle of 2 $^{\circ}$. The 3D surface plot is presented in Appendix I.

**ii.      hardness at constant transverse speed**

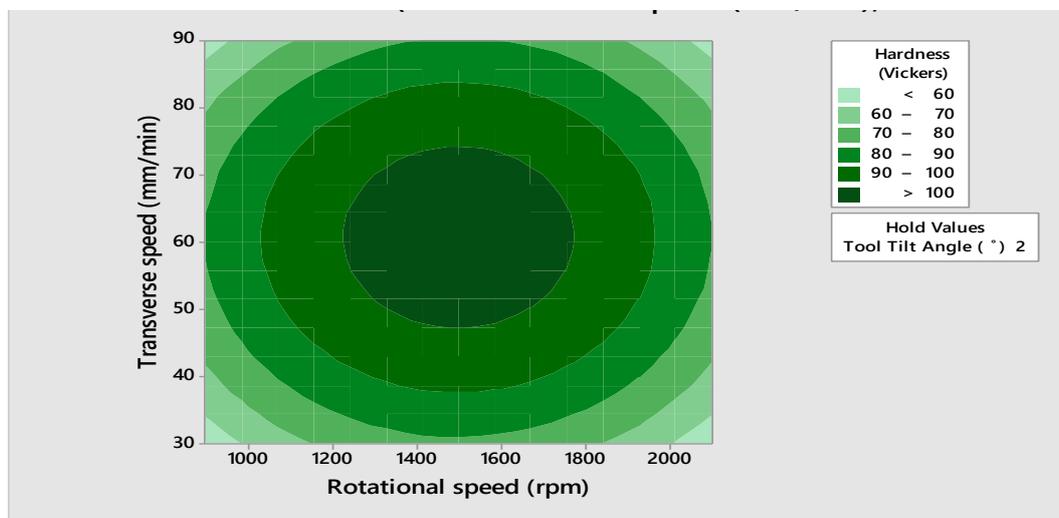The contour plot for the hardness of the weldment at constant transverse speed is shown in Figure 4.34
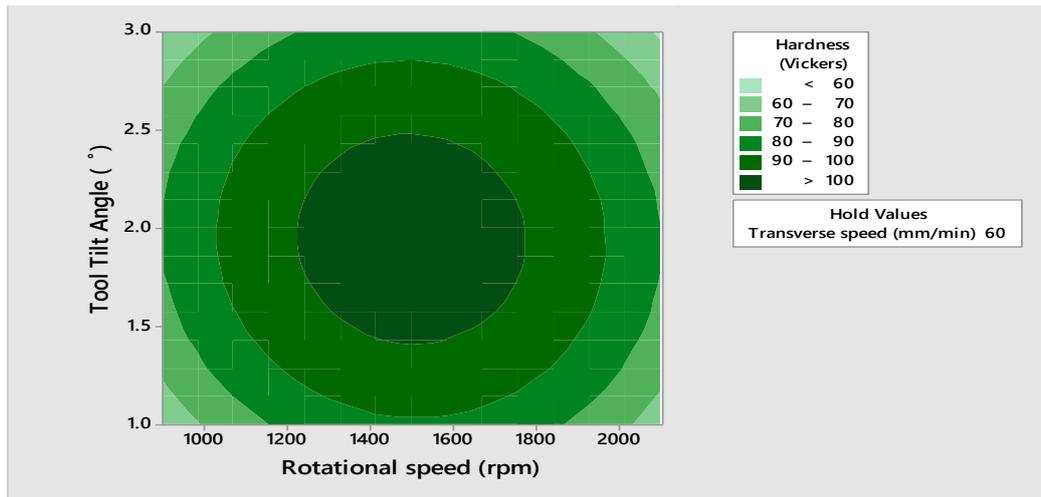
**Figure 4.34: Contour plot for hardness at constant transverse speed**

The contour plot indicates how change in the tool tilt angle ( ˚ ) and tool rotational speed (rpm) and affects the hardness (Vickers) of the weldment while keeping transverse speed (mm/min) constant at 60 mm/min. The result indicates that a hardness of 90-100 HV can be achieved using tilt angle of $2^{°}$ and RS of 1200 rpm or Hardness value of 80-90 HV can be achieved using tilt angle of 1.2 ˚, 1100 rpm and 60 mm/min transverse speed. The 3D surface plot is presented in Appendix J.

### iii. hardness at constant rotational speed

The contour plot for the hardness of the weldment at constant rotational speed is presented in Figure 4.35.



**Figure 4.35: Contour plot for hardness at constant rotational speed**

The contour plot indicates how change in the tool tilt angle (˚ ) and transverse speed (mm/min)  affects the hardness (Vickers) of the weldment while keeping tool rotational speed (rpm)  constant at 1500 rpm. The result indicates that a hardness of 90-100 HV can be achieved using tilt angle of $2^{°}$ and TS of 40 mm/min. The 3D surface plot is presented in Appendix K.

**4.5.2.2 UTS at various constant process parameters**

**i.      UTS at constant tilt angle**

The contour plot for the UTS of the weldment at constant tilt angle is presented in Figure 4.36



**Figure 4.36: Contour plot for UTS at constant tilt angle**

The contour plot indicates how change in tool rotational speed (rpm) and transverse speed (mm/min) affects the UTS values of the weldment while keeping the tool tilt angle constant at $2^{°}$.  The result indicates that UTS Values of 150-160 MPa can be achieved using TS of 60 mm/min and RS of 1200 rpm. The 3D surface plot is presented in Appendix L.

122

### ii. UTS at constant transverse speed

Contour plot for the UTS of the weldment at constant transverse speed is shown in Figure 4.37.



**Figure 4.37: Contour plot for UTS at constant transverse speed**

The contour plot indicates how change in tool tilt angle and tool rotational speed (rpm) affects the UTS values of the weldment at constant transverse speed of at 60 mm/min. The result indicates that UTS Values of 150-160 MPa can be obtained with tilt angle of $2^{°}$ and RS of 11500 rpm. The 3D surface plot is presented in Appendix M.

### iii. UTS at constant Rotational speed

The contour plot for the UTS of the weldment at constant rotational speed is shown in Figure 4.38.



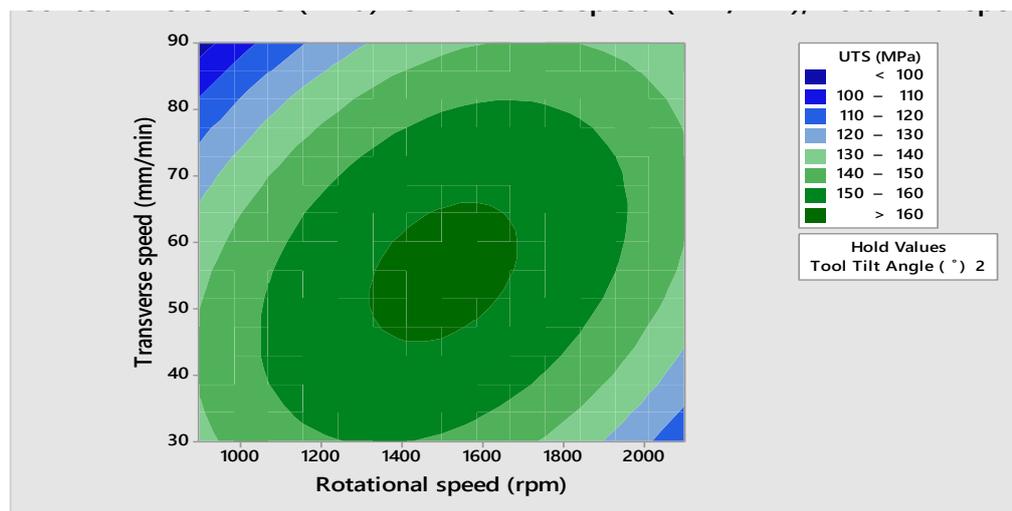**Figure 4.38: Contour plot for UTS at constant rotational speed**

The contour plot indicates how change in tool tilt angle and transverse speed (mm/min) affects the UTS values of the weldment while keeping the rotational speed (rpm) constant at 1500 rpm. The result indicates that UTS Values of 150-160 MPa can be achieved using tilt angle of 2° and TS of 48 mm/min. The 3D surface plot is presented in Appendix N.

**4.5.2.3 Impact energy at various constant process parameters**

**i        impact energy at constant tilt angle**

The contour plot for the impact energy of the weldment at constant tilt angle is shown in Figure 3.9.
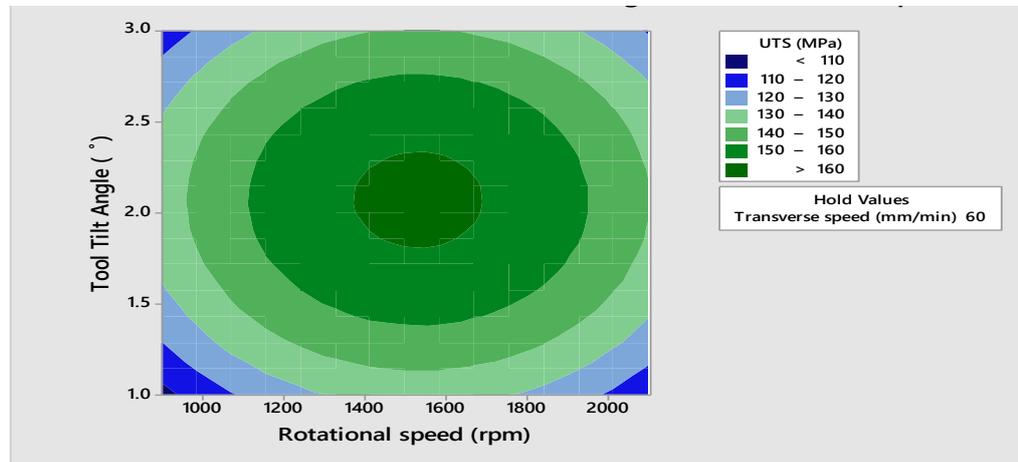


**Figure 4.39: Contour plot for impact energy at constant tilt angle**

The contour plot indicates how change in tool rotational speed (rpm) and transverse speed (mm/min) affects the impact energy of the weldment while keeping the tool tilt angle

constant at 2˚. The result indicates that impact energy values of 10-12.5 J can be achieved using TS of 60 mm/min and RS of 1200 rpm.

**ii.      Impact energy at constant transverse speed**

The contour plot for the impact energy of the weldment at constant transverse speed is shown in Figure 4.40
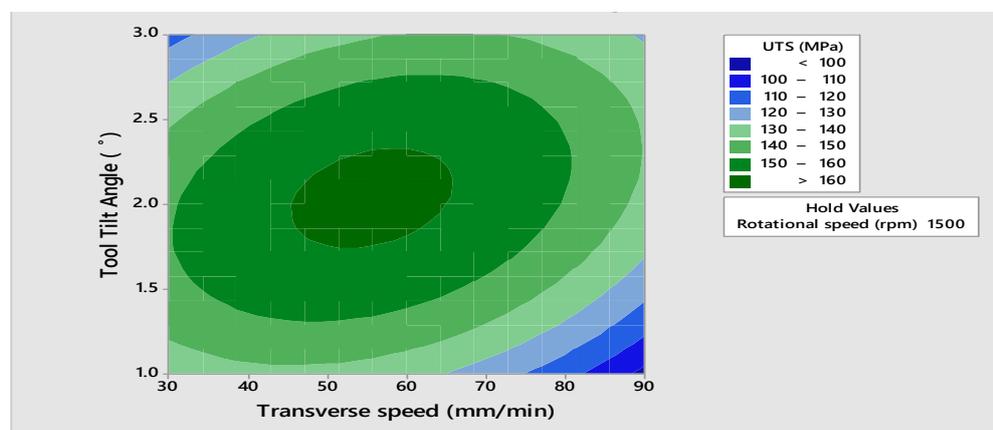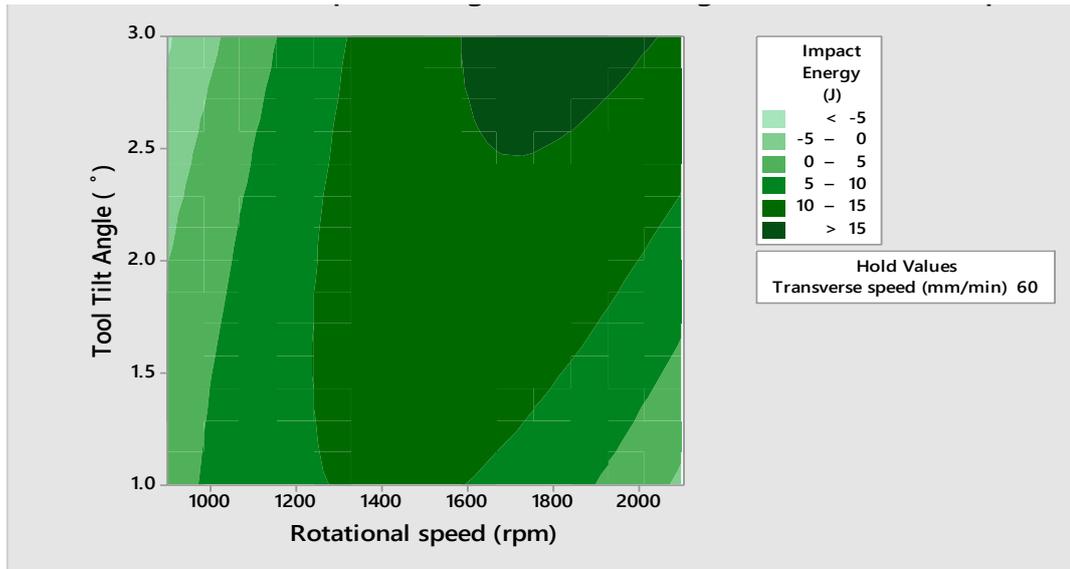


**Figure 4.40: Contour for impact energy at constant transverse speed**

The contour plot indicates how change in tool tilt angle (˚) and tool rotational speed (rpm) affects the impact energy of the weldment while keeping transverse speed (mm/min) constant at 60 mm/min. The result indicates that impact energy values of 5-10 J can be achieved using tilt angle of 2 ° and RS of 1350 rpm.

**iii.      Impact energy at constant rotational speed**

The contour plot for the impact energy of the weldment at constant rotational speed is shown in Figure 4.41
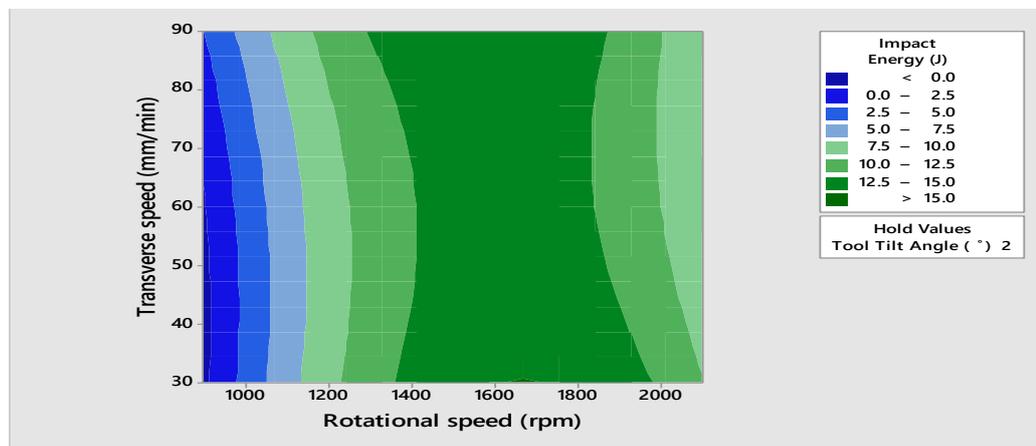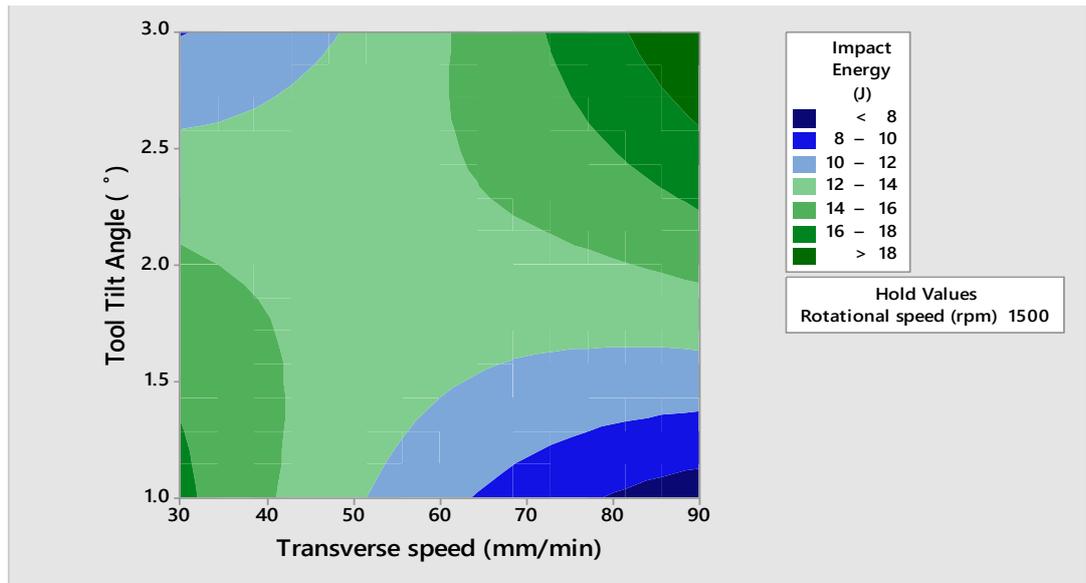
**Figure 4.41: Contour plot for impact energy at constant rotational speed**

The contour plot indicates how change in tool tilt angle (˚) and tool rotational speed (rpm) affects the impact energy of the weldment while keeping transverse speed (mm/min) constant at 60 mm/min. The result indicates that impact energy values of 16-18 J can be achieved using tilt angle of 2.5 ° and TS of 90 mm/min.

## 4.6    Single Response Optimisation

### 4.6.1    Single response optimisation for TT weldment

#### a.    Signal to noise (S/N) ratio analysis (TT)

The S/N ratio values for TT are shown in Table 4.12. The calculation was done using larger the better attributes as shown in Equation 3.1. The S/N ratio for hardness ranges between 36.15 to 39.97 dB, while for UTS it was 40.94 to 43.66 dB and for impact energy it was -4.43 to 26.60 dB. These values were plotted in order to obtain their respective main effect plots which are presented in Figures 4.42 to 4.44.

**Table 4.12: Experimental Response and Signal-to Noise ratio values for Tapered Tool (TT)**

| Runs | Rotational speed (rpm) | Transverse speed (mm/min) | Tool Tilt Angle ( ˚) | Hardness (Vickers) | UTS (MPa) | Impact Energy (J) | S/N for Hardness (dB) | S/N for UTS (dB) | S/N for Impact Energy (dB) |
|------|------|------|------|------|------|------|------|------|------|
| 1 | 1150 | 45 | 1.5 | 73.78 | 128.79 | 8.9 | 37.35 | 42.19 | 18.98 |
| 2 | 1850 | 45 | 1.5 | 74 | 122.47 | 10.9 | 37.38 | 41.76 | 20.74 |
| 3 | 1150 | 75 | 1.5 | 76.21 | 122.53 | 0.6 | 37.64 | 41.76 | -4.43 |
| 4 | 1850 | 75 | 1.5 | 85.5 | 126.81 | 6 | 38.63 | 42.06 | 15.56 |
| 5 | 1150 | 45 | 2.5 | 72.25 | 111.81 | 2.9 | 37.17 | 40.96 | 9.24 |
| 6 | 1850 | 45 | 2.5 | 84.65 | 125.5 | 10.1 | 38.55 | 41.97 | 20.08 |
| 7 | 1150 | 75 | 2.5 | 77.01 | 123.76 | 5.2 | 37.73 | 41.85 | 14.32 |
| 8 | 1850 | 75 | 2.5 | 64.26 | 122.68 | 4.1 | 36.15 | 41.77 | 12.25 |
| 9 | 900 | 60 | 2 | 66.85 | 111.51 | 3.4 | 36.50 | 40.94 | 10.62 |
| 10 | 2100 | 60 | 2 | 75.68 | 117.09 | 5.7 | 37.57 | 41.37 | 15.11 |
| 11 | 1500 | 30 | 2 | 81.99 | 126.04 | 12.9 | 38.27 | 42.01 | 22.21 |
| 12 | 1500 | 90 | 2 | 77 | 128.37 | 5.4 | 37.72 | 42.16 | 14.64 |
| 13 | 1500 | 60 | 1 | 70.22 | 123.32 | 6.4 | 36.92 | 41.82 | 16.12 |
| 14 | 1500 | 60 | 3 | 66 | 112.2 | 4.7 | 36.39 | 40.99 | 13.44 |
| 15 | 1500 | 60 | 2 | 98.58 | 151.54 | 21.4 | 39.87 | 43.61 | 26.60 |
| 16 | 1500 | 60 | 2 | 99.72 | 151.3 | 11.4 | 39.97 | 43.59 | 21.13 |
| 17 | 1500 | 60 | 2 | 97.91 | 150.51 | 10.7 | 39.81 | 43.55 | 20.58 |
| 18 | 1500 | 60 | 2 | 98.8 | 151.88 | 10.8 | 39.89 | 43.63 | 20.66 |
| 19 | 1500 | 60 | 2 | 98.87 | 151.99 | 11.4 | 39.90 | 43.63 | 21.13 |
| 20 | 1500 | 60 | 2 | 99.19 | 152.48 | 11.3 | 39.92 | 43.66 | 21.06 |

**b.    Main effect plot for Responses**

The main effect plots for all the responses were obtained with the use of the Minitab 17 software.

**i.    Hardness**

The main effect plot for signal to noise ratios (S/N) of the response (hardness) is shown in Figure. 4.42.
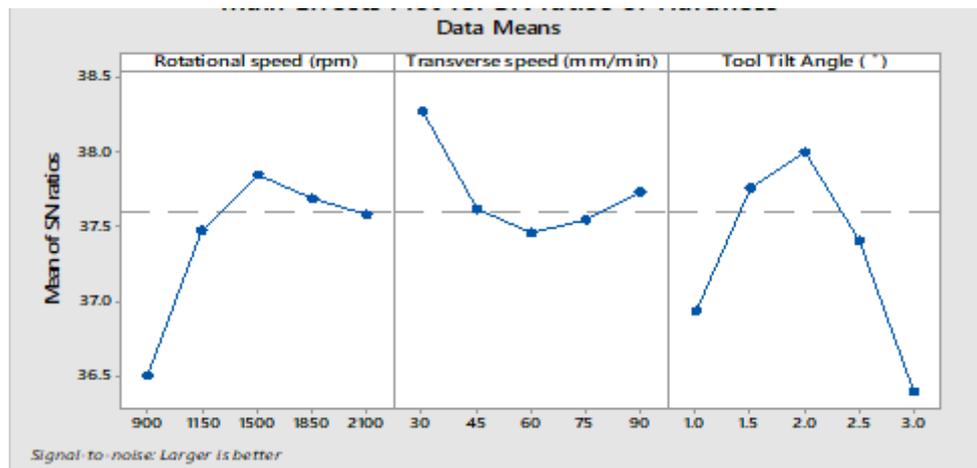


**Figure 4.42: Main effects plot for signal to noise ratios (S/N) of hardness**

As shown in Figure 4.42, it can be observed that the optimal hardness can be obtained using RS of 1500 rpm, TS of 30 mm/min and TTA of $2°$ as optimal welding parameters when using TT for welding.

**ii. UTS**

 The main effect plot for signal to noise ratios (S/N) of the response (UTS) is shown in Figure 4.43.

**Figure 4.43: Main effect plot for signal to noise ratios (S/N) of UTS**

As shown in Figure 4.43, it can be observed that the optimal UTS value can be obtained using RS of 1500 rpm, TS of 90 mm/min and TTA of $2^\circ$ as optimal welding parameters when using TT for welding.

### iii.     Impact Energy

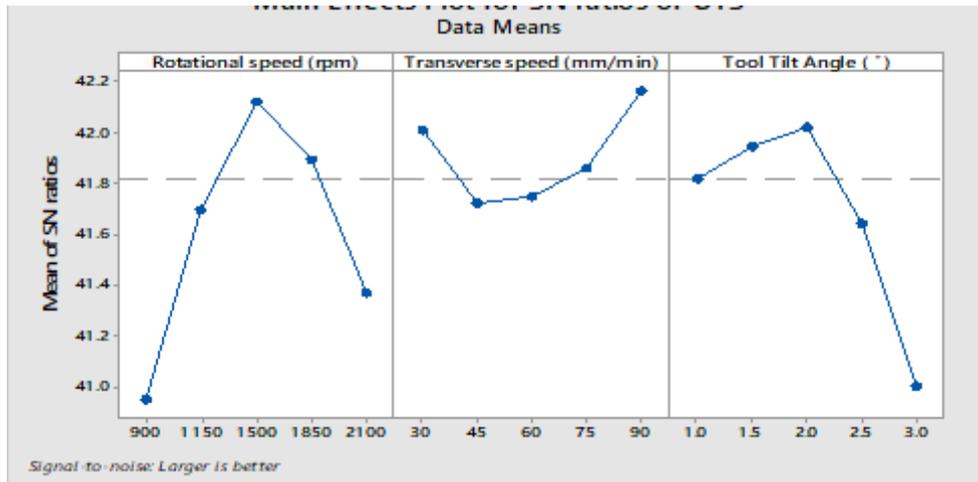The main effect plot for signal to noise ratios (S/N) of the response (impact energy) is shown in Figure 4.44.



**Figure 4.44: Main effect plot for signal to noise ratios of UTS**

As shown in figure 4.44, it can be observed that the optimal impact energy can be obtained using RS of 1500, TS of 30 mm/min and TTA of $2^\circ$ as optimal welding parameters when welding with TT.

**4.6.2    Single response optimisation for TTT weldment**

**a.       Signal to noise (S/N) ratio analysis (TTT)**

The S/N ratio values for TTT are shown in Table 4.13. The calculation was done using larger the better attributes as shown in Equation 3.1. The S/N ratio for hardness ranges between 37.81 to 40.48 dB, while for UTS it was 42.31 to 44.22 dB and for impact energy it was -3.09 to 27.38 dB. These values were plotted in order to obtain their respective main effect plots which are presented in Figures 4.45 to 4.47.

**Table 4.13: Experimental Response and Signal-to Noise ratio values for Tapered Threaded Tool (TTT)**

| Runs | Rotational speed (rpm) | Transverse speed (mm/min) | Tool Tilt Angle ( ˚) | Hardness (Vickers) | UTS (MPa) | Impact Energy (J) | S/N for Hardness (dB) | S/N for UTS (dB) | S/N for Impact Energy (dB) |
|---|---|---|---|---|---|---|---|---|---|
| 1 | 1150 | 45 | 1.5 | 86.5 | 138.35 | 9.9 | 38.74 | 42.81 | 19.91 |
| 2 | 1850 | 45 | 1.5 | 86.04 | 138.42 | 10.2 | 38.69 | 42.82 | 20.17 |
| 3 | 1150 | 75 | 1.5 | 85.5 | 136.81 | 8.8 | 38.63 | 42.72 | 18.88 |
| 4 | 1850 | 75 | 1.5 | 88.28 | 141.08 | 9.1 | 38.91 | 42.98 | 19.18 |
| 5 | 1150 | 45 | 2.5 | 83.76 | 144.13 | 1.5 | 38.46 | 43.17 | 3.52 |
| 6 | 1850 | 45 | 2.5 | 84.91 | 130.53 | 10.4 | 38.57 | 42.31 | 20.34 |
| 7 | 1150 | 75 | 2.5 | 84.82 | 141.14 | 6.9 | 38.56 | 42.99 | 16.77 |
| 8 | 1850 | 75 | 2.5 | 83.28 | 158.77 | 12.6 | 38.41 | 44.01 | 22.00 |
| 9 | 900 | 60 | 2 | 81.21 | 135.59 | 0.7 | 38.19 | 42.64 | -3.09 |
| 10 | 2100 | 60 | 2 | 79.82 | 143.45 | 10.7 | 38.04 | 43.13 | 20.58 |
| 11 | 1500 | 30 | 2 | 77.8 | 162.66 | 16.9 | 37.81 | 44.22 | 24.55 |
| 12 | 1500 | 90 | 2 | 81.77 | 126.45 | 14.7 | 38.25 | 42.03 | 23.34 |
| 13 | 1500 | 60 | 1 | 88.8 | 136.51 | 8.7 | 38.96 | 42.70 | 18.79 |
| 14 | 1500 | 60 | 3 | 85.15 | 140.27 | 18.41 | 38.60 | 42.93 | 25.30 |
| 15 | 1500 | 60 | 2 | 105.25 | 161.8 | 23.4 | 40.44 | 44.17 | 27.38 |
| 16 | 1500 | 60 | 2 | 104.85 | 161.18 | 12 | 40.41 | 44.14 | 21.58 |
| 17 | 1500 | 60 | 2 | 105.52 | 162.21 | 11.8 | 40.46 | 44.20 | 21.43 |
| 18 | 1500 | 60 | 2 | 105.28 | 161.84 | 10.6 | 40.44 | 44.18 | 20.50 |
| 19 | 1500 | 60 | 2 | 105.75 | 162.57 | 11 | 40.48 | 44.22 | 20.82 |
| 20 | 1500 | 60 | 2 | 104.91 | 161.27 | 12.7 | 40.41 | 44.15 | 22.07 |

## b.    Main effect plot for Responses

The main effect plots for all the responses were obtained with the use of the Minitab 17 software.

## i.    Hardness

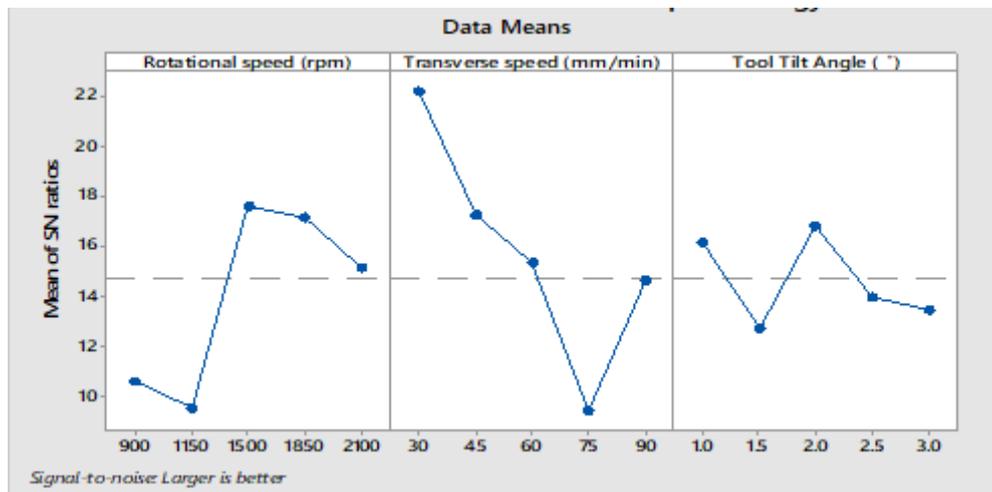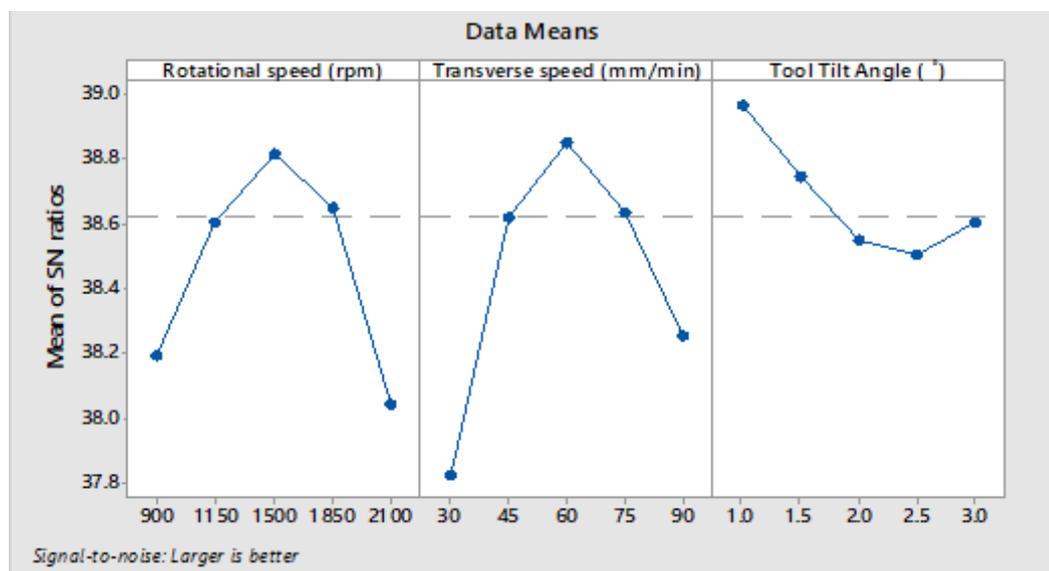The main effect plot for signal to noise ratios (S/N) of the response (hardness) is shown in Figure 4.45.



**Figure 4.45: Main effect plot for signal to noise ratios (S/N) of hardness**

As shown in Figure 4.45, it can be observed that the optimal hardness can be obtained using RS of 1500 rpm, TS of 60 mm/min and TTA of  $1°$  as optimal welding parameters when using TTT for welding.

## ii.    UTS

The Main effect plot for signal to noise ratios (S/N) of the response (UTS) is shown in Figure 4.46.

**Figure 4.46: Main effect plot for signal to noise ratios (S/N) of UTS**

As shown in Figure 4.46, it can be observed that the optimal UTS can be obtained using RS of 1500 rpm, TS of 30 mm/min and TTA of $2°$ as optimal welding parameters when using TTT for welding.

### iii.    Impact energy

The main effect plot for signal to noise ratios (S/N) of the response (impact energy) is shown in Figure 4.47
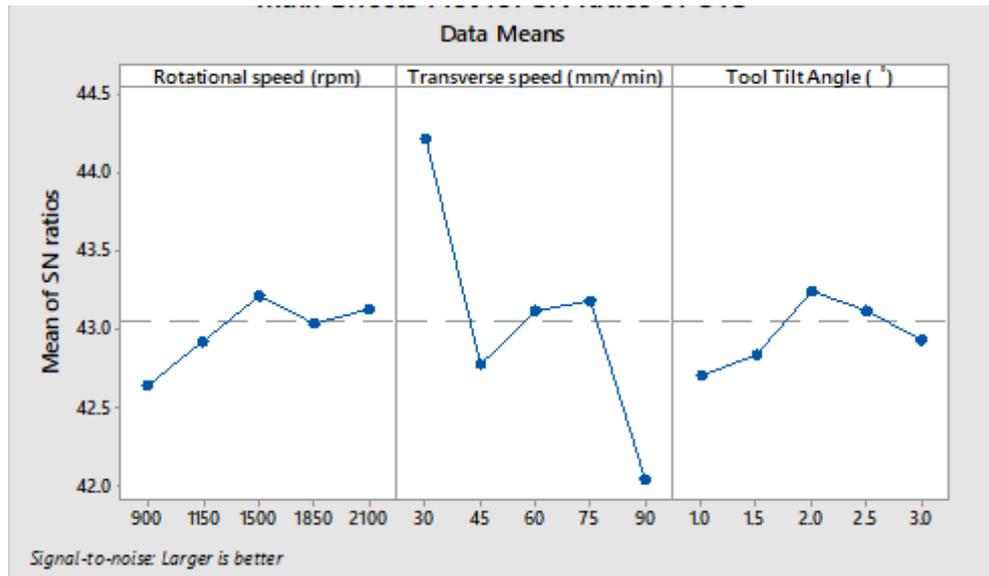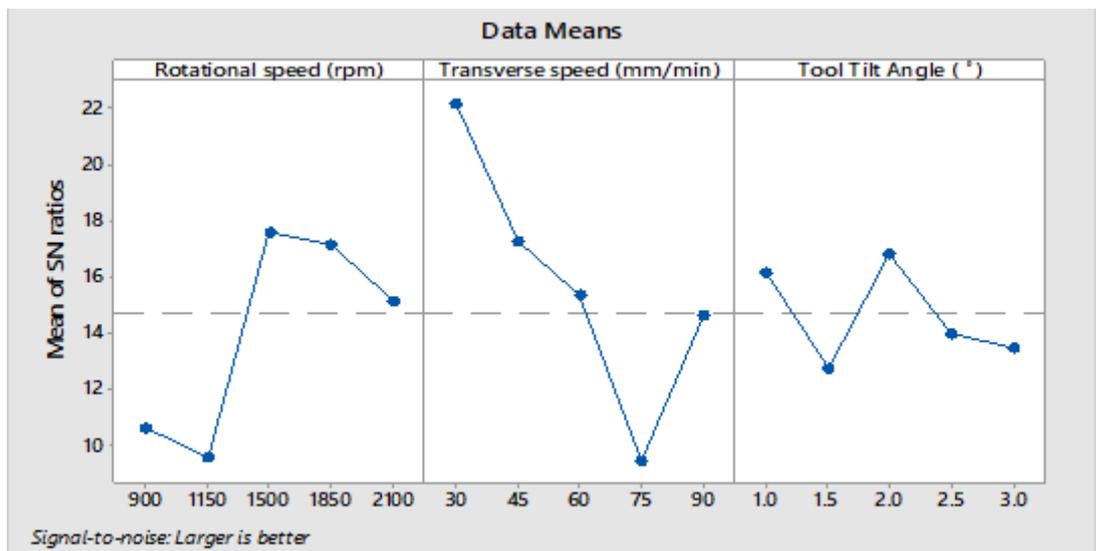


**Figure 4.47: Main effect plot for signal to noise ratios (S/N) of impact energy**

As shown in Figure 4.33, it can be observed that the optimal hardness can be obtained using RS of 1500 rpm, TS of 30 mm/min and TTA of $2°$ as optimal welding parameters when using TT for welding.

## 4.7     Multi-Response Optimisation

### 4.7.1   Multi-response optimisation for TT weldment

### i        Grey relational analysis

The calculated values of grey relational generation, grey relational coefficient (GRC), and grey relational grade (GRG) are presented in Table 4.14, while the process parameters resulting factor effects are as presented in table 4.15 (the optimal levels for each process parameters are presented in bold form). The values in Table 4.15 were used in obtaining the main effect plots.

**Table 4.14: Results of GRG, GRC and grades**

| Scenario | GRG | | | GRC | | | Grade |
|---|---|---|---|---|---|---|---|
| | Hardness | UTS | Impact Energy | Hardness | UTS | Impact Energy | |
| X0 | 1.000 | 1.000 | 1.000 | - | - | - | - |
| 1 | 0.318 | 0.460 | 0.755 | 0.423 | 0.481 | 0.671 | 0.525 |
| 2 | 0.325 | 0.300 | 0.811 | 0.426 | 0.417 | 0.726 | 0.523 |
| 3 | 0.393 | 0.301 | 0.000 | 0.452 | 0.417 | 0.333 | 0.401 |
| 4 | 0.658 | 0.411 | 0.644 | 0.594 | 0.459 | 0.584 | 0.546 |
| 5 | 0.270 | 0.009 | 0.441 | 0.406 | 0.335 | 0.472 | 0.405 |
| 6 | 0.635 | 0.378 | 0.790 | 0.578 | 0.446 | 0.704 | 0.576 |
| 7 | 0.417 | 0.333 | 0.604 | 0.462 | 0.428 | 0.558 | 0.483 |
| 8 | 0.000 | 0.305 | 0.538 | 0.333 | 0.418 | 0.520 | 0.424 |
| 9 | 0.091 | 0.000 | 0.485 | 0.355 | 0.333 | 0.493 | 0.394 |
| 10 | 0.377 | 0.156 | 0.630 | 0.445 | 0.372 | 0.575 | 0.464 |
| 11 | 0.561 | 0.391 | 0.858 | 0.533 | 0.451 | 0.779 | 0.588 |
| 12 | 0.417 | 0.450 | 0.615 | 0.462 | 0.476 | 0.565 | 0.501 |
| 13 | 0.204 | 0.322 | 0.662 | 0.386 | 0.424 | 0.597 | 0.469 |
| 14 | 0.062 | 0.020 | 0.576 | 0.348 | 0.338 | 0.541 | 0.409 |
| 15 | 0.986 | 0.980 | 1.000 | 0.972 | 0.962 | 1.000 | 0.978 |
| 16 | 1.012 | 0.975 | 0.824 | 1.025 | 0.953 | 0.739 | 0.906 |
| 17 | 0.970 | 0.958 | 0.806 | 0.944 | 0.923 | 0.721 | 0.862 |
| 18 | 0.991 | 0.987 | 0.809 | 0.982 | 0.975 | 0.723 | 0.894 |
| 19 | 0.993 | 0.990 | 0.824 | 0.985 | 0.980 | 0.739 | 0.902 |
| 20 | 1.000 | 1.000 | 0.821 | 1.000 | 1.000 | 0.737 | 0.912 |

**Table 4.15: Resulting factor effect of process parameters factors (average GRG)**

| Factor | Axial points | | Cubic points | | Centre point |
|---|---|---|---|---|---|
| | Level 1 | Level 5 | Level 2 | Level 4 | Level 3 |
| Rotational speed | 0.3937 | 0.4639 | 0.453242 | 0.517007 | **0.742005** |
| Transverse speed | 0.5877 | 0.5008 | 0.50701973 | 0.4632301 | **0.71891566** |
| Tool tilt angle | 0.4690 | 0.4088 | 0.498496 | 0.471754 | **0.7400** |

## ii    Optimum welding process parameters

The optimum weldment can be obtained using the optimal process parameters of 1500 rpm rotational speed, 60 mm/min welding speed and 2 $^{\circ}$ tilt angle as shown in Figure 4.34 and Table 4.18.
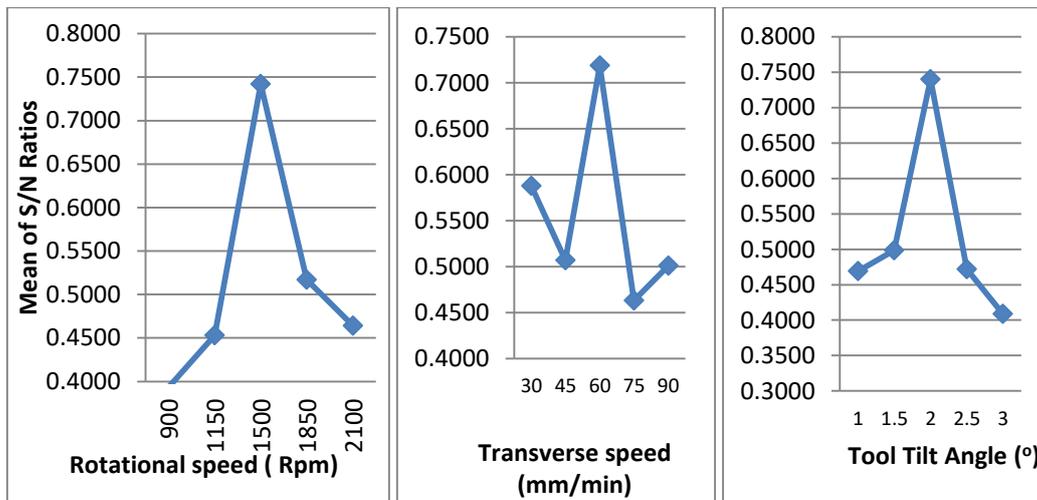


**Figure 4.48: Plots of factor effects**

## 4.7.2    Multi-response optimisation for TT weldment

## i    Grey relational analysis

The calculated values of grey relational generation, grey relational coefficient (GRC), and grey relational grade (GRG) are presented in Table 4.16, while the process parameters

resulting factor effects are as presented in Table 4.17 (the optimal levels for each process

parameters are presented in bold form). The values in Table 4.17 were used in obtaining

the main effect plots.

**Table 4.16: Results of GRG, GRC and grades**

| Scenario | GRG | | | GRC | | | Grade |
|---|---|---|---|---|---|---|---|
| | **Hardness** | **UTS** | **Impact Energy** | **Hardness** | **UTS** | **Impact Energy** | |
| $X_0$ | 1.000 | 1.000 | 1.000 | - | - | - | - |
| 1 | 0.345 | 0.357 | 0.755 | 0.433 | 0.438 | 0.671 | 0.514 |
| 2 | 0.328 | 0.359 | 0.763 | 0.427 | 0.438 | 0.679 | 0.515 |
| 3 | 0.307 | 0.313 | 0.721 | 0.419 | 0.421 | 0.642 | 0.494 |
| 4 | 0.412 | 0.435 | 0.731 | 0.459 | 0.469 | 0.650 | 0.526 |
| 5 | 0.240 | 0.520 | 0.217 | 0.397 | 0.510 | 0.390 | 0.432 |
| 6 | 0.285 | 0.126 | 0.769 | 0.411 | 0.364 | 0.684 | 0.486 |
| 7 | 0.281 | 0.436 | 0.652 | 0.410 | 0.470 | 0.590 | 0.490 |
| 8 | 0.222 | 0.904 | 0.824 | 0.391 | 0.839 | 0.739 | 0.656 |
| 9 | 0.140 | 0.277 | 0.134 | 0.368 | 0.409 | 0.366 | 0.381 |
| 10 | 0.084 | 0.501 | 0.777 | 0.353 | 0.500 | 0.692 | 0.515 |
| 11 | 0.000 | 1.000 | 0.907 | 0.333 | 1.000 | 0.844 | 0.726 |
| 12 | 0.162 | 0.000 | 0.868 | 0.374 | 0.333 | 0.791 | 0.499 |
| 13 | 0.431 | 0.304 | 0.718 | 0.468 | 0.418 | 0.639 | 0.508 |
| 14 | 0.294 | 0.412 | 0.932 | 0.415 | 0.460 | 0.880 | 0.585 |
| 15 | 0.985 | 0.979 | 1.000 | 0.970 | 0.960 | 1.000 | 0.977 |
| 16 | 0.972 | 0.964 | 0.810 | 0.947 | 0.932 | 0.724 | 0.868 |
| 17 | 0.993 | 0.989 | 0.805 | 0.986 | 0.978 | 0.719 | 0.895 |
| 18 | 0.985 | 0.980 | 0.774 | 0.972 | 0.961 | 0.689 | 0.874 |
| 19 | 1.000 | 0.998 | 0.785 | 1.000 | 0.996 | 0.699 | 0.898 |
| 20 | 0.974 | 0.966 | 0.826 | 0.951 | 0.936 | 0.742 | 0.876 |

**Table 4.17: Resulting factor effect of process parameters factors (average GRG)**

| Factor | Axial points | | Cubic points | | Centre point |
|---|---|---|---|---|---|
| | **Level 1** | **Level 5** | **Level 2** | **Level 4** | **Level 3** |
| Rotational speed | 0.3809 | 0.5150 | 0.4825819 | 0.5459229 | **0.7705491** |
| Transverse speed | 0.7256 | 0.4992 | 0.486784 | 0.541721 | **0.737654** |
| Tool tilt angle | 0.5084 | 0.5846 | 0.512225 | 0.51628 | **0.7508** |

**ii    Optimum welding process parameters**

The optimum weldment can be obtained using the optimal process parameters of 1500 rpm rotational speed, 60 mm/min welding speed and 2 $^{\circ}$ tilt angle as shown in Figure 4.49 and Table 4.18.
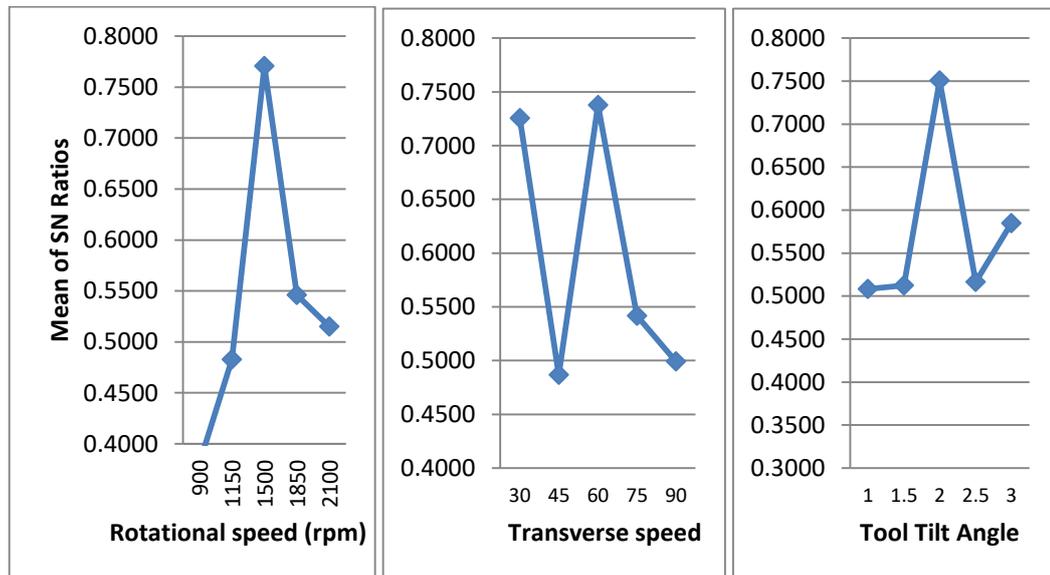


**Figure 4.49: Plots of factor effects**

**Table 4.18: Optimal level of factors (TT &TTT)**

| Tool geometry | Rotational speed (rpm) | Transverse speed (mm/min) | Tool tilt angle (˚) | Joint efficiency (%) |
|---|---|---|---|---|
| Tapered tool (TT) | 1500 | 60 | 2 | 84.71 |
| Tapered threaded tool (TTT) | 1500 | 60 | 2 | 90.32 |

### 4.7.3 Confirmation test

The empirical regression models were validated using the optimised values obtained from GRA. These results are presented in Table 4.19.

**Table 4.19 Confirmation test**

| Properties | Tapered tool (TT) | | | Tapered threaded tool( TTT) | | |
|---|---|---|---|---|---|---|
| | Experimental value | Calculated value | Error (%) | Experimental value | Calculated value | Error (%) |
| Hardness (Vickers) | 99.72 | 99.102 | 0.62 | 105.75 | 104.18 | 1.48 |
| Tensile strength (MPa) | 152.48 | 150.99 | 0.977 | 162.21 | 161.2 | 0.622 |
| Impact energy (J) | 21.4 | 20.0399 | 6.355 | 23.4 | 22.15 | 0.40 |

Based on the results presented in Table 4.19, it can be observed that TTT performed better than TT. Also, the calculated values are in close agreement with the experimental values, this implies that the regression equations (models) are valid and can be applied in the prediction of mechanical properties of TTT and TT welded joints.

## 4.8 Characterisation of Optimal Weldment

The optimal weldments for the two tools (tapered and tapered threaded tools) were further characterized by performing the corrosion test and microstructural analysis on the optimized weldment for the two tools.

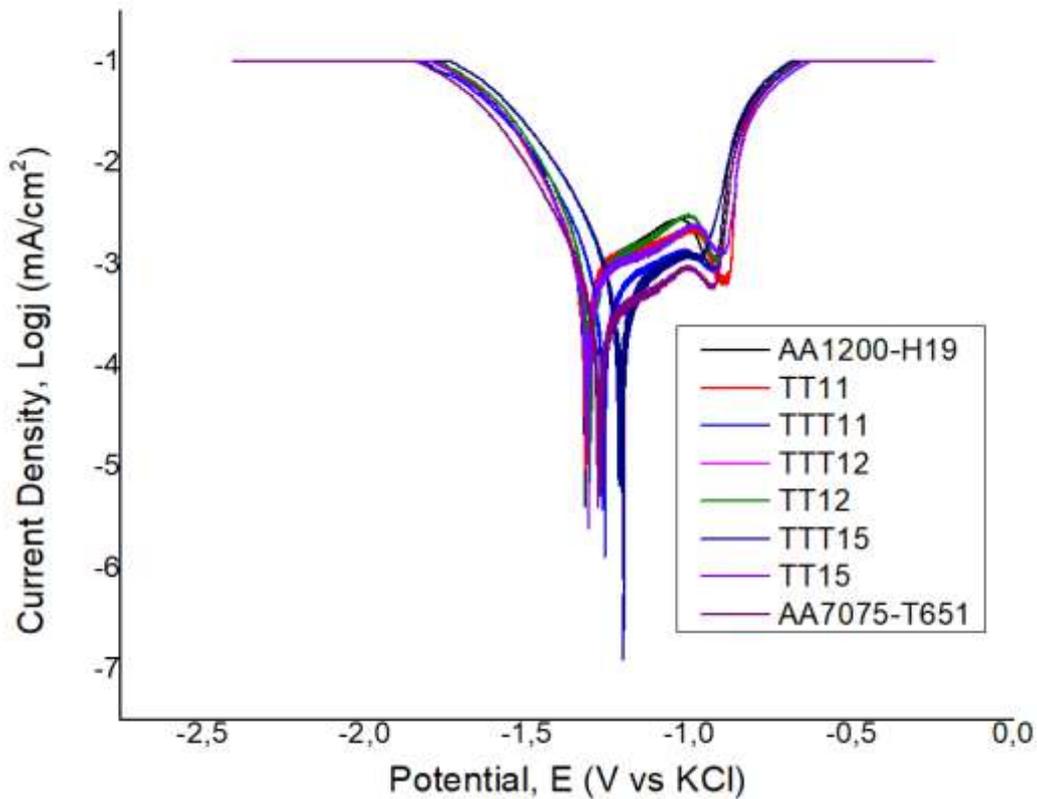### 4.8.1 Corrosion results for the base-metals and friction stir welded samples

The corrosion rate of the metal in each setting is the velocity at which the metal degrades. This depends on the metal and the material used. Calculation of the corrosion risk helps to determine the useful life of the material. The size of the grains of each material in the sample also determines the corrosion rate of the sample. The research shows that finer grains have been found to increase the hardness of material and thus encourage the formation of a passive layer, thereby reducing the corrosion risk of the material. The loss due to corrosion happens only gradually over time. Despite this, coarse grains often facilitate the development of a less passive film, which increases corrosion rate (Ikumapayi *et al.*, 2020). The findings of the corrosion test are shown in Table 4.20 where TT11, TT15, TT12 and TTT11, TTT15, TTT12 represents weldment produced with tapered tool and tapered threaded tools respectively at 1500 rpm rotational speed, 30 mm/min transverse speed, $2^0$ tool tilt angle, 1500 rpm rotational speed, 60 mm/min transverse speed, $2^0$ tool tilt angle and 1500 rpm rotational speed, 90 mm/min transverse speed, $2^0$ tool tilt angle, respectively. These weldments were evaluated to check the effect of the parameters on their corrosion behaviour. The open circuit potential (OCP) and Tafel plot for the base metals and friction stir welded samples are shown in figures 4.50 and 4.51 respectively.

**Table 4.20: Corrosion result for the base metals and friction stir welded Samples**

| Samples | Corrosion Current | Open Circuit Potential | Anodic Tafel Slope | Corrosion Rate | Chi-Square Value | Polarization Resistance | Cathodic Tafel Slope | Corrosion Potential | % Inhibition Efficiency |
|---------|-------------------|------------------------|--------------------|----------------|------------------|-------------------------|----------------------|---------------------|-------------------------|
| | $j_{corr}$ ($\mu A/cm^2$) | OCP (V) | \|ba\| (mV/dec) | Cr (mm/year) | $\chi^2$ | Pr ($\Omega$) | \|bc\| (mV/dec) | $E_{corr}$ (mV) | % IE |
| AA7075 | 402 | -0.969 | 156.65 | 4.529 | 2.79 E-06 | 49.52 | 53.61 | -1328 | - |
| AA1200 | 187 | -1.032 | 96.64 | 1.624 | 6273300 | 69.16 | 238.24 | -1424 | 53.48 |
| TT 11 | 96.2 | -0.995 | 114.3 | 0.676 | 54365 | 478.28 | 183.77 | -1450.2 | 76.07 |
| TT 12 | 132 | -0.984 | 59.14 | 0.783 | 4.92 E-07 | 223.90 | 87.53 | -1325.1 | 67.16 |
| TT 15 | 79.9 | -0.976 | 88.29 | 0.698 | 3.13E-07 | 403.14 | 45.37 | -1282.3 | 80.12 |
| TTT 11 | 88.2 | -1.056 | 23.18 | 0.464 | 1.84 E-08 | 956.17 | 53.45 | -1321.6 | 78.06 |
| TTT 12 | 69.4 | -1.043 | 98.61 | 0.574 | 4.97 E-07 | 798.78 | 23.05 | -1293.4 | 82.73 |
| TTT 15 | 48.4 | -0.99884 | 36.52 | 0.497 | 5.42 E-05 | 895.75 | 36.51 | -1282.5 | 87.96 |
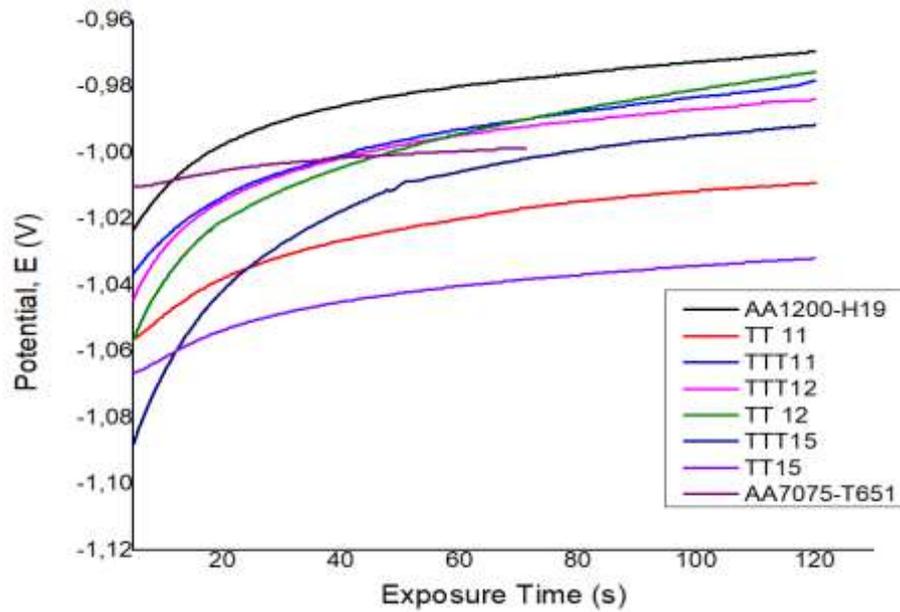


**Figure 4.50:** *OCP* **versus exposure time**

**Figure 4.51: Tafel Plot for the Base-Metals and Friction stir welded sample**

The result of the corrosion test revealed that the TTT15 weldment produced the highest polarization resistances (Pr) of 956.17 $\Omega$ as compared to TT15 with polarization resistance (Pr) of 403.14 $\Omega$ while the base metal AA7075-T651 and AA1200-H19 resisted the corrosion least with 69.16 $\Omega$ and 49.52 $\Omega$, respectively. It also revealed that the corrosion rate (Cr) was 0.497 mm/year for TTT15 as compared to TT15 with corrosion rate (Cr) of 0.698 mm/year while the base metals received the highest attack of corrosion with corrosion rates 4.529 and 1.624 mm/year for AA7075 and AA1200, respectively. From Table 4.20, the percentage inhibition performance efficiency was far higher with the TTT15 weldment resulting in 87.96 % percentage protection as against 80.12 % for TT15.

Also, the corrosion rate for TT11 is 0.676 mm/year and increased to 0.698 mm/year for TT15 with increase in transverse speed from 30 to 60 mm/min and increased further to 0.783 mm/year for TT12 with increase in transverse speed from 60 to 90 mm/min while for TTT 11, TTT15 and TTT12 it increased from 0.464 mm/year to 0.497 mm/year and further to 0.574 mm/year with increase in transverse speed from 30 to 60 and 60 to 90 mm/min respectively. This is because the polarisation resistance decreases with increase in transverse speed from 30 to 60mm/min and then to 90 mm/min and polarization resistance is directly related to corrosion rate hence the higher the polarisation resistance, the lower the corrosion rate and vis-avis (Toshev & Kostadinov 2006).

The polarisation resistance decreased from 478.28 $\Omega$ at TT11 condition to 403.14 $\Omega$ with increase in transverse speed from 30 to 60 mm/min (TT15) and decreased further to 223.90 $\Omega$ with increase in transverse speed from 60 to 90 mm/min. TTT weldment followed that same pattern by decreasing from 956.17 $\Omega$ at TTT11 to 895.75 $\Omega$ at TTT15 condition and at TTT 12 decreased further to 798.78 $\Omega$. This is because the higher the polarization resistance the lower the corrosion rate.

The inhibition efficiency was optimal for both TT15 and TTT15 weldment at 80.12 % and 87.96%, respectively with a transverse speed of 60 mm/min and changes with temperature. Inhibition efficiency decreases with increase in temperature (Chakravarthy *et al.,* 2014).

### 4.8.2 SEM images of base metal, optimised weldment and corroded samples

Morphological characteristics and surface topography for the corroded samples of both inhibited samples which are weldment of the two dissimilar alloys AA7075-T651 and AA1200-H19 aluminum alloys and uninhibited samples which were base metal AA7075-T651 and AA1200-H19 aluminium alloys were studied using TESCAN VEGA 3 LMH scanning electron microscope. All the SEM micrographs were taken at a magnification

of 500X with accelerating voltage of 20 kV and beam intensity of 10 having a varying working distance ranging from 13.46 mm to 14.72 mm. The morphologies of the corroded samples that revealed the extent of corrosion attacks were captured by scanning electron microscopy and presented in Plates XIX (a and b). In plate XIX (a) for sample (a), pits corrosion attacks were seen in AA7075-T651 which indicates that it is susceptible to corrosion attack while for corroded friction stir welded alloys (the two optimal weldment) a considerable number of pit attacks as well as micro cracks in its surface topography occurred as a result of intergranular corrosion on the surface.
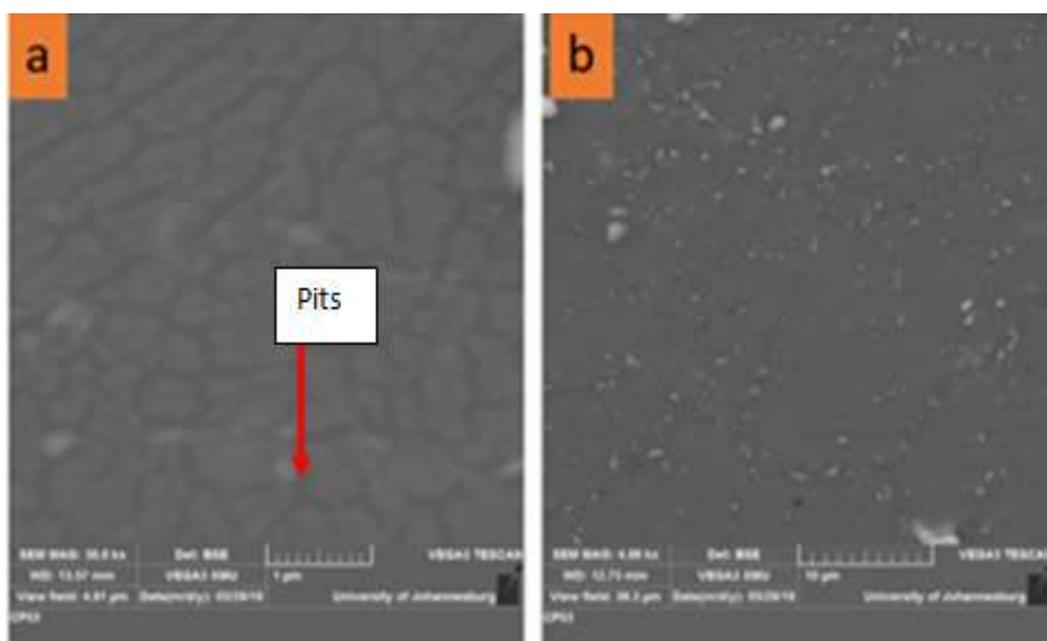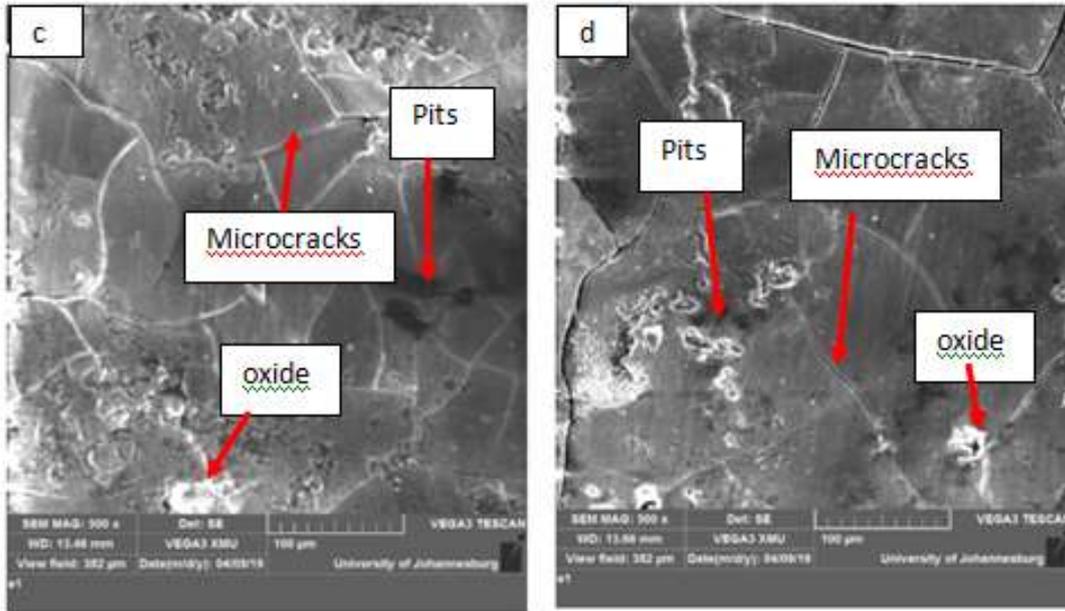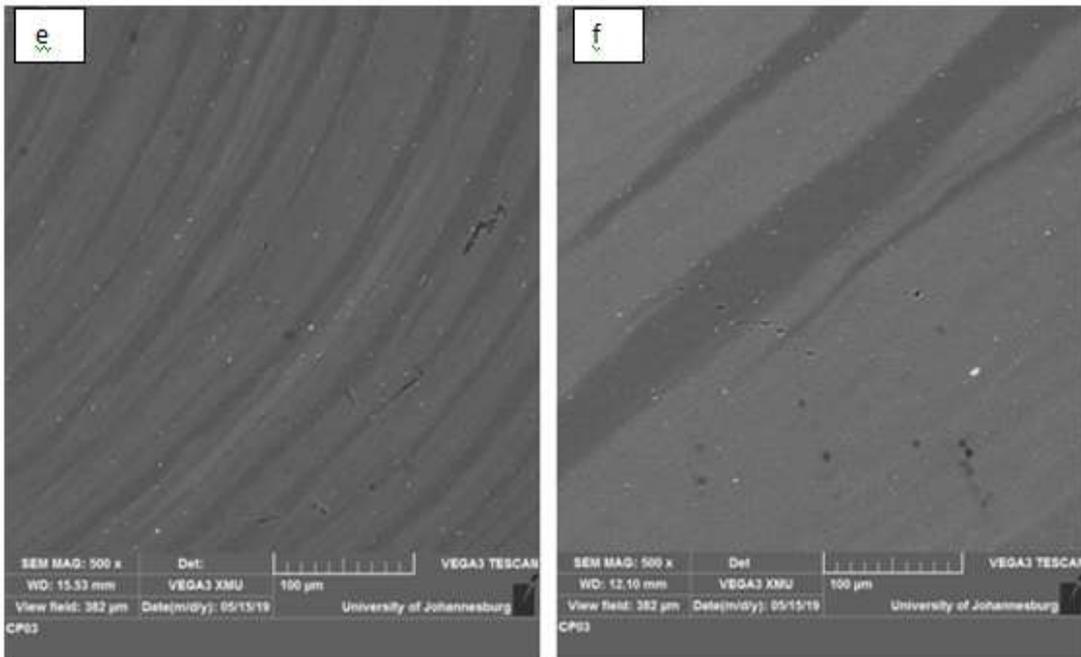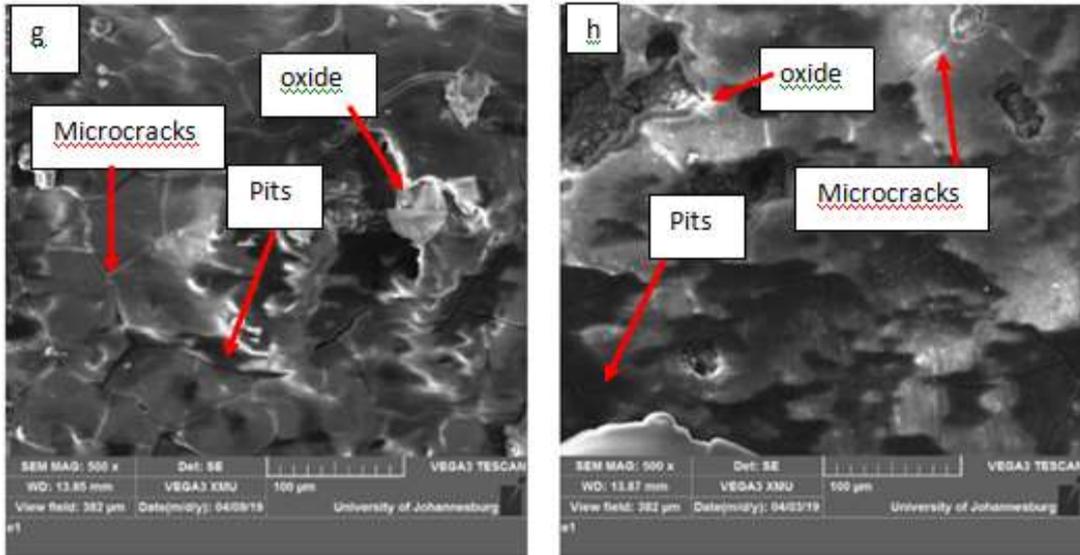
**Plate XIX (a): Magnification at 500X for (a) AA7075 (b) 1200 (c) corroded AA7075 (d) corroded AA1200**

**Plate XIX (b) : Magnification at 500X for (e) optimal weldment TT15 (f) optimal weldment TTT15 (g) corroded optimal TT15 (h) corroded optimal TTT15**
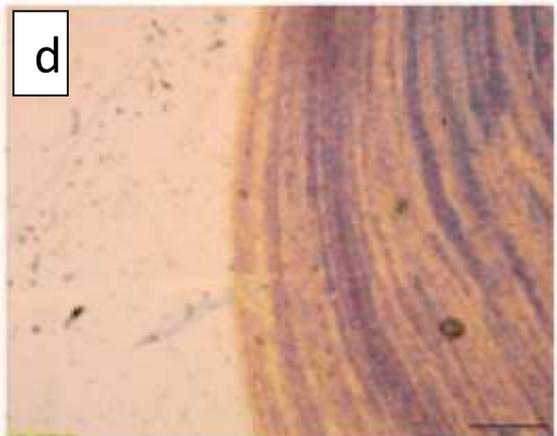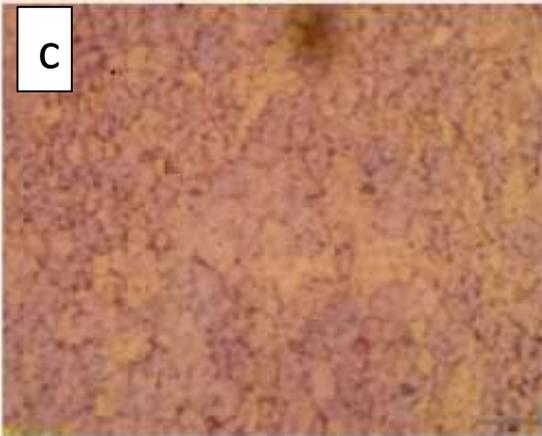
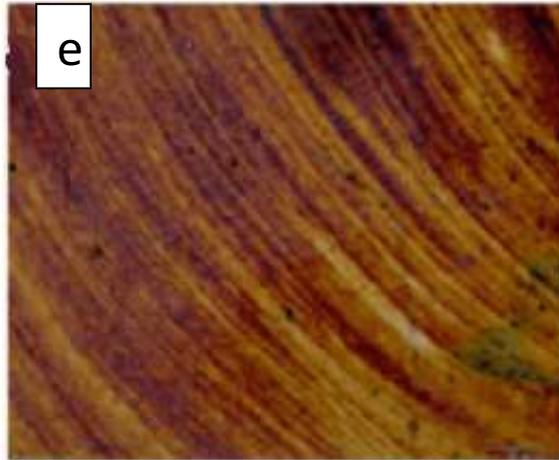### 4.8.3 Microstructure of optimised weldment

The mixing of the two dissimilar alloys occurred as a result of rotational action of the tool at the tool-metal interface. The mixing pattern and material flow has been revealed through microstructure and microstructural observations at the weld zones. The microstructure as shown in micrographs in plates XX(a) and XXI(a) revealed that there is sufficient heat for plastic deformation and material coalescence at the optimal welding parameters for both tapered and tapered threaded tool weldment (TT and TTT). There are microstructural variations along the length and across the breath of the weld zones resulting into three distinct regions which are mixed flow, mechanically mixed and unmixed regions. This is in agreement with the results obtained by several researchers (Abolusoro & Akinlabi, 2019, Abolusoro & Akinlabi, 2020, Ouyang & Kovacevic, 2002). The unmixed region is at the upper part of the joint close to the tool shoulder (Plates XX (c) and XXI(c)). The heat generated by the rotating action of the tool and the tool shoulder- workpiece interface impacts on the microstructure leading to grain refinement and resulting in dynamic recrystallization during the welding. The mechanically mixed

region is a combined microstructure of both AA7075-T651 and AA1200-H19 aluminium alloys (Plates XX (d) and XXI (d)). Etching with Weck,s reagent indicated that 7075-T651 alloy was lighter than the 1200-H19 aluminium alloy. Substantial material mixing was achieved at the optimal parameters for the two tools, onion ring structures of material flow were seen at these levels (Plates XX (b) and XXI (b)). The mixed region also comprises of microstructure of both alloys as the materials flow into each other in alternate layers (XX (e), XXI (e)).
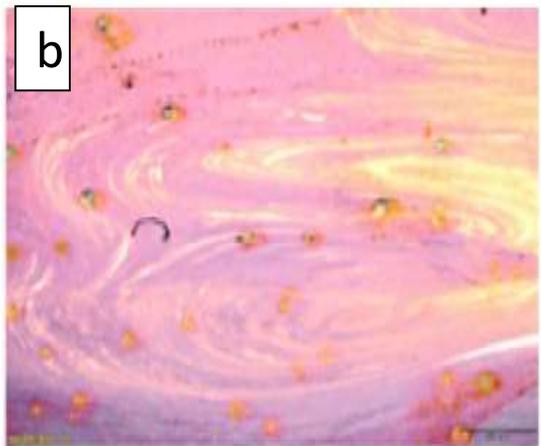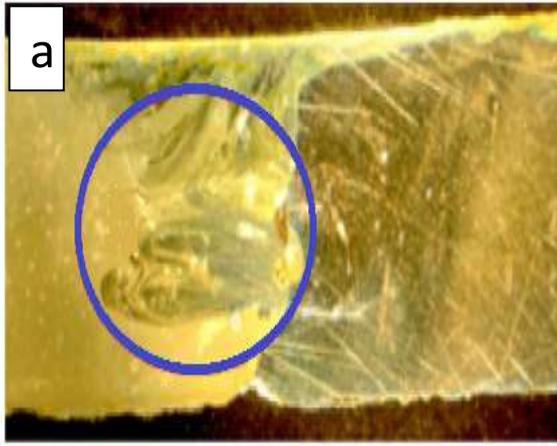
**Plate XX: Optical images of material flow pattern and microstructure of nugget zone of tapered tool optimal weldment at 100X magnification: (a) Micrograph of joint, (b) material flow pattern, (c) unmixed, (d) mechanically mixed, (e) mixed region, (j) joint interface**
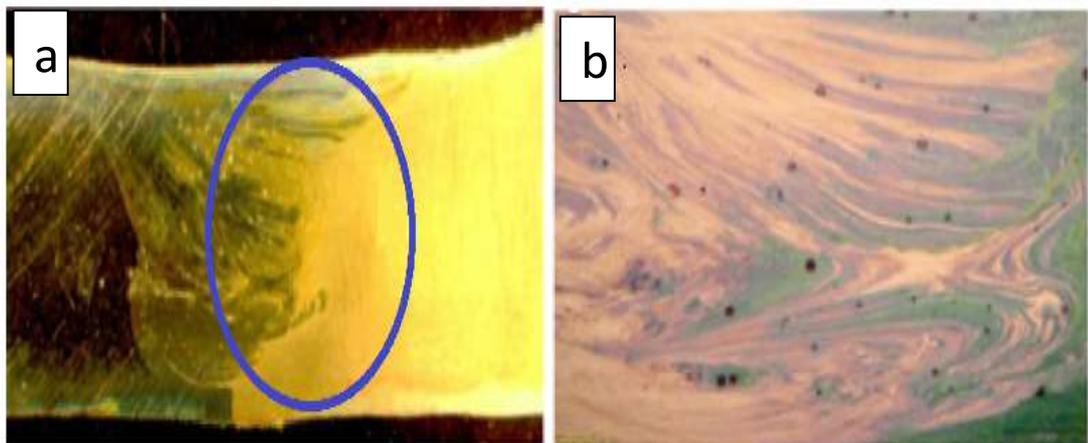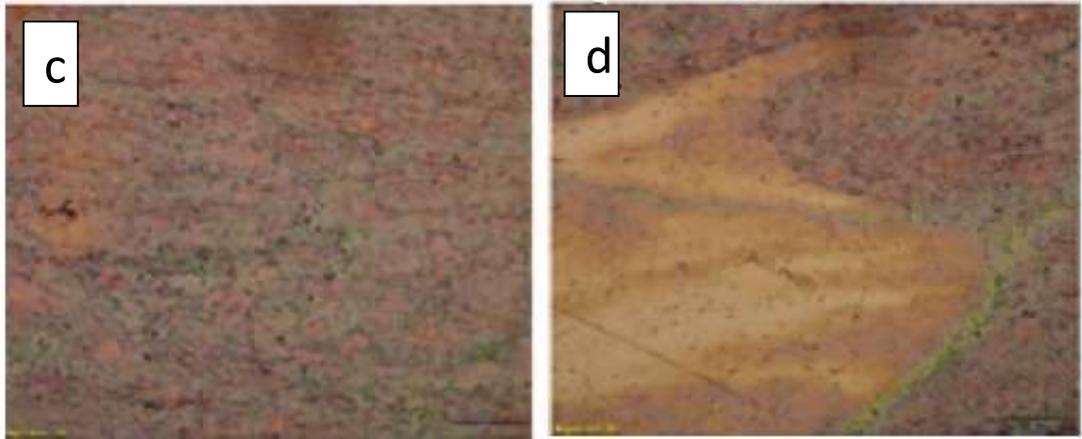
**Plate XXI: Optical images of material flow pattern and microstructure of nugget zone of tapered threaded tool optimal weldment at 100X magnification :(a) Micrograph of joint, (b) material flow pattern, (c) unmixed, (d) mechanically mixed, (e) mixed region, (j) joint interface**

**CHAPTER FIVE**

**5.0          CONCLUSION AND RECOMMENDATIONS**

**5.1     Conclusion**

The investigation on friction stir welding parameters of dissimilar aluminium alloys AA 7075 and AA 1200 butt joints has been successfully undertaken in this work. From the analysis of experiments conducted, it was revealed that:

Effect of friction stir welding parameters (rotational speed, transverse speed and tool tilt angle) of two dissimilar aluminium alloys has been successfully determined. Mechanical properties increase with increase in process parameters up to a certain limit then begins to decrease. The average hardness of both TT increased from 81.99 to 98.58 and then dropped to 77 HV as welding speed increased from 30 to 60 mm/min and 60 to 90 mm/min. While for TTT following the same trend, it increased from 77.8 to 105.25 and dropped to 81.77 HV. Hardness at optimal levels was 98.58 and 105.25 HV, respectively.

The UTS increased from 128.79 at 1150 rpm to 152.48 MPa at 1500 rpm and then dropped to 122.47 MPa at 1850 rpm. While for TTT, it increased from 138.35 to 162.21 at 1500 rpm and then dropped to 138.42 at 1850 rpm. The impact energy followed a similar trend and was optimal for TT and TTT at 20.03 and 21.4 J, respectively.

From the ANOVA for hardness of tapered tool, the tool tilt angle has the highest percentage contribution of 41.79 % on hardness as against rotational and transverse speeds with percentage contributions of 34.45 and 19.44 %, respectively. The rotational speed has the highest percentage contribution based on the ANOVA of the UTS with percentage contribution of 35.03 %, followed by tilt angle with a value of 33.72 and then transverse speed (30.23 %). While, for the impact energy AVOVA, rotational and welding speeds as well as tilt angle have percentage contributions of 37.45, 32.00 and

27.02 %, respectively. From the ANOVA for hardness of tapered threaded tool, the tool transverse speed has the highest percentage contribution of 39.69 % on hardness as against rotational speed and tool tilt angle with percentage contributions of 36.97 and 22.18 %, respectively. The transverse speed has the highest percentage contribution on the UTS based on the ANOVA of the UTS with percentage contribution of 41.29 %, followed by tilt angle with a value of 28.24% and then transverse speed (25.4 6 %). While for the impact energy AVOVA, rotational speed, tilt angle and transverse speed have percentage contributions of 52.57, 24.29 and 19.32 %, respectively.

The optimal welding parameters as revealed by the grey relational analysis for both tapered tool and tapered threaded tools (TT and TTT) was tool rotational speed of 1500 rpm, Transverse speed of 60 mm/min and tilt angle of $2°$.

Tapered threaded tool weldment performed better in terms of their mechanical properties as well as in corrosion resistance as the corrosion rate for threaded tapered tool (0.497 mm/yr) was lower than that of tapered threaded tool (0.68 mm/yr).

The microstructure of the optimal weldments for tapered tool (TT) and tapered threaded tools (TTT) considered were similar with both having presence of onion ring formation which is an indication of proper mixing of the alloys leading to superior mechanical properties.

From the developed regression models for tapered tool (TT), hardness, tensile strength and impact energy of 99.102 HV, 150.99 MPa and 20.0399 J were obtained with each having an error margin of 0.62, 0.977 and 6.355 %, respectively when compared to the experimental values. While for the tapered threaded tool (TTT) weldments, they were hardness, tensile strength and impact energy of 104.18 HV, 161.2 MPa and 22.15 J with

each having an error margin of 1.48, 0.622 and 0.40 %, respectively when compared to the experimental values.

## 5.2    Recommendations

The following recommendations are made:

1.   Compressive and Bending Strengths of the weldment of the two dissimilar aluminium alloys should be evaluated.

2.  Friction stir welding in lap configuration arrangement should be conducted on the two dissimilar aluminium alloys for other application purposes.

3. Further research should be performed on the effect of residual stress on the weldment.

4. The effect of the axial downward force on the mechanical properties of the weldment should be investigated.

## 5.3    Contribution to Knowledge

The study developed a joining parameter for dissimilar welding of AA 1200-H19 and AA 7075-T651 aluminium alloys. The joint efficiencies of the weld were found to be 84.17 % and 90.32 % for tapered tool and tapered threaded tool weldments respectively. The study also established an optimum welding rotational speed of 1500 rpm, welding speed of 60 mm/min and tilt angle of $2^°$ for dissimilar welding of AA 1200-H19 and AA 7075-T651 aluminium alloys.

# REFERENCES

Abutu, J., Lawal, S.A., Ndaliman, M. B., Lafia-Araga, R.A., Adedipe, O. & Choudhury, I.A. (2018). Effects of process parameters on the properties of brake pad developed from seashell as reinforcement material using grey relational analysis. *International Journal of Engineering Science and Technology* 21(1), 787-797.

Abdulaziz, I.A. (2020). Review the common defects in friction stir welding. *International Journal of Scientific and Technology Research*, 8(11) 318-329.

Abolusoro, O. P & Akinlabi, E. T. (2019). Experimental investigations of tool pin geometry and process parameter influence on mechanical property of friction stir welded 6101-T6 and 7075-T651 aluminium alloys. *Journal of Physics*: Conference series 1378 032077 In: *International conference on engineering for sustainable world*, Covenant University Ota, Nigeria p 1378. doi:10.1088/1742-6596/1378/3/032077.

Abolusoro, O. P. & Akinlabi, E. T. (2020). Effect of processing parameters on mechanical, Material flow and wear behaviour of friction stir welded 6101-T6 and 7075-T651aluminium alloys. *Manufacturing Review*. 7(1), 1-14. http://doi.org/10.1051/mreview.

Aby, K., Sritharan, V. & Danesh, G. M. (2016). Optimization of Process parameters of Friction Stir Welding of Dissimilar Aluminium Alloys (AA6063-AA5052) *International Research Journal of Engineering Technology,* 3 (12), 501-504.

Agus, D.A, Bibit, S., Agus, H., Subroto & Sarjito, S. (2017). Mechanical Behaviour Investigation of Aluminium Alloy Tailor Welded Blank Developed By Using Friction Stir Welding Technique *J. Phys.: Conf. Ser. 914 012031 International Conference on Materials Physics and Mechanics: Journal of Physics: Conf. Series* 914(1) 012-031 DOI:10.1088/1742-6596/914/1/012031.

Akinlabi, E.T (2010). Characterisation of Dissimilar Friction Stir Welds between 5754 aluminium alloy and C11000 Copper. PhD Dissertation, Faculty of Engineering, The built Environment and Information Technology, Nelson Mandela Metropolitan University, Port Elizabeth, South Africa.

Akinlabi, E. T., Madyira, D. M. & Akinlabi, S. A. (2011). Effect of Heat Input on the Electrical Resistivity of Dissimilar Friction Stir Welded Joints of Aluminium and Copper, *Institute of Electrical & Electronics Engineering Conference, Africon 2011 - The Falls Resort and Conference Centre,* 13th – 15th September, Livingstone, Zambia.

Akinlabi, E. T. (2012). Effect of shoulder size on weld properties of dissimilar metal friction stir Welds. *Journal of Materials Engineering Performance*. 2(1), 1514-1519. DOI: 10.1007/s11665-011-0046- 6.

Akinlabi, E. T. & Akinlabi, S. A. (2012). Effect of Heat Input on the Properties of Dissimilar Friction Stir Welds of Aluminium and Copper. *American Journal of Materials Science,* 2(5): 147-152, *DOI: 10.5923/j.materials.20120205.03*

Akinlabi, E.T. & Akinlabi, S.A. (2014). Friction Stir Welding of Aluminium and Copper: Fracture Surface Characterizations. *Proceedings of the World Congress on Engineering,* 2 (1), 1525-1528. July 2nd - 4th, London, U.K.

Akinlabi, E.T., Annelize, E. & Patrick, J. M. (2012). Effect of Travel speed on Joint properties of Dissimilar Metal Friction Stir Welds. *Second International Conference on Advances in Engineering and Technology, 20th -21st December,* Noida, India, 155-161.

Amit, G., Punit, K. R & Atul, K. K. (2017). Optimization of Friction Stir Welding Parameters for AA3003 Aluminum Alloy Joints Using Response Surface Methodology. *International Journal of Mechanics and Solids*, 12 (1), 15-26.

Anil -Kumar , H. M., Venakata, R.V. & Shanmuganathan, S.P. (2017). Study of Process Parameters on Dissimilar Friction Stir Welding Using AA2024 T351 and AA7075T6 Aluminium Alloy. *International Journal of Engineering Research and Technology,* 6 (4), 225-228.

Ashish, G., Mohit, S., Manjeet, B. & Sunil, D. (2017). Joint Analysis of Aluminium Alloys AA2014 welded to AA5052 by Friction stir welding using Taguchi method. International Journal of Current Engineering and Technology International Journal of Current Engineering and Technology, 7(5), 1733-1736.

Aonuma, M. & Nakata, K. (2012). Friction stir welding of aluminium based alloys *Journal of Materials Science and Engineering*, 177(2), 543-548.

Bakavos, D., Chen, Y. C., Beabout, L., & Prangnell, P. B. (2011). Material interactions in a novel pinless tool approach to friction stir spot welding thin aluminium sheet,' *Metallurgical Material Transaction*, 42(A), 1266–1282.

Bakavos, D. & Prangnell, P. B. (2009). Effect of reduced or zero pin length and anvil insulation on friction stir spot welding thin gauge 6111 automotive sheet, *Science and Technology of welded Joints* 14(1), 443– 456.

Bhatt, K. D. & Pillai, B. (2012). Simulation of peak temperature and flow stresses during Friction Stir welding of AA7050-T7451 Aluminium Alloy using hyperworks, *International Journal of Emerging Technology and Advanced Engineering, ISSN* 2250-2459, 2(5), 212-216.

Bied-Charreton, A. D (2016). Friction Stir Welding Effects of Defects in Glare. Msc Thesis Submitted to Faculty of Mechanical Engineering/ Aerospace Engineering, Department of Biomedical Engineering (Mechanical Engineering) and Aerospace Structures and Materials (Aerospace Engineering), Delft University of Technology, Netherland.

Bozkurt, Y, & Duman, S. (2011). The effect of welding parameters on the mechanical and microstructural properties of friction stir welded dissimilar AA 3003-H24 and 2124/SiC/25p-T4 alloy joints, *Scientific Research and Essays*. 6(17), 3702-3716, Available online at http://www.academicjournals.org/SRE.

Buchibadu, V., Reddy, G.M. & De, A. (2017). Probing torque, transverse torque and tool durability in friction stir welding of aluminium alloys, *Journal of Material Processing Technology* 241(1) 86-92. doi:1016/j.matprotec.2016.11.008.

Byung-Wook, A., Chang-Yong, L. & Don-Hyun, C. (2010). Effect of Pin Shapes on Joint Characteristics of Friction Stir Spot Welded AA5J32 Sheet, *Materials Transaction*, 51 (5) 1028-1032.

Caio-Palumbo, D.A., Isolda, C., Harcilio, G.D., Nadine, P., Bernard, T. & Vincent, V. (2017). Multiscale electrochemical study of welded aluminium joined by friction stir welding. Journal of electrochemical society, 164(13) 735-746.

Carlone, P., Astarita, A., Palazzo, G.S., Paradiso, V. & Squillace, A. (2015). Microstructural aspects in Al–Cu dissimilar joining by FSW, The *International Journal of Advanced Manufacturing Technology,* 79 (5), 1109-1116.

Carlone, P., Astarita., A., Rubino, F. & Pasquino, N. (2016). Microstructural Aspects in Friction Stir Welding and TIG Welding of Cast ZE41A Magnesium Alloy, *Metallurgical and Materials Transactions B*, 47B, 1340-1346.

Chaitanya, S., Dwivedi, D. K., & Kumar, P. (2013). Effect of post weld heat treatments on microstructure and mechanical properties of friction stir welded joints of Al-Zn-Mg alloy AA7039: *Materials and Design Journal*, 43(1): 134-143.

Chakravarthy, M.P., Mohana, K.N. & Pradeep-Kumar., C. B. (2014). Corrosion inhibition effect and adsorption behaviour of nicotinamide derivatives on mild steel in hydrochloric acid solution, *International Journal of Industrial Chemistry*, 5 (19),1-21, DOI 10.1007/s40090-014-0019-3.

Chetan, P., Hemant, P. & Hiralal, P. (2016). Investigation of Weld Defects in Similar and Dissimilar Friction Stir Welded Joints of Aluminium Alloys of AA7075 and AA6061 by X-ray Radiography *American Journal of Materials Engineering and Technology,* 4(1), 11-15.

Daswes, C.J., Threadgill, P.L., Spurgin, E.J.R & Staines, D. G. (2007) Development of the New Friction Stir technique for welding aluminium- Phase II, The Weld Institute Member report 5651/35/95. Nov 1995. In: *Friction stir welding and processing*. Mishra RS, Mahoney MW (eds.) Materials Park Ohio; ASM International.

Dinaharan, I., Kalaiselvan, K., Vijay, S.J. & Raja, P. (2012). Effect of material location and tool rotational speed on microstructure and tensile strength of dissimilar friction stir welded aluminium alloys, *Archives of Civil and Mechanical Engineering*, 12(1), 446-454.

Ding, R. J. & Oelgoetz P. A. (2012). Auto-adjustable probe tool for friction stir welding, US Patent no. 5893507.

Ding, R. J. (2013). Force characterization on the welding pin of a friction stir welding retractable pin tool using aluminium-lithium 2195, *Proceedings. 2nd International Conference on 'Friction stir welding*, September 10th -13th Gothenburg, Sweden, 220-226.

Divya, D. D., Anuj, S. & Charit, V. (2014). Optimisation of Friction Stir Welding Parameters for AA 6061 and AA 7039 Aluminium Alloys by Response Surface Methodology (RSM). *International Journal of Advanced Mechanical Engineering*.
4 (5) 565-571.

Elathrasan, G & Senthil Kumar, V.S (2012). Modelling and Optimization of Friction Stir welding parameters for Dissimilar Aluminium Alloys using Response Surface Methodolgy, *International Conference on Modeling, Optimization and Computing*, *Procedia Engineering*, 38(1), 3477 – 3481.

Elangovan, K., Balasubramanian, V. & Babub, S. (2009). Predicting tensile strength of Friction stir welded AA6061 aluminium alloy joints by a mathematical model *Materials and Design Journal.* 30 (1), 188-193.

Esmaeili, A., Besharati, G.M.K & Zareie, R. H.R (2011). A metallurgical and mechanical study on dissimilar Friction Stir welding of aluminium 1050 to brass (CuZn30). *Material Science and Engineering* 1(A), 528(1) 7093-7102.

Ewuola, O. O., Akinlabi, E.T. & Madyira, D. M. (2016). Effect of Plunge Depth on Weld Integrity of Friction Stir Welds of Dissimilar Aluminium and Copper. *Proceedings of the World Congress on Engineering 2016 Vol II WCE 2016*, June 29th - July 1st, London, U.K. 1157-1160, http://handle.net/10210/93322.

Fereiduni, E., Movahedi, M. & Kokabi, A.H. (2015). Aluminum/steel joints made by an alternative friction stir spot welding process, *Journal of Materials Processing Technology,* 224 (1)*, 1–10.

Frigaard, O., Grong, O. & Midling, O. T. (2001). A process model for friction-stir welding of age hardening aluminium alloys". *Metallurgical and Material Transactions.* 32A(5), 1189-1200, 1189-1190, DOI:10.1007/s11661-001-0128-4.

Fukumoto, M., Yasui, T., Shinoda, Y., Tshubaki, M. & Shinoda, T. (2004). Butt welding Between dissimilar metals by friction stirring. *5th International Friction Stir Welding Symposium*, September 14th -16th, Metz, France.14-16.

Galvao, I., Oliveira, J. C., Loureiro, A & Rodrigues, D .M .(2012). Formation and distribution of brittle structures in friction stir welding of Aluminium and copper: Influence of shoulder geometry. *Journal of Intermetallics*. 22(1) 122-128.

Gesto, D., Pintos, V., Vazquez, J. Rasilla, J., & Barreras, S. (2008). Application of Friction stir welding in ship building. *Proceedings of TWI,s 7th Int. Symposium on Friction stir welding*', May 4th-7th , Awaji Island, Japan.227-232.

Guo, J. F., Chen, H.C., Sun, C.N., Bi, G., Sun, Z. & Wei, J. (2014). Friction Stir Welding of Dissimilar Materials Between AA6061 and AA7075 Al alloys effects of Process Parameters. *Materials and Design* 56(C), 185-192.

Gurvir, S. S., Gurmeet, K. & Jasbir, S .G. (2016). Optimization of Process Parameters of Friction Stir Welding of Dissimilar Aluminum Alloys AA6061-T6 and AA6082-T6. Indian Journal of Science and Technology, 9 (36), 1-5 DOI: 10.17485/ijst/2016/v9i3 6/101460.

Heena, K. S, Kamlesh, B, Krunal S & Unnati, J (2016). Experimental Analysis of Friction Stir Welding of Dissimilar Alloys AA6061 and Mg AZ31 Using Circular Butt Joint Geometry, 3rd International Conference on Innovations in Automation and Mechatronics Engineering, ICIAME 2016 *Procedia Technology,* 23 (1) 566 –572.

Hua, T. (2006). Monitoring and Intelligent Control for Complex Curvature Friction Stir Welding. D.Tech Thesis. Faculty of Engineering, Nelson Mandela Metropolitan University, Port Elizabeth South Africa.

Hussain, A.K. & Quadri, S.A.P. (2010). Evaluation of parameters of friction stir welding for aluminium AA6351 Alloy, *International Journal of Engineering Science and Technology*, 2 (10) , 5977-5984.

Hwang, Y. M., Pan, P.L & Lin, C.H. (2010). Experimental study on friction stirWelding of copper metals. *Journal of material processing Technology* 210(1) 1667-1672.

Ikumapayi, O.M., Akinlabi, E.T., Majumdar, J.D., Fayomi, O.S.I & Akinlabi, S.A. (2020). Corrosion study and quantitative measurement of crystallite size of high strength Aluminum hybrid composite developed via friction stir processing. *Materialwiss. Werkstofftech.*, 51(1), 732–739.

Ilangovan, M., Rajendra, S. B. & Balasuramanian, V. (2015). Effect of tool pin profile on microstructure and tensile properties of friction stir dissimilar AA 6061 and AA 5086 aluminium alloy joints. *Journal of Defence Technology* 11(1), 174-184.

Jagesvar, V., Ravindra, V., Taiwade, Chandraprakash Reddy & Rajesh K. K (2017). Effect of Friction Stir Welding Process Parameters on Mg-AZ31B/Al-AA6061 Joints. *Journal of Materials and Manufacturing Processes,* 33 (3), 308-314.

Jambulingam, S. (2015). Optimization of process parameters of friction stir welding for dissimilar aluminium alloys AA7075 and AA3014, *International Journal of Emerging Researches in Engineering Science and Technology*, 2(1), 234-251.

João-Pedro, R. P., (2014). Sealant Joints in Aircraft Integral Fuel Tanks, Master of Science Degree thesis, Technico Lisboa, Portugal, 27-60.

Jitender, K & Hari, S. (2016). Friction Stir Welding of Dissimilar Aluminium Alloys: Effect of Process Parameters on Mechanical Properties, *Engineering Solid Mechanics* 4(1), 125-132.

Kamran, A. & Farhad, G. (2016). Influence of Welding Speed on Corrosion Behaviour of Friction Stir Welded AA5086 Aluminium Alloy. *Journal of Centenary South University,* 23(1), 1301−1311.

Khaled, T. (2005). An outsider looks at Friction stir welding. Federal Aviation Administration. Report number: ANM-112N-05-06. 7-9. Retrieved on November 12 2017 from http://googlescholar.com.

Khrishna, K. N. (2002). On the formation of Onion ring in friction stir welds. *Material Science and Engineering, A.* 327(2) 246-251. doi: 10.1016/S0921-5093(01)01474-5.

Kumar, K., Kailas, V. & Satish, I. (2008). The role of friction stir welding tool on material flow and Weld formation*: Materials Science and Engineering*, 485(1): 367-374.

Kumbhar, N.T., & Bhanumurthy, K (2017). Friction Stir Welding of Aluminium 5052 with Al6061. *Journal of Metallurgy,* 2012(1), doi:10.1155/2012/303756, 1-7.

Lakshminarayanan, A. K., Malarvizhi, S. & Balasubramanian, V. (2011). Developing friction stir welding window for AA2219 aluminium alloy. *Transactions of Nonferrous Metals Society of China.* 21(1) 2339-2347.

Leal, R. M., Loureiro, A., Rodrigues, D. M., & Galvao, I. (2010). Material flow in heterogeneous friction stir welding of aluminium and copper thin sheets, *Science and Technology of Welding and Joining,* 5(8), 654- 660.

Lee, C. Y., Lee, W. B., Kim, J. W., Choi, D. H., Yeon, Y. M. & Jung, S. B. (2008). Lap joint Properties of friction stir welded dissimilar formed 5052 Al and 6061 Al alloys with different thickness," *Journal of Materials Science*, 43(9), 3296–3304.

Li, X., Zhang, D., Qiu., C & Zhang, W. (2012). Microstructure and Mechanical Properties of dissimilar pure copper/1350 aluminium alloy butt joint by friction stir welding. *Transactions of Non-ferrous Metals society of China* 22(1), 1298-1306.

Lienert, T. J., Stellwag, W. L., Grimmett, J. B. B. & Warke, R .W. (2013). Friction Stir Welding Studies on mild steel, *American Welding Society, Supplement to the Welding Journal.* 35(1) 210-224.

Maalekian, M., Kozeschnik, E., Branntner, H.P., & Cerjak, H. (2008). Finite element modelling of orbital Friction Welding of Eutectoid Steel Bars. *Metallurgical and Materials Transaction,* 39(A), 844-852.

Mahoney, M.W., Rhodes, C.G., Flintoff, J.G., Bingel, W.H.,Spurling, R.A.(1998). Properties of Friction Stir Welded 7075-T651 Aluminium. *Metallurgical and Materials Transactions A* 29(1) 1955-1964. doi: 10.1007/s11661-998-0021-S.

Marie, F., Allehaux, D & Esmiller, B. (2004). Development of the bobbin tool technique on various Aluminium Alloys,' *Proceedings. 5th International Conference on friction stir welding,* September 5th- 8th Metz, France, 1-8

Midling, O. T., Kvåle, J. S & Dahl, O. (1999). Industrialisation of the Friction Stir Welding Technology in Panels Production for the Maritime Sector. *Proceedings*

*of TWI 1st International Symposium on 'Friction stir welding,* June 2nd- 5th 1999, Thousand Oaks, CA, USA, 255-259.

Montgomery, D.C., Runger, G.C, Hubele, N.F. (1998). Engineering statistics, First Edition, John Willey and Sons, Inc, Ney York, USA.

Murr, L.E., Liu, G.J. & McClure, J.C. (1997). Dynamic Recrystallisation in Friction Stir welding of aluminium alloy 1100. *Journal of Material Science Letters*. 16(22):1801-1803. doi:10.1023/A.1018556332357.

Myers, R. H., & Montgomery, D.C. (2002). Response Surface Methodology: process and product optimization using designed experiment, A Wiley-Interscience Publication. New York, USA.

Nandan, R., Roy, G. & Debroy, T. (2013). Numerical simulation of three-dimensional heat Transfer and plastic flow during friction stir welding, *Metal Material Transactions,* A(37), 1247-1259.

Navaneethakrishnan, T. & Ganesh, P. (2015). Effect of Welding Parameters on Friction Stir Welded Dissimilar Aluminum Alloys 7075 and 6082 with Various Tool Pin Profiles. *International Conference on Recent Advancement In Mechanical Engineering & Technology*, *Journal of Chemical and Pharmaceutical Sciences,* Special Issue 9, 463-468.

Olivier, L., Veronique, F., Hamid, Z., & Didier, L (2010). Understanding the material flow path of friction stir welding process using unthreaded tools, *Journal of Materials Processing Technology* 1(1). 603-609. https://hal.archives-ouvertes.fr/hal-02456305.

Ouyang, J. H. & Kovacevic, R (2002). Material flow and microstructure in the Friction stir butt welds of the same and dissimilar aluminum alloys. *Journal of Manufacturing Engineering and Performance*, 11 (1):51-63.

Ozel, T., Hsu, T. K. & Erol, Y. Z . (2005). Effect of cutting edge geometry, work piece Hardness, feed rate and cutting speed on surface roughness and forces in finish hard turning of hardened AISI H 13 steel, *International Journal of Advanced Manufacturing Technology*, 25 (1), 262-269.

Pankaj, N, D. T. & Pranav, K. P. (2014). Optimization of Friction stir welding parameters in joining dissimilar aluminium alloys using SPSS and Taguch, *Journal of Basic and Applied Engineering Research*, 1(1), 25-27.

Pantelis, D. I. (2014). School of Naval Architecture and Marine Engineering, Greek Section. Technical meeting. Retrieved on November 12 2017 from http://googlescholar.com.

Paradiso, V., Rubino, F Carlone, P. & Palazzo, G. S (2017). Magnesium and Aluminium alloys Dissimilar Joining by Friction Stir Welding, *17th International Conference on Sheet Metal, SHEMET17 Procedia Engineering* 183 (1), 239-244.

Park, J. C. &. Kim, S. J. (2010). The effect of traveling and rotation speeds on mechanical properties during friction stir welding of dissimilar Al alloys, *Defect and Diffusion Forum*, 297 (301), 590–595.

Park, S. K., Hong, S. T., Park, J. H., Park, K. Y., Kwon, Y. J. &. Son, H. J. (2013). Effect of Material locations on properties of friction stir welding joints of dissimilar Aluminium alloys, *Science and Technology of Welding and Joining*, 15(4). 331-336.

Patil, H. S & Soman, S. N. (2013). Effect of Weld Parameter on Mechanical and Metallurgical Properties of Dissimilar Joints AA6082–AA6061 In T6 Condition Produced By Friction Stir Welding. *Frattura ed Integrità Strutturale,* 24 (1) 151-160,DOI: 10.3221/IGF-ESIS.24.16.

Pierce Industries (2018). Friction Welding. Retrieved on 25th March 2021 from www.pierceindustries .

Podrzaj, P., Jerman, B. & Klobcar, D. (2015).Welding Defects at Friction Stir Welding, METABK 54(2) 387-389.

Pradeep, A. & Muthukumaran, S. (2013). An analysis to optimize the process parameters of friction stir welded low alloy steel plates, *International Journal of Engineering, Science and Technology,* 5(1), 25-35.

Qi, X. & Chao, Y. J. (1999*).* Heat transfer and Thermo-Mechanical analysis of friction stir joining of 6061-T6 plates. *1st International Symposium on friction stir welding. Thousand Oaks, USA:* Retrieved on October 28 2017 from http://www.scielo.br.

Rai, R., De, A., Bhadeshia, H.K.D.H., & DebRoy, T. (2011). Review: friction stir welding tools. *Science & Technology Welding and Joining*, 16(1):325–42.

Rajkumar, V., Venkatesh, K. & Arivazhagan, N. (2017). Friction Stir Welding of aluminium alloys, aluminium alloys – Recent Trends in Processing, Characterization, Mechanical behavior and Applications, http://dx.doi.org/10.5772/intechopen.70233, Retrieved on March 17, 2018 from: http://www.intechopen.com/books/aluminium-alloys-recenttrends-inprocessing-characterization-mechanical-behavior-and-applications.

Rajesh, K .G., Hrishikesh D. & Tapan K. P. (2012). Influence of Processing Parameters on Induced Energy, Mechanical and Corrosion Properties of FSW Butt Joint of 7475 AA. *Journal of Materials Engineering Performance*, 21:1645–1654 _ASM International. DOI: 10.1007/s11665-011-0074-21.

Raju, P.M., Rahul, B., Surya, K.P., Harshaseep, S.J.& Siddhartha, D.A. (2016). A study on mechanical properties in friction stir lap welding of AA 6061-T6 and AISI 304. *Materials Science & Engineering A,* 652(1)136–144.

Ramachandran, K.K., Murugan, N & Shashi, K.S. (2015). Friction Stir Welding of Aluminum Alloy Aa5052 and HSLA Steel, *Welding Journal*, 94 (1), 291-300.

Ratanathavorn, W. & Melander, A. (2015). Dissimilar joining between aluminium alloys (AA6111) and thermoplastics using friction stir welding. *Science and Technology of Welding and Joining*, 20 (3), 222-228.

Raza, M., P.M., Farazila, Y., Hassan, M.A. & Rahmat, S. M. (2015). Effect of tool rotational speed on force generation, microstructure and mechanical properties of friction stir welded Al-Mg- Cr-Mn (AA 5052-O) alloy. *Material Design,* 66 (1), 118-128.

Record, J. H., Covington, J. L., Nelson, T. W., Sorensen, C.D. & Webb, B.W. (2004). *Fundamental characterisation of friction stir welding*. 5th International Friction Stir Weilding Symposium Metz, France. September 14th -16th. The Weld Institute (UK). Retrieved: CDROM.

Robert, J. C., Spyros, A. K., Gregory C. S. & Giannoula, C. (2019). Joint strength or "efficiency" factors of steel lap welded joints for use water conveyance. Utility Engineering & Surveying Institute (UESI) pipelines conference, July 21-24, Nashvile, Tennessee USA. https://doi.org/10.1061/9780784482506.048.

Rusdi, N., Ahmad, Z. S. & Muhammad, A. S (2017). Mechanical Properties on Friction Stir Welding of Aluminium AlIoy 5052. *ARPN Journal of Engineering and Applied Sciences Asian Research Publishing Network (ARPN).*12 (15). 4445-4450.

Sajid, A. K.H., Fathal, A., Hashim, A. & Al-Rouba, O. (2012). Mechanical properties and Microstructure of 6061-T651 aluminium alloy by friction stir welding, *The Iraqi Journal for Mechanical and Material Engineering,* 12(4), 723-734.

Sandeep, V.J. & Sandeen, E.S. (2016). Friction Stir welding of dissimilar aluminium Alloys between AA5052 and Steel. *International Journal of Advanced Manufacturing Technology,* 30(2), 225-236.

Selamat, N.F.M., A.H. Baghdadi, A.H., Sajuri, Z. & Kokabi, A.H (2016). Friction stir Welding of similar and dissimilar aluminium alloys for automotive applications. *International Journal of Automotive and Mechanical Engineering*, 13(2), 3401 -3412, September 5th- 7th. *Universiti Malaysia Pahang Publishing* DOI: https://doi.org/10.15282/ijame.13.2.2016.9.0281.

Shanavas, S., Edwin, R. D. J. & Murugan, N. (2018). Weldability of marine grade AA 5052 aluminum alloy by underwater friction stir welding. *The International Journal of Advanced Manufacturing Technology*, 95(1), 4535-4546. https://doi.org/10.1007/s0 0170-017-1492-6.

Shaikh, G. I. & Dabade, U.A. (2015). Experimental Investigation on friction stir welding of dissimilar metals, *5th National conference on Recent Advances in Manufacturing*, Sarder Vallabhbhai National Institute of Technology, Surat, India, 15-17. Retrieved on October, 29 2017 from http;//www.reserachgate.net.

Shaikh, M. S & Yagnesh, B. C. (2015). Optimization of friction stir welding process parameters for welding aluminum alloys, *International Journal of Science Technology & Engineering* 2(2), 69-75.

Skinner, M. & Edwards, R. L. (2003). Improvements to the friction stir welding process using the self-reacting technology. *Material Science Forum*, 426(1), 2849–2854.

Smith, C. B., Hinrichs, J. F., & Ruehl, P. C.  (2012). Friction Stir and Friction Stir Spot Welding - Lean, Mean and Green. Retrieved on October 20 2017 from: www.frictionstirlink/Pub14AwssmcLeanMeanGreen-UnitedStates.

Sunil, K., Yasir, Z. & Raghuvir, K. (2018). A review on modelling and optimisation techniques in turning processes. *International Journal of Mechanical Engineering and Technology*. 8(3), 1146-1156.

Suriya, P., Pradit, S. & Kittipong, K. (2015).  Friction Stir Spot Welding of AA5052 Aluminum Alloy and C11000 Copper Lap Joints *International Journal of Advanced Culture Technology,* 3(1), 145-152. http://dx.doi.org/10.17703/IJACT.2015.3.1.145.

Suhuddin, U.F.H.R., Mironov, S., Sato, Y.S., Kokawa, H & Lee, C.W (2009). Grain structure evolution during friction stir welding of Az31 magnesium alloy. *Acta Materialia*. 57(1) 5406-5418.

Sylva, G., Edwards, R.  & Sassa, T. (2004). A feasibility study for selecting pin tool welding of thin section aluminium,' Proceedings. 5th International Conference on Friction stir welding, September 5th – 8th, Metz, France.

Thomas, M.W., Nicholas, E.D., Needham, J. C., Murch, T.A.G., Templesmith, P & Dawes, C.J. (1991). Improvements Relating to Friction Stir Welding. *International Patent Application. PCT/GB92/02203.*

Tozaki, Y., Uematsu, Y. & K. Tokaji (2010). A newly developed tool without the probe for friction Stir spot welding and its performance,' *Journal of Material Process Technology* 210(1), 844–851.

Toshev, Y.  & Kostadinov, K. (2006). Protective coating of Zinc and Zinc alloys for Industrial applications. 2nd International conference on Multi-Material Micro Manufacture. Forschumgszentrum Karlsruhe, Germany, 23-25th September.

Tri-state Fabricators (2010). Types of Welding. Retrieved on 28th February, 2018 from: triastatefabricators.com.

TWI (2015). What is welding? Definition, processes and types of welds. Retrieved on 25th March, 2021 from www.twi-global.com.

Uthaya- Kumar, M., Prabhakaran, G. & Arvindam, S. (2012). Influence of cutting force on bimetallic piston machining by cubic boron nitrides tool (CBN), *Journal of Material Manufacturing Process*, 27(1), 1078-1083.

Valero, O.F., Kenedy, C., Murr, L.E., Brown, D., Snidhar, P.,Brook, M.W & Mcclure, J. C. (1998). Micro Structural Issues in friction Stir Welded aluminum alloy. *Scripta Materialia*, 38(5), 703-708.

Vinayak, D. Y. & Bhatwadekar, S. G. (2015). Friction Stir Welding of Dissimilar Aluminium alloys AA1100 to AA6101-T6. *International Journal of Research In Aeronautical and Mechanical Engineering*, 3(1) 2321-3051.

Vivekanandan, P., Arunachalam, V., P, Prakash, T. & Savadamuthu, L. (2012). The Experimental Analysis of Friction Stir Welding on Aluminium Composites. *International Journal of Metallurgical Engineering,* 1(4): 60-65 DOI: 10.5923/j.ijmee.20120104.03. *Materialia*, 38(5), 703-708.

Vinayak, D. Y. & Bhatwadekar, S.G. (2014). Friction stir welding of dissimilar materials between AA6101 aluminium and pure Copper, *International Journal of Engineering Sciences & Research Technology*, 3(12), 505-508.

Vural, M. (2014). Welding and Bonding Technologies. Comprehensive Metal Processing, Elsevier Limited, Istanbul, Turkey, 6(1), 3-48 DOI:10.1016/B978-0-08-0965321.006038.

Wang, Y., Tong, J. & Congqing, L. (2009). Application of friction stir welding on large aircraft structures (China Friction Centre, BAMTRI) Retrieved on 24th May 2019 from: www.cfswt.com.

Wayne, M.T., Keith, I.J. & Christoph, S. W. (2003). Friction Stir Welding. Recent Development in Tool and Process Technologies. Advanced Engineering Materials, The weld Institute Abington, Cambridge, United Kingdom 5 (7), 485-490.

Wei, Y., Li, J., Xiong, J., Huang, F., Zhang, F. & Raza S. H. (2012). Joining Aluminium to titanium Alloy by friction stir lap welding with cutting pin. *Journal of Material Characterization*. 71(1), 1-5.

Xu, W. F., Liu, J. H., Chen, D. L., Luan, G.H & Yao, J. S. (2012). Improvements of strength and ductility in aluminium alloy joints via rapid cooling during friction stir welding. *Materials Science and Engineering* 1(A), 548, 89-98.

Yaduwanshi, D. K., Bag, S. & Pal, S. (2016). Effect of Tool offset in hybrid Friction Stir Welding of Copper and Aluminium alloys. Materials and Manufacturing Processes, 33(3), 227-289.

Yan, Y., Zhang, D., Qiu, C. & Zhang, W. (2010). Dissimilar frictions stir welding between 5052 aluminium alloy and AZ31 magnesium alloy. *Transactions of Nonferrous Metals Society of China.* 20(1), 619-623.

Yoo, T., Yoon, J., Min, K. & Lee, H. (2015). Effect of friction stir welding process parameters on mechanical properties and macro structure of Al-Li alloy, *2ⁿᵈ International Materials, Industrial, and Manufacturing Engineering Conference*, February 4ᵗʰ -6ᵗʰ, Bali Indonesia. Retrieved on November 12 2017 from http://www.sciencedirect.com.

Yoshikawa, K. (2003). A joining criterion for lap welding of dissimilar metal materials of aluminium and stainless steel. *4th International friction stir welding symposium*, Park City, Utah. USA 14-16.

Yufeng, S., Nobuhiro, T. & Hidetoshi, F. (2016). Microstructure and Mechanical Properties of Dissimilar Friction Stir Welding between Ultrafine Grained 1050 and 6061-T6 Aluminum Alloys, *Metals*, 1-12, doi:3390/met6100249.

Zhang, G., Su, w., Zhang, J., Wei, Z., & Zhang, J. (2010). Effects of shoulder on interfacial bonding during friction stir Lap welding of Aluminium thin sheets using tool without pin. *Transaction of non-ferrous metal society of China*, 20(1) 2233-2228.

Zhang, F., Su, X., Chen, Z. & Nie, Z. (2015). Effect of welding parameter on microstructure and mechanical properties of friction stir welded joints of a super high strength Al–Zn–Mg–Cu aluminum alloy, *Journal of Materials and Design* 67(1), 483–491.
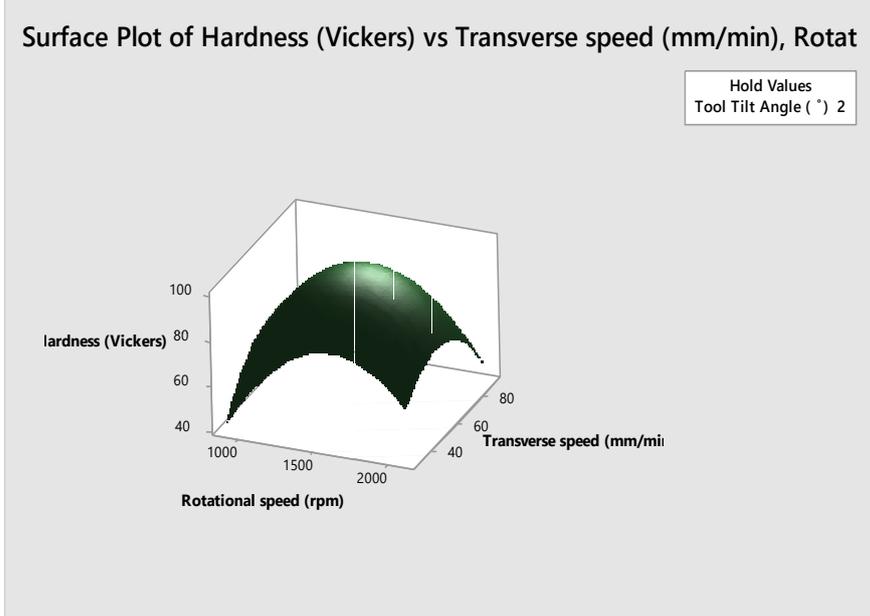
APPENDIX A (i): Interaction plot for UTS (TT)
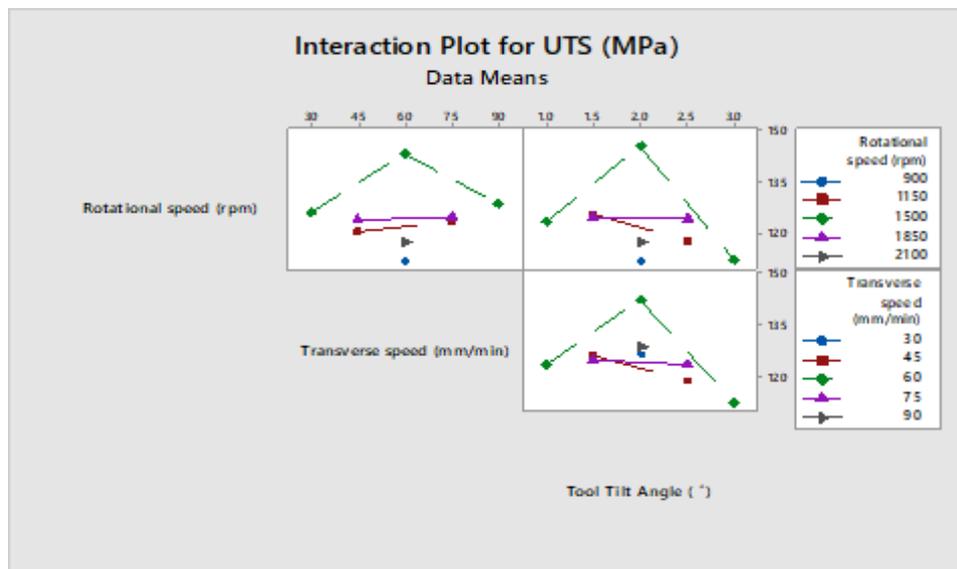


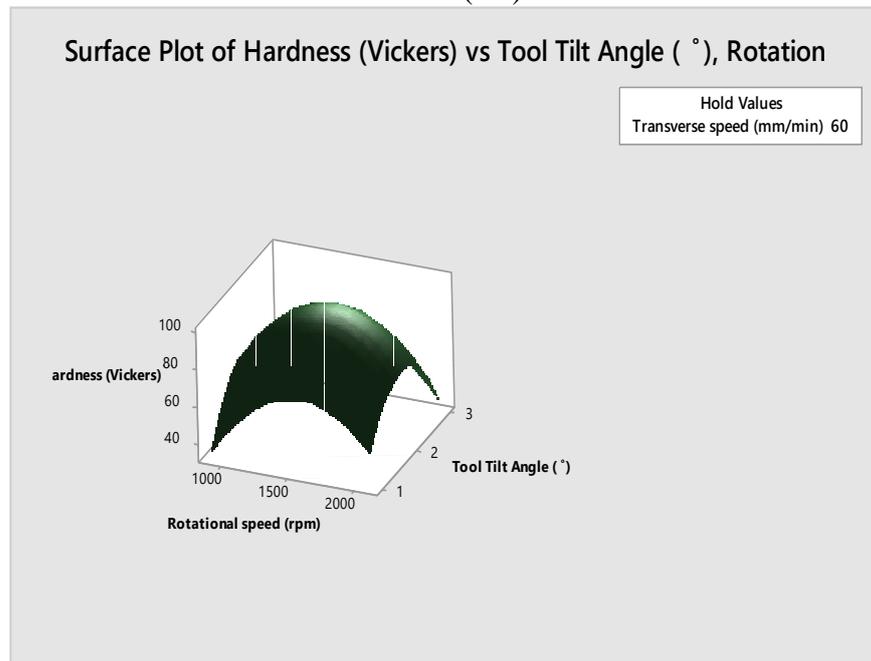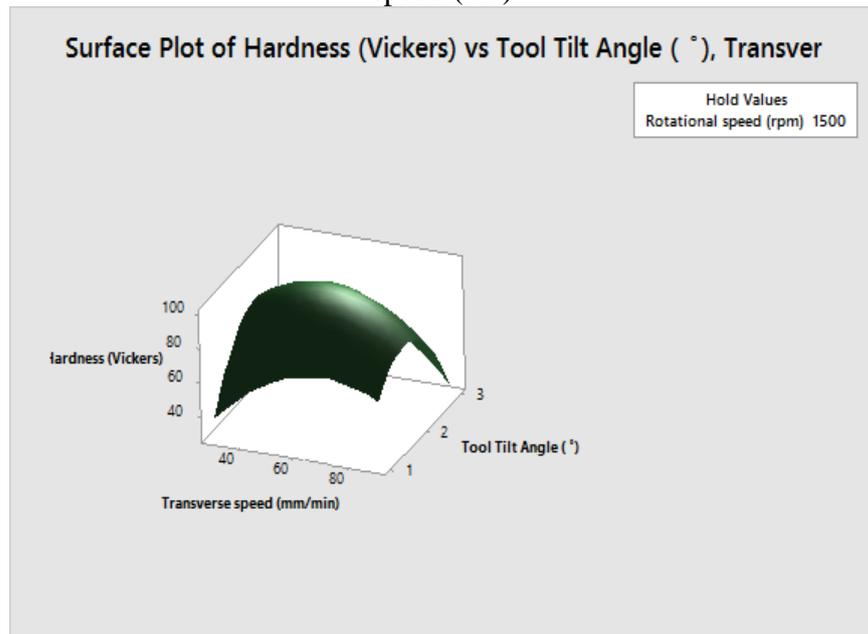(ii): Interaction plot for impact energy
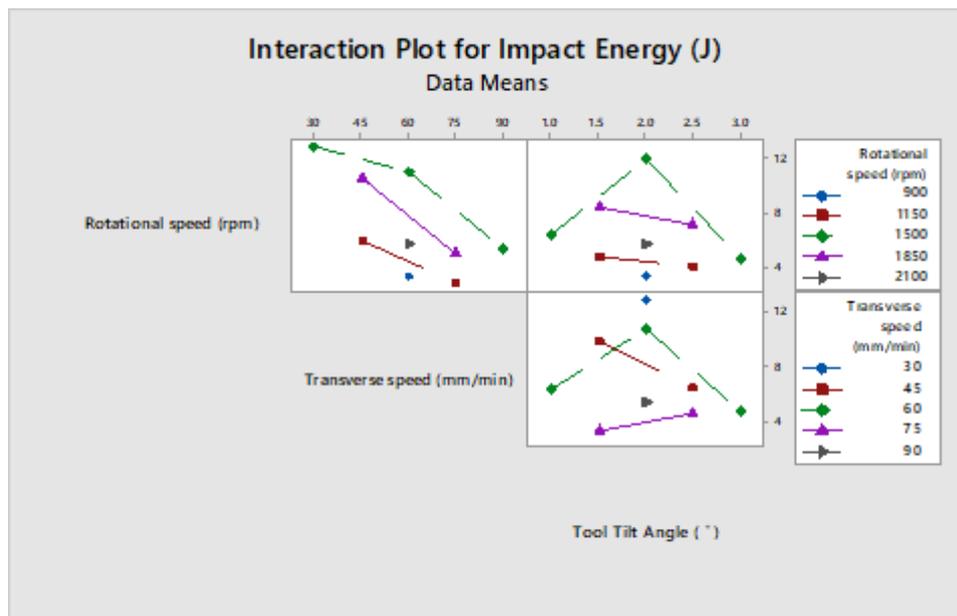
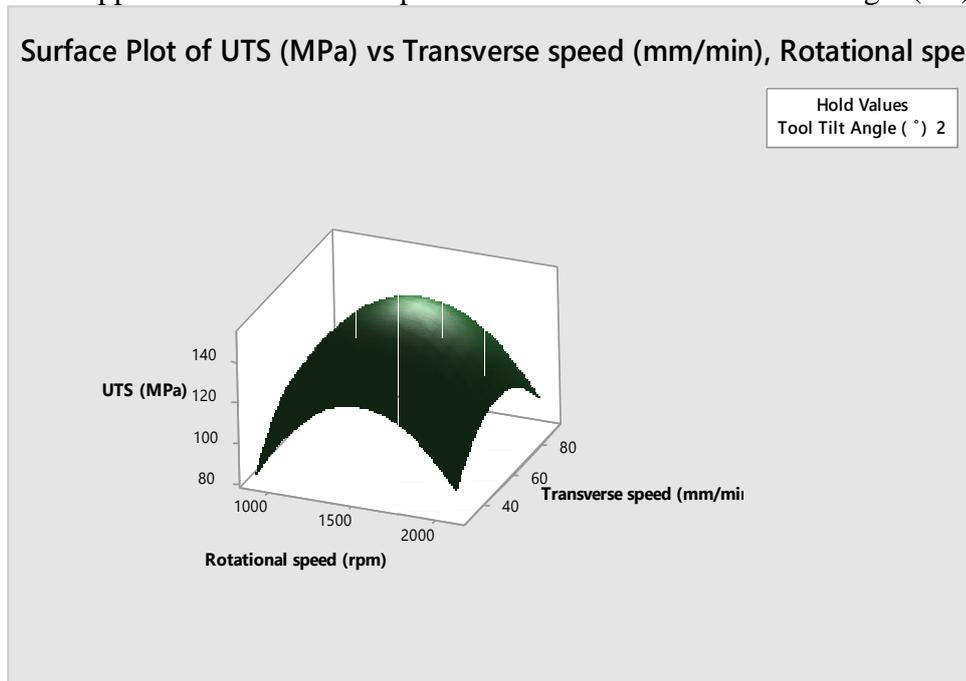APPENDIX B: 3D Surface plots for hardness at constant tilt angle (TT)



Surface Plot of Hardness (Vickers) vs Transverse speed (mm/min), Rotat

APPENDIX C: 3D Surface plots for hardness at constant traverse speed (TT)



Surface Plot of Hardness (Vickers) vs Tool Tilt Angle ( ˚), Rotation

APPENDIX D: 3D Surface plots for hardness at constant rotational speed (TT)



Surface Plot of Hardness (Vickers) vs Tool Tilt Angle ( ˚ ), Transver

Hold Values
Rotational speed (rpm) 1500

Appendix E: 3D Surface plots for UTS at constant tool tilt angle (TT)



Surface Plot of UTS (MPa) vs Transverse speed (mm/min), Rotational spe

Hold Values
Tool Tilt Angle ( ˚ ) 2

APPENDIX F: 3D Surface plots for UTS at constant traverse speed (TT)



Surface Plot of UTS (MPa) vs Tool Tilt Angle ( ˚ ), Rotational speed

Hold Values
Transverse speed (mm/min) 60
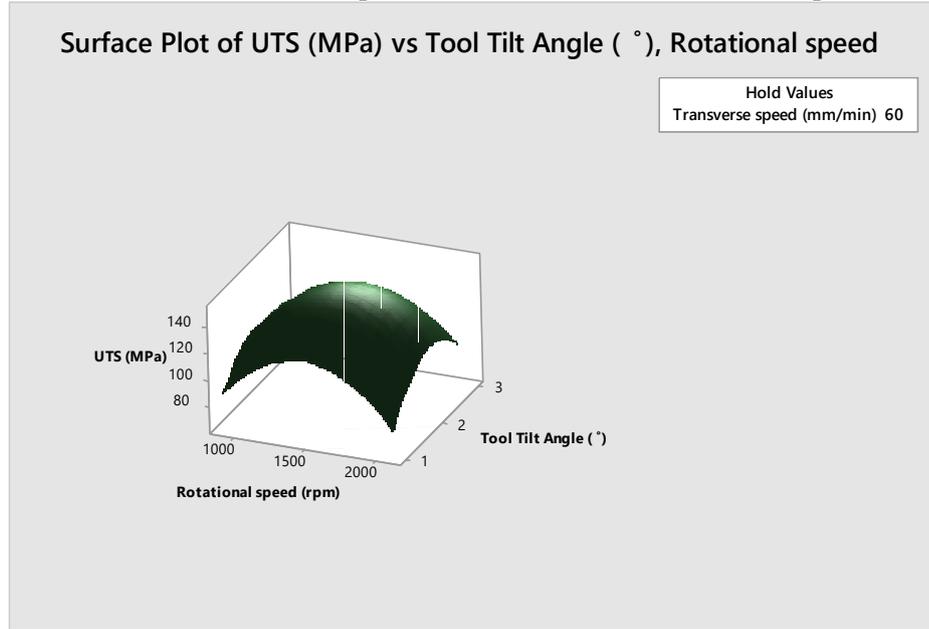
APPENDIX G: 3D Surface plots for UTS at constant rotational speed (TT)



Surface Plot of UTS (MPa) vs Tool Tilt Angle ( ˚ ), Transverse speed

Hold Values
Rotational speed (rpm) 1500
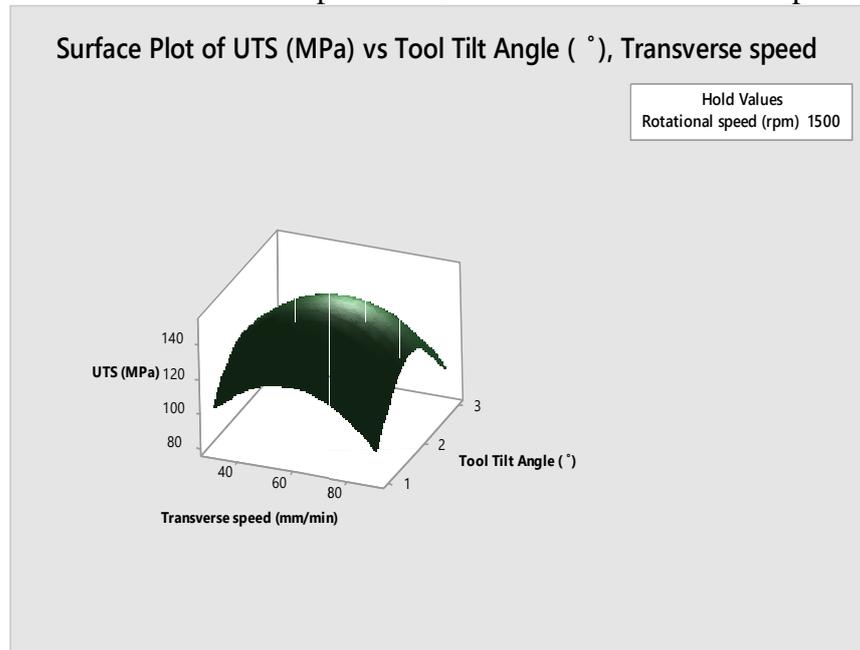
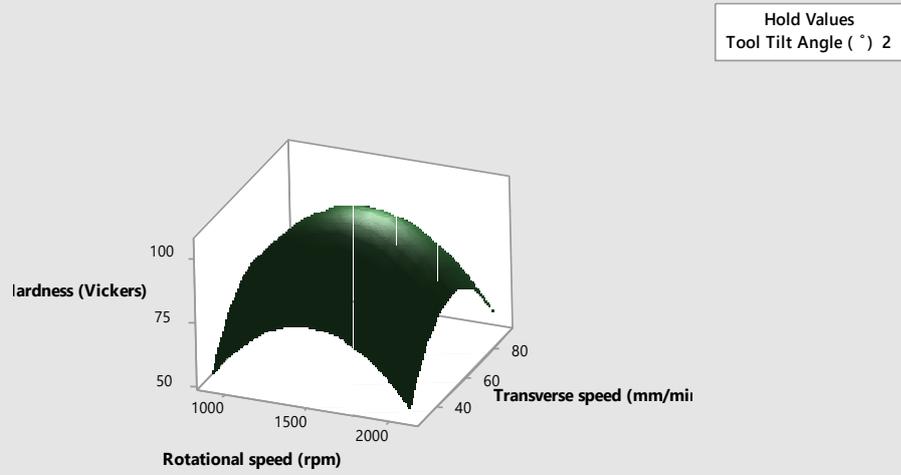APPENDIX H (I): Interaction Plot for UTS (TTT)
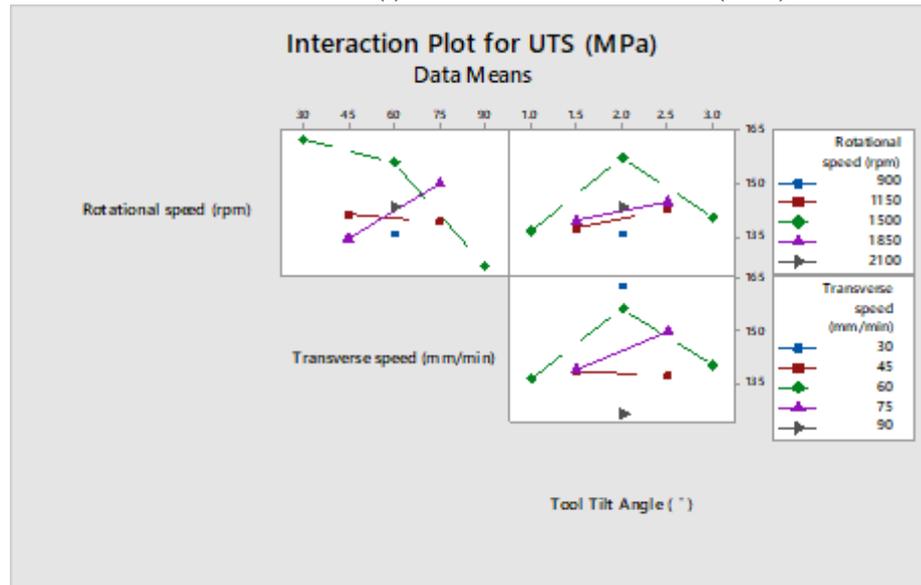


(ii): Interaction Plot Impact (TTT)
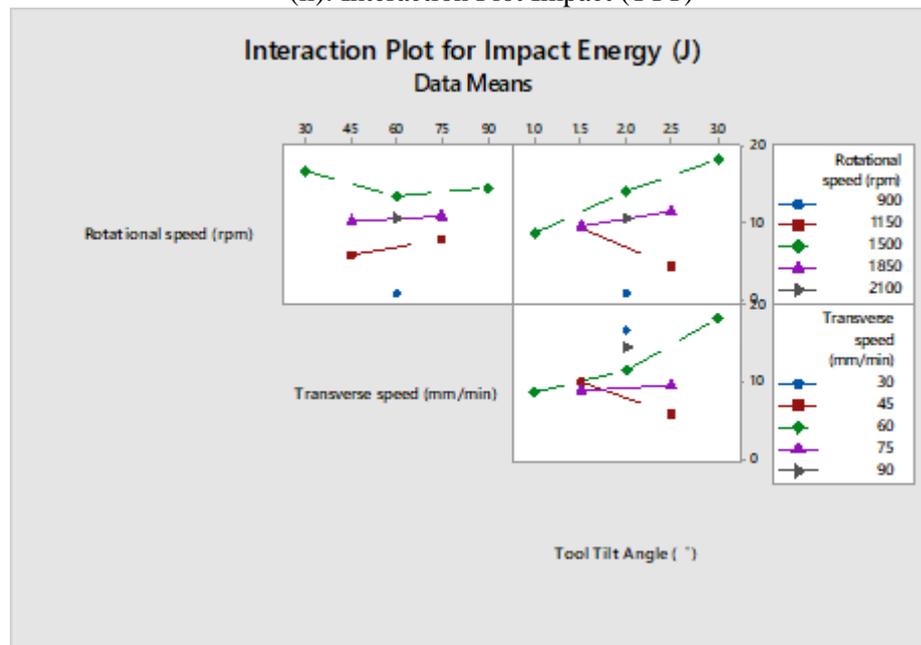
APPENDIX I: 3d surface plots for hardness at constant tool tilt angle (TTT)

**Surface Plot of Hardness (Vickers) vs Transverse speed (mm/min), Rotat**

Hold Values
Tool Tilt Angle ( ˚) 2



APPENDIX J: 3d surface plots for hardness at constant traverse speed (TTT)

**Surface Plot of Hardness (Vickers) vs Tool Tilt Angle ( ˚), Rotation**

Hold Values
Transverse speed (mm/min) 60
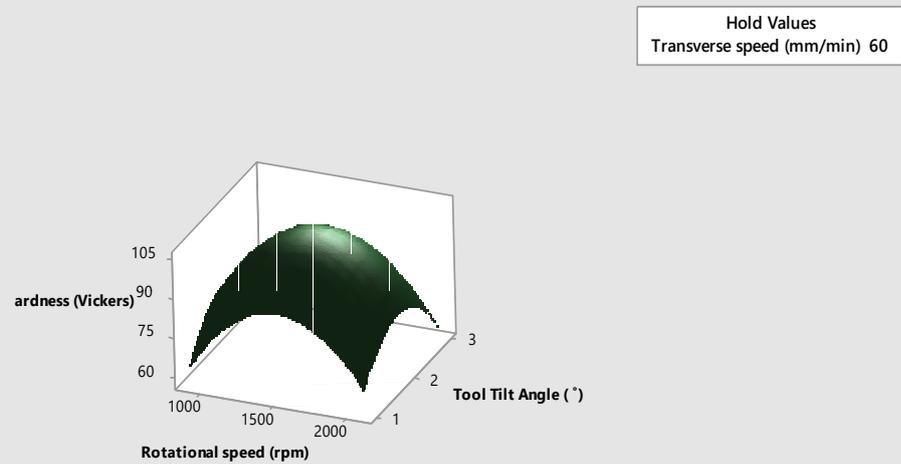
APPENDIX K: 3D Surface plots for hardness at constant rotational speed (TTT)

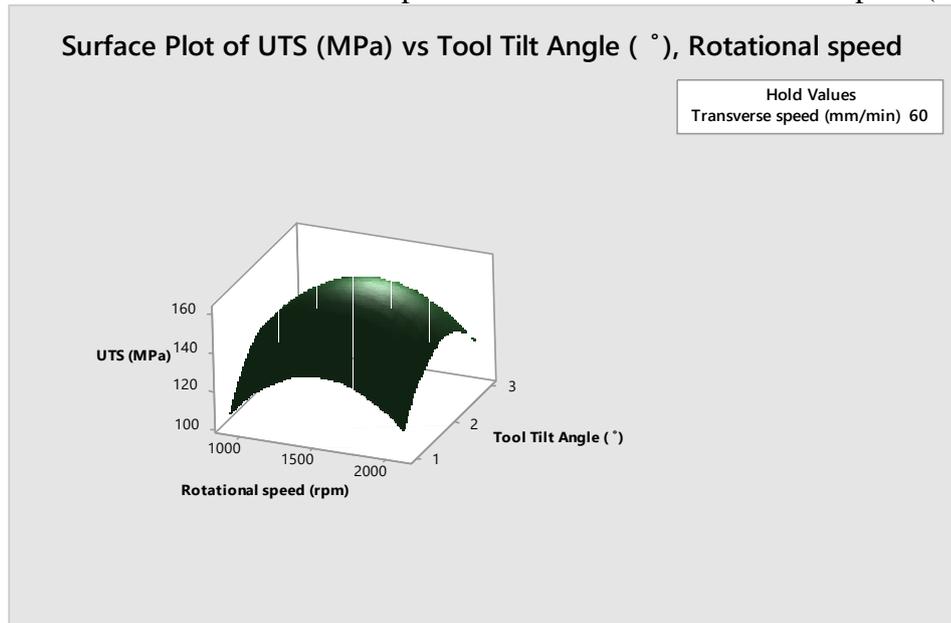**Surface Plot of Hardness (Vickers) vs Tool Tilt Angle ( ˚), Transver**

Hold Values
Rotational speed (rpm)  1500
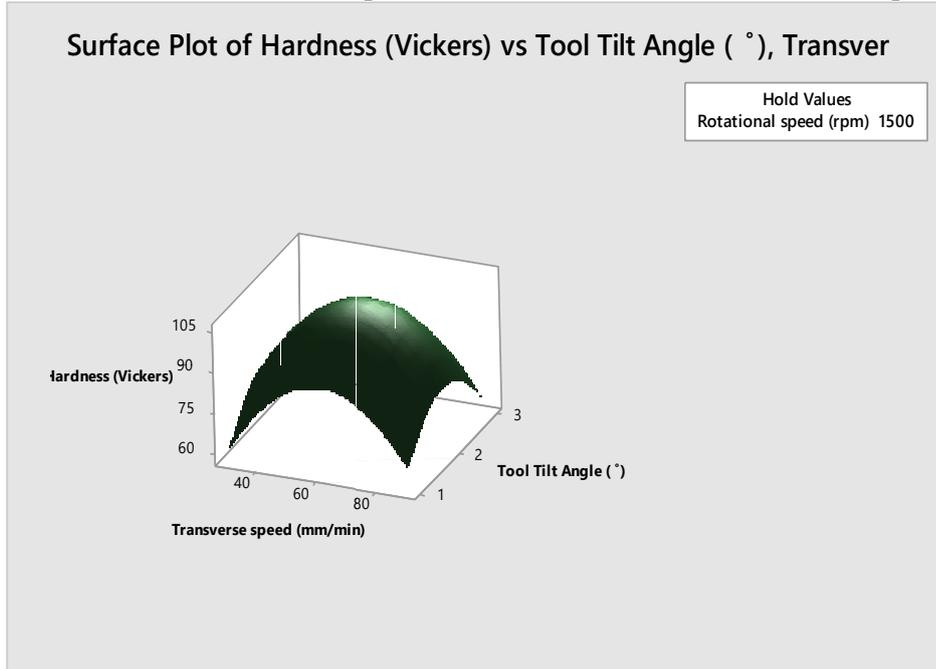


APPENDIX L: 3D Surface plots for UTS at constant tool tilt angle (TTT)

**Surface Plot of UTS (MPa) vs Transverse speed (mm/min), Rotational spe**

Hold Values
Tool Tilt Angle ( ˚)  2

APPENDIX M: 3D Surface plots for UTS at constant traverse speed (TTT)



Surface Plot of UTS (MPa) vs Tool Tilt Angle ( ˚ ), Rotational speed

Hold Values
Transverse speed (mm/min) 60

APPENDIX M: 3D Surface plots for UTS at constant rotational speed (TTT)



Surface Plot of UTS (MPa) vs Tool Tilt Angle ( ˚ ), Transverse speed

Hold Values
Rotational speed (rpm) 1500